TITLE

GEOCHEMICAL SIGNATURES OF KOMATIITES

AND ORIGIN OF THE STOUGHTON-ROQUEMAURE GROUP,

ABITIBI GREENSTONE BELT, CANADA.

By

James Suma-Momoh

A thesis submitted to the Faculty of Graduate Studies and Research, in partial fulfillment of the requirements for the degree of Master of Science.

Saint Mary's University

December, 2006.

© James Suma-Momoh, 2006.

i

NOTICE:
The author has granted a non-exclusive license allowing Library and Archives Canada to reproduce, publish, archive, preserve, conserve, communicate to the public by telecommunication or on the Internet, loan, distribute and sell theses worldwide, for commercial or non-commercial purposes, in microform, paper, electronic and/or any other formats.

AVIS:
L'auteur a accordé une licence non exclusive permettant à la Bibliothèque et Archives Canada de reproduire, publier, archiver, sauvegarder, conserver, transmettre au public par télécommunication ou par l'Internet, prêter, distribuer et vendre des thèses partout dans le monde, à des fins commerciales ou autres, sur support microforme, papier, électronique et/ou autres formats.

The author retains copyright ownership and moral rights in this thesis. Neither the thesis nor substantial extracts from it may be printed or otherwise reproduced without the author's permission.

L'auteur conserve la propriété du droit d'auteur et des droits moraux qui protège cette thèse. Ni la thèse ni des extraits substantiels de celle-ci ne doivent être imprimés ou autrement reproduits sans son autorisation.

In compliance with the Canadian Privacy Act some supporting forms may have been removed from this thesis.

Conformément à la loi canadienne sur la protection de la vie privée, quelques formulaires secondaires ont été enlevés de cette thèse.

While these forms may be included in the document page count, their removal does not represent any loss of content from the thesis.

Bien que ces formulaires aient inclus dans la pagination, il n'y aura aucun contenu manquant.

Canada

CERTIFICATION

Name: James Suma-Momoh

Degree: Master of Science in Applied Science

Title of Thesis: Geochemical Signatures of Komatiites and Origin of the

Stoughton-Roquemaure Group, Abitibi Greenstone Belt, Canada.

Examining Committee:

Dr. Marcos Zentilli, External Examiner.
Department of Earth Sciences, Dalhousie University,
Halifax, Nova Scotia.

Dr. Jaroslav Dostal, Senior Supervisor (Geology)

Dr. J. Victor Owen, Supervisory Committee (Geology)

Dr. Robert Singer, Supervisory Committee (Chemistry)

Dr. Malcolm Butler, Program Coordinator and Dean of Science.

Dr. Philip Giles, Graduate Studies Representative.

Date Certified: December 15, 2006.

© James Suma-Momoh, 2006

ii

TABLE OF CONTENTS

CHAPTER 1

INTRODUCTION 1

CHAPTER 2

GEOLOGICAL SETTING 17

iv

CHAPTER 5

LIST OF PLATES

LIST OF FIGURES

LIST OF ACRONYMS

BA-A: basaltic andesites and andesites

BON: boninites

Cpx: clinopyroxene

HFSE: high field strength element

HMG: hunter mine group

HREE: heavy rare earth element

IAT: island arc tholeiites

LILE: large ion lithophile element

LREE: light rare earth element

MORB: mid-ocean ridge basalts

NVZ: northern volcanic zone

OFB: ocean-floor basalts

REE: rare earth element

SRG: stoughton-roquemaure group

SVZ: southern volcanic zone

VAB: volcanic arc basalts

WOPB: within ocean plate basalts

WPA: within plate alkali basalts

WPT: within plate tholeiitic basalts

X_{Mg}:   mole fraction of magnesium

ACKNOWLEDGMENTS

First and foremost, I must say thanks to God for giving me the opportunity and making it possible for me to achieve this level of education. Secondly, I want to express gratitude and appreciation to the International Council for Canadian Studies and the Faculty of Graduate Studies and Research for their generosity, funding and moral support.

This thesis is the result of significant encouragement, direction and assistance for which I am greatly indebted to my thesis supervisor, Dr. Jaroslav Dostal. The trust and advice you gave to me brought extra determination and confidence in carrying out the research. Thanks to Dr. J. Victor Owen and Dr. Robert Singer for serving on my thesis committee. Special commendation and appreciation is given to Dr. Pierre Jutras, Dr. Andrew MacRae, Dr. Georgia Pe-Piper, Dr. Jerry Byers and Dr. Pawan Lingras for their interest and encouragement over the duration of this research. I wish to thank Patricia Stoffyn-Egli and Brian Fryer for providing priceless, expert analytical work. The administrative assistance of Barb Meunier and the technical support of Randolph Corney and Nikolas Tsoukalas cannot be forgotten.

Several individuals have been instrumental in making this thesis a success. The support and brotherhood received from member of the Sierra Leone-Canadian Association is gratefully acknowledged, with special thanks to Dr. Kelleh Gbawuru Mansaray, Dr. Joseph Bangura, Thomas Allie, Abdul Wurie, Nobizizwe Sizwe, Rosamond Luke, Lucy Swaray, Josephine Tommy, Denisia Allie and Ariatu Wurie. Many thanks to all my friends, including Ahmed Ahmed, Katie Flood, Tony Barresi, Colin Garroway, Fan Luo,

Brent LaPierre, Jason McLeod, Erica Oberndorfer, Kathleen Gould, Kevin Murphy and Aaron Retzlaff. You guys were greatly helpful in reducing every form of stress and making life much livelier during the entire research period.

Finally, I want to thank my family for their love. Although they are currently far away from me, they have remembered me in their prayers by wishing success and God's richest blessings.

ABSTRACT

Geochemical Signatures of Komatiites
and Origin of the Stoughton-Roquemaure Group,
Abitibi Greenstone Belt, Canada.

By: **James Suma-Momoh**

The genesis of sub-greenschist-facies-metamorphosed komatiitic rocks of the Stoughton-Roquemaure Group (SRG) in the Abitibi Greenstone belt, Canada, is evaluated based on the geochemistry of preserved primary clinopyroxenes. This study tries to distinguish between two main models of origin by the application of major and trace elements.

In general, clinopyroxenes in the SRG ultramafic komatiites, komatiites and basaltic komatiites are similar in composition. They contain low atomic proportions of non-quadrilateral components (e.g., Ti, Al and Na). The tectonic discrimination diagrams of Nisbet and Pearce (1977) and Leterrier et al. (1982) suggest both a plume and subduction origin for these rocks, whereas, those of Beccaluva et al. (1989) are compatible with a subduction origin. The SRG clinopyroxenes are seen to have similar compositions to those from Barberton (South Africa) and Belingwe komatiites (Zimbabwe), but they differ from Gorgona komatiites (Colombia). In addition, they can be compared with very low- and low-Ti ophiolitic basalts, island arc tholeiites, boninites, and basaltic andesites and andesites thought to evolve in subduction zones.

The SRG trace element data indicate that the rare earth elements (REE) have been immobile during metamorphism. REE patterns show depletion in the light REE ($[La/Sm]_N < 0.3$) and unfractionated heavy REE ($[Gd/Y]_N = 0.8$-1.18). The clinopyroxenes are depleted in high field strength elements (Nb, Zr, Ti and Y) relative to the more incompatible REE but show enrichment in large ion lithophile elements (Rb, Sr). These characteristics are attributed to a subduction zone origin. The overlap between plume and subduction affinity in the discrimination diagrams, and the subduction affinity from the trace element data make it difficult to assign a particular palaeotectonic setting. A parallel line of descent is proposed in which a rising mantle plume intercepted a subducting slab at shallow depth.

December, 2006.

CHAPTER 1

INTRODUCTION

1.1   What are Komatiites?

Komatiites are ultramafic volcanic rocks that occur mainly in Archaean greenstone belts (Nisbet and Walker, 1982; Thurston, 1994; Parman et al., 1997; Ayer et al., 1999). The Abitibi greenstone belt in the Superior Province of the Canadian Shield contains some of the greatest abundances of well-preserved komatiitic rocks in the world (Davis et al., 1994), and they indicate the composition, structure and physical conditions of the Archaean mantle (Chown et al., 1992; Arndt, 1994). Komatiites (named after the Komati River Formation) were first recognized by Viljoen and Viljoen (1969) in the Barberton Mountainland greenstone belt of South Africa.

Komatiites typically have low SiO_2 content (45-50 %). The features that make these rocks distinctive is their high MgO content of 18-30 wt %, compared to 10-15 wt % for the most mafic mid-ocean ridge basalts or ocean island basalts (Le Bas and Streckeisen, 1991; Sproule et al., 2002a, b; Grove and Parman, 2004; Nna-Mvondo and Martinez-Frais, 2005); and their large, skeletal, platy, or acicular and parallel or disoriented crystals of olivine in a finer-grained groundmass, which Viljoen and Viljoen (1969) formally called 'crystalline quench textures'. Nesbitt (1971) introduced the term 'spinifex' for this texture. Thus, komatiites from the type locality were first distinguished on the basis of chemistry and texture. Arndt (1994) established that the spinifex texture originated as a result of magma quenching during emplacement, promoted by rapid cooling of melt with

1

low nucleation rate and high growth rate of crystals at large degree of supercooling (Donaldson, 1982). According to the experimental data of Green (1975), the MgO content of the magma is proportional to its melting temperature, higher MgO contents indicating hotter magmas. This very first experiment on komatiites was interpreted to imply melting conditions in excess of 1600°C (compared to 1250-1350°C for modern mid-ocean ridge basalts — MORB).

Komatiites were produced most commonly in the Archaean (3.8-2.5 Ga) and late Archaean. Few were produced in the Proterozoic (2.5-0.56 Ga), and they were infrequent in the Phanerozoic eon (< 0.56 Ga). The preponderance of komatiites in the Archaean signifies primary differences between early and current mantle conditions (Nna-Mvondo and Martinez-Frais, 2005). Decrease in the degree of melting of the mantle due to secular cooling up to ~ 500 °C since the Archaean (Fig. 1) has been suggested for the decline in abundance of komatiites from the Archaean to Phanerozoic (Davis, 1993; Parman et al., 2001; Grove and Parman, 2004). This interpretation suggests that komatiites are potential 'thermometers' of the Earth's cooling (Nna-Mvondo and Martinez-Frais, 2005). The oldest known ultramafic rocks on Earth (Barberton komatiites) yield ages of 3.6-3.2 Ga (Lopez-Martinez et al., 1992) and have MgO content up to ~ 30 wt % (Parman et al., 2003), hence, the high temperatures inferred for their source region seem to fit well with the concept of a hot early Earth. Komatiites from the Superior Province in Canada (Munro komatiites) were the next to be well studied (Pyke et al., 1973; Arndt, 1976). These were younger (2.7 Ga) than the Barberton komatiites and had lower MgO content (up to ~ 24 wt %), consistent with a cooling Earth (Grove and Parman, 2004).

2
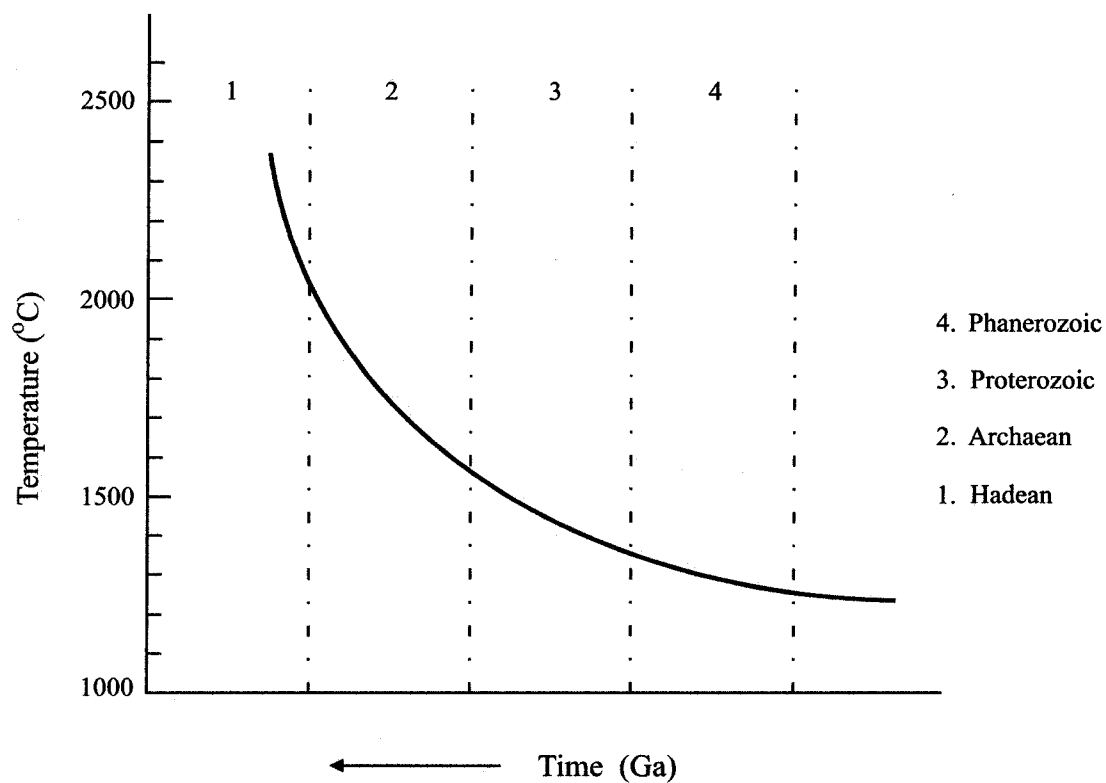
Fig. 1: Schematic temperature-time diagram illustrating evolution of mantle potential temperatures with time. The curve shows drop in temperatures from the Archaean to the Phanerozoic suggesting that the Earth has cooled with time. *Modified after Davis (1993)*

3

The most outstanding representatives of Phanerozoic komatiites are the Mesozoic komatiites from Gorgona Island, Colombia, South America. They are the youngest known komatiitic lava (0.089 Ga) and have much lower MgO content (~ 18 wt %) (Kerr et al., 1996). Their occurrence indicates unusually high temperatures in the mantle during the late Mesozoic era (Nna-Mvondo and Martinez-Frais, 2005). Younger komatiites are less common as compared to Barberton and Munro komatiites. One assumption is related to a progressive dehydration of hydrous phases in the upper mantle during the mid to late Archaean, such that, Mesozoic komatiites appearance may be as a result of local hydration of the upper mantle (Inoue et al., 2000).

There are two main types of komatiites, distinguished by their major and rare earth element contents: Al-depleted and Al-undepleted. The Al-depleted komatiites have comparatively low Al_2O_3/TiO_2 ratios (~ 10), high CaO/Al_2O_3 (>1), and fractionated heavy REE (rare earth element) patterns. They are referred to as 'Barberton-type komatiites'. In contrast, Al-undepleted komatiites have high Al_2O_3/TiO_2 ratios (~ 20), low CaO/Al_2O_3 (<1) and unfractionated heavy REE patterns. They are referred to as 'Munro-type komatiites' (Dostal and Mueller, 1997; Nna-Mvondo and Martinez-Frais, 2005).

1.2   What is the Problem?

Komatiites represent some of the oldest ultramafic magmatic rocks preserved in the Earth's crust (Kroner et al., 1991; Lopez-Martinez et al., 1992). For this reason, they have

4

been used to investigate the evolution of the Archaean crust. Numerous studies of komatiites dealing with their stratigraphic position (Anhaeusser, 1971; Tomlinson et al., 1998; Sproule et al., 2002b; Parman et al. 2003) and geochemistry (Arndt and Nesbitt, 1982; Hollings et al., 1999; Rollinson, 1999; Parman et al., 2001, 2003) have been published, but the original tectonic settings of komatiites remain enigmatic (Dostal and Mueller, 1997).

Several views have been proposed for the origin of these rocks. The original interpretation of Viljoen and Viljoen (1969) was that komatiites represent the first crust formed on Earth as a result of a catastrophic melting event triggered by convective overturn during core formation. A meteoritic impact origin for komatiites was proposed by Green (1972) and has recently been supported by Abbott and Isley (2002). Fyfe (1978) suggested that komatiites formed in an Archaean plume-dominated environment. Based on chemical data and field observations, Glikson (1971) and de Wit et al. (1987) proposed that komatiites formed in mid-ocean ridge environments. The similarity between modern mafic arc lavas and komatiitic lavas was noted by Brooks and Hart (1974) and Cameron et al. (1979), implying komatiite generation in a subduction zone. Likewise, the origin of komatiites in the wet melting environment of a subduction zone was proposed by Allègre (1982). Parman et al. (1997) and Grove and Parman (2004) pointed out the uniqueness of komatiites and suggested that they could not be related to a particular tectonic setting.

5

Of these several schools of thought, two have become prevalent in recent years. The first is that komatiites were produced by plumes, and the second, by subduction processes. Of these two, the plume model has become the most widely accepted explanation for the emplacement of komatiites (Grove and Parman, 2004).

1.2.1 Plume Model

The plume hypothesis was initially proposed by Fyfe (1978) for the origin of komatiites. It has earned considerable support from various workers, e.g., Arndt and Nisbet (1982), de Wit et al. (1987), Campbell et al. (1989), Arndt (1994), Dostal and Mueller (1997), and Sproule et al. (2002a).

Pressure-temperature constraints on the plume model are shown in Fig. 2. They follow fairly closely the models of adiabatic decompression melting used to explain the melting at mid-ocean ridges. In these environments, the temperature of a rising piece of mantle can be correlated with the major element composition of the magmas it produces (Herzberg, 1995).

The plume theory is explained by early secular cooling of the earth. Komatiitic magmas were generated from deep within the Earth at the core/mantle boundary when the mantle was about 500 °C hotter in the Archaean. Melts produced during this early stage of extreme temperature and pressure would have higher MgO and FeO contents but lower Na_2O, Al_2O_3 and SiO_2 contents than melts produced under the later cooler mantle

6

conditions (Grove and Parman, 2004). Komatiites would form by melting in the hot axial jet of the rising mantle plume (Fig. 3), whereas, basaltic komatiites (12-18 wt % MgO) would have been produced by melting in the cooler plume head (Campbell et al., 1989; Dostal and Mueller, 1997; Sproule et al., 2002b). Subsequent cooling, due to the need to transfer heat from the core, provided for the resulting emplacement of komatiites at consecutively shallower depths and lower temperatures (Grove and Parman, 2004).

Aitken and Echeverria (1984) reported the discovery of Phanerozioc komatiites on the island of Gorgona in South America. These komatiites have even lower MgO contents and melting temperatures than the Munro komatiites, again consistent with the idea of a cooling Earth. Originally, the tectonic setting of Gorgona was ambiguous, apparently corresponding either to the orogenies that affect mainland South America or to the Galapagos hotspot (Echeverria, 1980). Recent work on Gorgona suggests that they are related to the Galapagos hotspot. This information, therefore, buttresses the paradigm that komatiites were produced by plumes (Echeverria and Aitken, 1986; Arndt et al., 1998).

The high MgO contents in older komatiites and their decrease in younger samples indicates that komatiites are generated in a plume environment. Plume advocates also focus on the low SiO_2 komatiites, such as those from Munro and Gorgona, and point to the compositional similarity of modern ocean island basalts (Grove and Parman, 2004). However, melting experiments of representative mantle compositions under hydrous conditions (Inoue et al., 2000) have shown that Al-depleted Barberton-type komatiites are formed under low temperatures (~1300-1500 °C) and relatively low pressures (< 8 GPa)

7

in the solidifying hydrous magma ocean. This finding is at odds with a hotter Archaean mantle suggested for the origin of komatiites (Nna-Mvondo and Martinez-Frais, 2005).
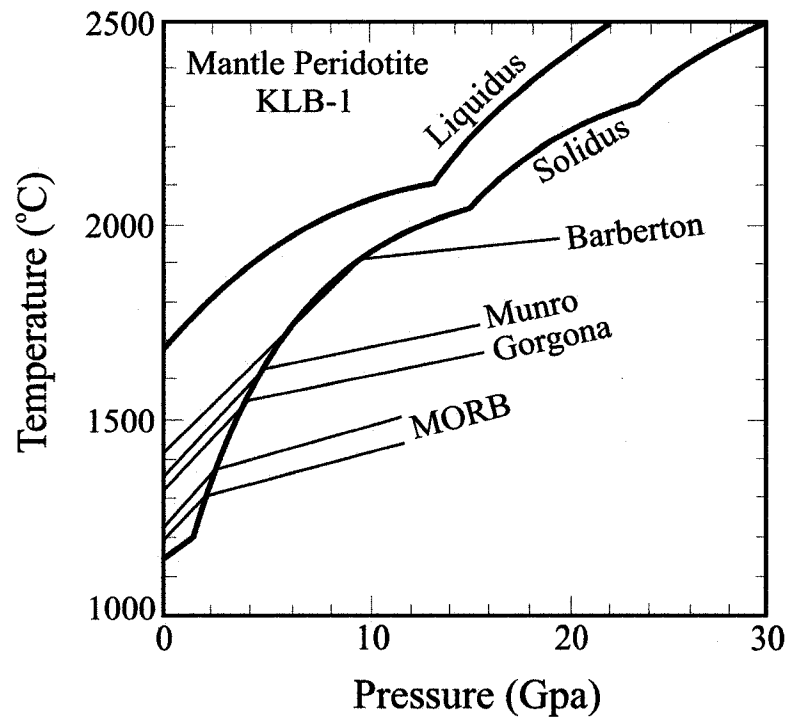
Fig. 2: Diagram illustrating depths and temperatures of melting of komatiites in a plume setting. The red lines show the pressure-temperature path experienced by a body of mantle as it ascends adiabatically towards the surface. The green lines are the solidus and liquidus of peridotite with representative mantle composition (sample KLB-1). The solidus is the first point at which the mantle will begin melting. The liquidus is the point at which the mantle would be completely molten. *Modified after Herzberg (1995)*

8
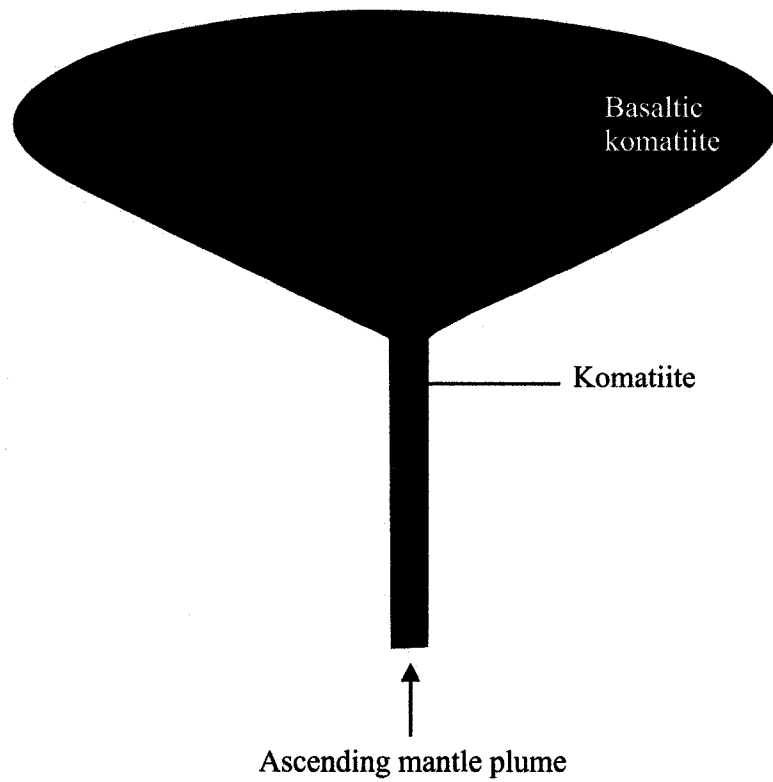
Fig. 3: Diagram illustrating a rising mantle plume from the core-mantle boundary. Komatiites will form in the hot axial jet and basaltic komatiites will be produced in the periphery of the cooler plume head.

9

1.2.2 Subduction Model

The generation of komatiites in a subduction zone (Fig. 4) was originally proposed by Brooks and Hart (1974). They pointed out that the major element chemistry of komatiites and basaltic komatiites is more closely related to modern mafic subduction-related magmas than those magmas produced by modern plumes. The initial evidence for a subduction origin for some komatiites is the elevated SiO_2 at high MgO contents; this feature is characteristic of the Commondale and Nondweni komatiites. These komatiites have much higher SiO_2 than Munro or Gorgona rocks and show some similarities to modern mafic subduction magmas (boninites) (Nna-Mvondo and Martinez-Frais, 2005). In general, the SiO_2 content of magmas decreases with increased melting pressures. The high SiO_2 content in these komatiites cannot be readily explained in a plume scenario (Grove and Parman, 2004).

Proponents of the subduction model (e.g., Brooks and Hart, 1974; Cameron et al., 1979; Allègre, 1982; Parman et al., 1997, 2003; and Wilson, 2003) suggest that hydrous melting at shallow mantle depths generated komatiite magmas in a subduction setting. In modern magmas, high H_2O contents are linked with melting in subduction zones. The introduction of water into the system was first proposed after the discovery of pargasitic amphibole in Fe-rich komatiites in Finland by Hanski (1992), and in a komatiite from the Abitibi belt, sampled by Stone et al. (1997). Subsequent experimental evidence showed that anhydrous experiments could not produce the crystallization sequence or phase composition of the Barberton komatiites. However, with the addition of H_2O, the experimental mineralogy was a good match.

10

1. Subduction initiation

Komatiitic crust
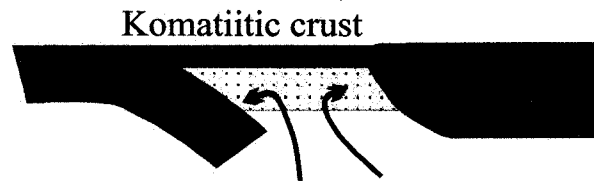
2. Mature subduction zone Calc-alkaline magmas

3. Subduction termination - continent collision
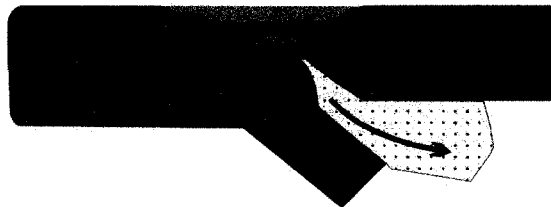
Highly depleted mantle

Lithosphere

Continent

Fig. 4: Subduction model for the origin of komatiites in subduction zones, based on boninite melting processes.

1: Boninite-like melting produces high MgO melts: komatiites, basaltic komatiites (dark-shaded portion) and highly depleted mantle residue.

2: Continued subduction of the lithosphere cools the mantle and the resulting low temperature magmas (calc-alkaline andesites) are emplaced on top of the high MgO, ultramafic crust.

3: Finally, ultramafic crust is then thrusted onto continents when subduction terminates during continental collisions. *Modified after Parman et al. (2004)*

11

Sun et al. (1989), Poidevin (1994), Wilson and Versfeld (1994), Kerrich et al. (1998), Hollings et al. (1999), Parman et al. (2001, 2003) and Wilson (2003), noted that many occurrences of komatiites have more compositional similarities to (or are interlayered with) modern boninitic lavas than any ocean island basalts. By virtue of such geochemical similarities, komatiites are expected to be produced by similar melting processes as have been proposed for modern boninites, but at higher mantle temperatures, assuming that the Archaean mantle was 100-500 °C hotter than the modern mantle (Nna-Mvondo and Martinez-Frais, 2005). Boninites are produced by high degrees of hydrous melting in subduction zones and have elevated SiO_2 at high MgO contents (Grove and Parman, 2004). According to Stern and Bloomer (1992), they are produced by melting conditions associated with the commencement of subduction. Hall et al. (2003) suggested that, in the early stages of a subduction zone, subduction is initiated along an active fault in the oceanic crust and the subducted plate rapidly sinks into the mantle, drawing hot, buoyant mantle asthenosphere into the forearc (Fig. 4). This early magmatism involves hydrated and depleted mantle. The addition of water and asthenospheric upwelling leads to massive degrees of melting. Eventually, as the subduction zone matures, this extreme form of melting ends and more normal island arc magmas predominate.

In summary, the origin of komatiites continues to be an on-going debate. Some workers advocate their formation during plume ascent whereas others favour a subduction zone setting. This perhaps suggests the emplacement of komatiites through various tectonic settings rather than a single type, as is the case of modern basalts (Parman et al., 1997; Grove and Parman, 2004). This study presents analytical data for Al-rich and Al-poor

komatiites from the Stoughton-Roquemaure Group (SRG) in the Abitibi Greenstone belt (~ 30 km NNW of Rouyn Noranda, Quebec), Canada, in order to substantiate which of the two competing models is more suitable for the area.

1.3   Previous work on the SRG

Lumbers (1962, 1963) was one of the earliest workers who mapped out the structural components of the SRG. He delineated the interface between the metavolcanic rocks which he termed *Bonis sequence*, and the metasedimentary rocks to the north of the belt. Eakins (1972) and Jensen (1978) reported that the SRG consists predominantly of komatiitic and magnesium- and iron-rich tholeiites. They noted that these metavolcanic rocks are interlayered with metasediments, such as, finely layered chert and iron formation horizons. Jensen and Langford (1985) outlined the stratigraphic sequence of rock units making up the SRG.

Dostal and Mueller (1997) described the geochemical characteristics and physical volcanology of komatiites and basaltic komatiites of the SRG. They discussed the evolution of the rocks, proposing a model involving a rising mantle plume beneath an arc (the Deloro assemblage) in which Al-depleted basaltic komatiites were generated by mantle melting, with garnet in the residue at the periphery of the plume, whereas Al-undepleted komatiites were formed by a higher degree of melting in the plume axis.

Sproule et al. (2002a) first mentioned that the Stoughton-Roquemaure Group (like the Pacaud assemblage) appears to represent lava channels or lava channel facies of

13

channelized sheet flows, compared to the Kidd-Munro and Tisdale assemblages which contain a greater abundance of meso- to adcumulate komatiitic peridotites and dunites. In addition, they observed that relatively low [Nb/Th] and [Th/Sm] mantle-normalized ratios in the SRG, which are much closer to depleted mantle, show that the lava was not contaminated. This implies a fundamental distinction either in the nature of the lithosphere through which the SRG komatiites ascended, or in magma discharge rates.

Sproule et al. (2002b) also studied spatial and temporal variations in the geochemistry of komatiites and basaltic komatiites in the Abitibi greenstone belt. They mentioned that the SRG is composed predominantly of Al-depleted, Ti-enriched basaltic komatiites, with subordinate low and high-Mg, abundant cumulate, Al-undepleted komatiites. They also postulated that the basaltic komatiites in the SRG may be primary melts derived from the peripheral parts of a plume head, consistent with the model proposed by Dostal and Mueller (1997). Sproule et al. (2002b) proposed a number of models suggesting plume ascent, plume dragging and stalling were responsible for the temporal variation in komatiite geochemistry in the Abitibi greenstone belt.

Based on U-Pb geochronology, Ayer et al. (2002) established an age range of 2725-2720 Ma for the SRG, indicating that the group was deposited in a relatively short time span. They reported that the chemical and isotopic signatures of the volcanic rocks deposited from about 2750-2700 Ma suggest a repeated tapping of both plume and subduction-related mantle sources.

Gibson et al. (2003) commented on the occurrence of several small volcanogenic massive sulphide deposits in the SRG. They observed that the rocks were not depleted in Pd and Pt, indicating that the magmas were not sulphide-saturated in the source region and that they did not reach sulphide saturation during ascent or emplacement. Gibson et al. (2003) concluded that such magmas represent a favourable source for Ni-Cu- (PGE) mineralization, as they contain a complete chalcophile element budget.

1.4   Objectives of Study

This work aims at determining the origin of Al-undepleted and Al-depleted komatiites from the Stoughton-Roquemaure Group (SRG) of the Abitibi greenstone belt. Emphasis is placed on the use of preserved, primary clinopyroxenes to shed light on the origin and palaeotectonic setting of these komatiites and related rocks by the application of relevant discrimination techniques.

1.5   Scientific Approach

The petrological and geochemical characteristics of volcanic rocks are directly related to their tectonic setting. However, post-emplacement alteration (including low temperature seawater-basalt interactions, high temperature hydrothermal water-basalt reactions, and regional metamorphism) may obscure the original mineralogical and geochemical characteristics of the volcanic rocks and thus prevent reconstruction of paleo-tectonic regimes. Moreover, it has been established that the geochemical characteristics of

15

primary clinopyroxenes preserved in some spilites and metabasites may be used to identify the original magmatic affinity (e.g., Beccaluva et al., 1989; Yaliniz and Goncuoglu, 1999; Koizumi and Ishiwatari, 2006).

Komatiites are old and altered rocks. However, clinopyroxenes are locally preserved, and can serve as important tools to determine the geotectonic setting in which they formed (e.g., Beccaluva et al., 1989; Yaliniz and Goncuoglu, 1999; Parman et al., 2003). The present study reports major and trace element compositions of clinopyroxenes in representative samples of komatiites and basaltic komatiites from the SRG, as determined by electron microprobe and laser ablation (ICP-MS). The geotectonic setting will be determined by employing various discrimination techniques previously published by Nisbet and Pearce (1977), Leterrier et al. (1982), and Beccaluva et al. (1989).

16

CHAPTER 2

GEOLOGICAL SETTING

2.1   The Superior Province

The Superior Province of Canada (Fig. 5) is the largest Archaean craton in the world. It underlies 1,572,000 km^2 (Goodwin, 1991, 1996) of the central part of the Canadian Shield. It is composed of volcano-plutonic, plutonic, metasedimentary, and high-grade gneiss sub-provinces (Thurston, 1991) that range in age between 3.3 – 2.55 Ga (Card, 1990). The boundaries of the sub-provinces are either major dextral, transcurrent, east-striking faults, or zones of plutonic and metamorphic transition. These subprovinces differ in aspects, such as, structural style, rock type, and metamorphic grade (Card and Ciesielski, 1986).

The volcano-plutonic (granite-greenstone) terranes contain volcanic arc-like rocks that have been metamorphosed to a low- or medium-grade. Stratigraphically, the lower of three recognized groups are komatiitic ultramafics and mafic volcanics with pillow lava structures. The second are andesites and calc-alkaline volcanics that are similar to island-arc type rocks. The top layers consist mainly of coarse sediments and smaller amounts of cherts, sandstones and limestones (Ayres and Thurston, 1985; Thurston and Chivers, 1990). Also present are large volumes of granitic plutons intruded into these volcanics and sediments.

17
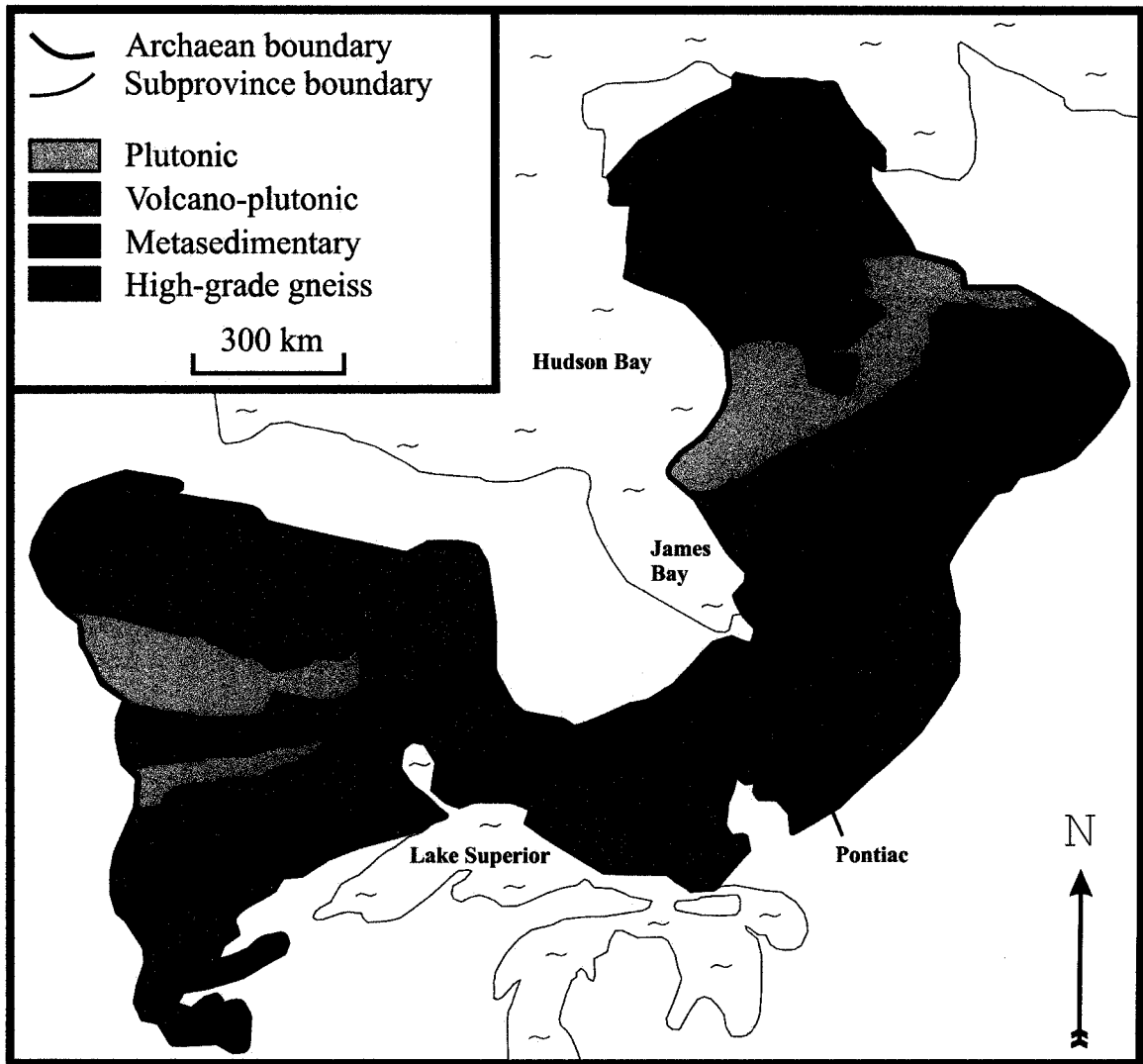
Fig. 5: Generalized map of the Superior Province illustrating major lithological subdivisions.

Modified after Card and Ciesielski (1986)

18

The greenstone terranes of the northeastern Superior Province contain the oldest metavolcanic rocks, dated in Ontario as much at 3013 ± 10 Ma (Fyon and Green, 1991). The greenstone terranes of the southeastern Superior Province contain metavolcanic rocks generally younger than 2800 Ma (Corfu and Grunsky, 1987).

The plutonic or intrusive terranes are composed of granitoid rocks, but differ from the granites in the volcano-plutonic terranes in the way they relate to other rocks. They compose entire subprovinces and were injected at a later time than the granites in the greenstone terranes. These Late Archaean granite intrusions emplaced into and adjacent to greenstone belts include: tonalite-granodiorite-granite, tonalite-diorite-monzonite-granodiorite and syenite (Smith and Williams, 1980; Stern et al., 1989).

Metasedimentary terranes comprise the metamorphic equivalents of greywacke, mudstone, tuff, conglomerate and banded iron formations (Goodwin, 1996); these are intruded by a wide range of rocks, from potassic granite to tonalite. The metamorphic grade varies from middle-amphibolite to granulite facies (Easton, 2000).

The gneissic terranes are usually the product of high-grade metamorphism. The rocks are massive to foliated (Fyon and Green, 1991) and are mostly represented by quartzofeldspathic gneiss of largely tonalitic to granodioritic composition. There are also granulites and complexes of more mafic gneisses derived from gabbro and anorthosite, as well as, metavolcanic amphibolites and metasediments. Rocks of the gneissic terrane range up to about 3.3 Ga (Goodwin, 1996).

19

2.2   The Abitibi Greenstone Belt

The Abitibi greenstone belt is located in the southeastern part of the Superior Province (Fig. 5), spanning northern Ontario and Quebec. It has an areal extent of approximately 115,000 km^2, making it the largest greenstone belt in the world (de Wit and Ashwal, 1997) and contains some of the greatest abundances of well-preserved komatiitic rocks (Sproule et al., 2002b), particularly in Munro Township. It is, as well, one of the youngest ($\sim$ 2.7 Ga) volcano-plutonic sub-provinces in the Superior Province. The ultramafic, mafic, and volcanic components make up 93% of the rocks; the remaining percentage being the felsic and calc-alkaline components (Fig. 6).

Komatiites and high-Mg tholeiites constitute about 12% of the volcanic rocks. The metamorphic grade varies from prehnite-pumpellyite to greenschist facies, but amphibolite facies rocks occur near late plutons. Due to the low-grade metamorphism and heterogeneous nature of the deformation, many of the primary textures and mineralogical assemblages within the lithological units have been preserved. Two periods of metamorphism have been determined: 2700-2688 and 2680-2670 Ma (de Wit and Ashwal, 1997).

Jackson et al. (1994) identified $\sim$ 50 small-scale lithotectonic assemblages. These have recently been revised by Ayer et al. (1999, 2002) into nine geochronologically- and stratigraphycally-distinct assemblages/groups, namely:

20

Timiskaming (2687-2675 Ma)

Porcupine (2696-2692 Ma)

Blake River (2701-2697 Ma)

Kinojevis (2702-2701 Ma)

Tisdale (2710-2703 Ma)

Kidd-Munro (2718-2710 Ma)

Stoughton-Roquemaure (2725-2720 Ma)

Deloro (2730-2725 Ma)   and

Pacaud (2750-2735 Ma)

| | Granitoid Rocks | | Mafic intrusions | | Middle Precambrian Sediments | | Early Precambrian Sediments | | Volcanic Rocks | | Ultramafic Rocks |
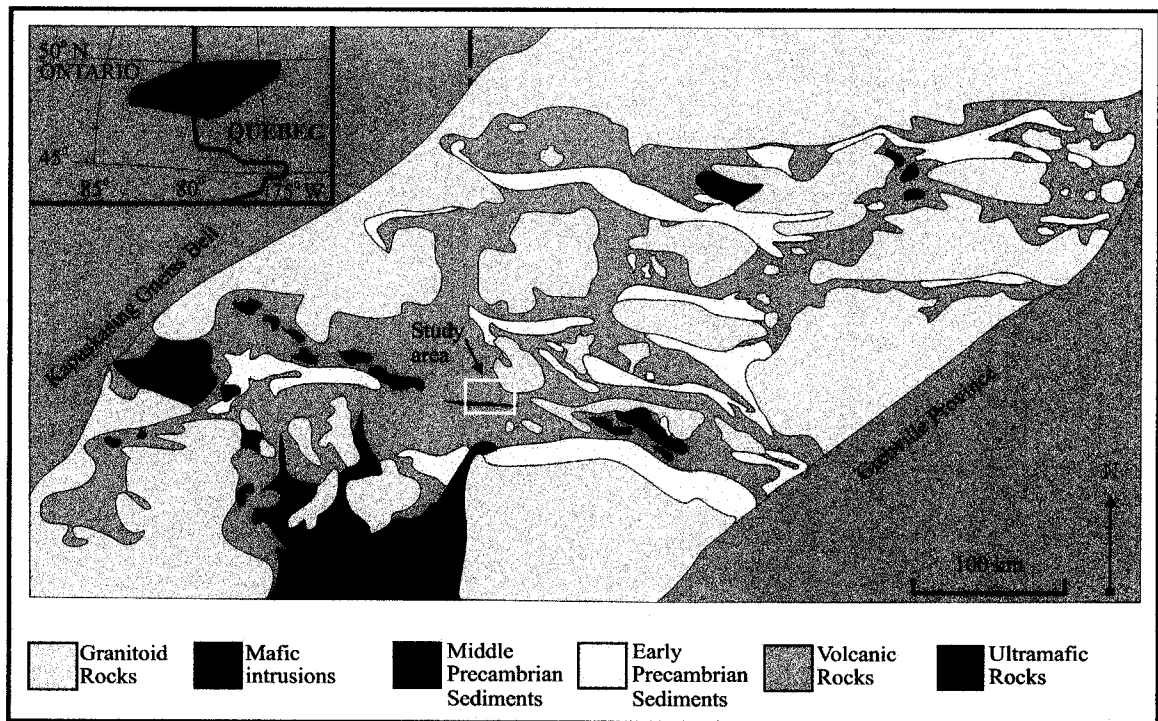
Fig. 6: General geological map of the Abitibi greenstone belt showing association of the various

rocks. *Modified from: http://user.uni-frankfurt.de/~lahaye/fieldtrip/html/abitibitx.html*

21

In the Abitibi greenstone belt, komatiitic rocks occur in only four of these lithotectonic groups: the Pacaud, Stoughton-Roquemaure, Kidd-Munro, and Tisdale groups. All komatiitic rocks in the Pacaud group are Ti-depleted komatiitic basalts; those in the Stoughton-Roquemaure Group are Al-depleted komatiites (ADK) and Al-undepleted komatiites (AUK). The majority of those in the Kidd-Munro and Tisdale assemblages are AUK with rare ADK and Ti-enriched komatiites (TEK) (Sproule et al., 2002b).

Goodwin and Ridler (1970) mapped and divided the belt into a Northern Volcanic Zone (NVZ) and a Southern Volcanic Zone (SVZ) (Fig. 7). These zones are the most fundamental subcomponents of the Abitibi greenstone belt (Chown et al., 1992). The NVZ is dominated by a cycle of 2730-2720 Ma volcanism and sedimentation. On the other hand, the SVZ comprises a mix of volcanic ages, but is largely characterized by 2720-2685 Ma volcanism. Magmatic associations in the SVZ include: (a) tholeiitic basalts and komatiites; (b) a depleted tholeiitic-boninite suite; (c) arc tholeiites and calc alkaline rocks; (d) adakites and high Mg# andesites; (e) syn-orogenic batholithic intrusions, and (f) pre- to post-orogenic shoshonites (Wyman et al., 2002).

Both zones are separated from one another by the steeply dipping, east-striking Destor-Porcupine fault (Chown et al., 1992). The fault zone has a strike length of over 300 kilometres (Jackson and Fyon, 1991).

22

23
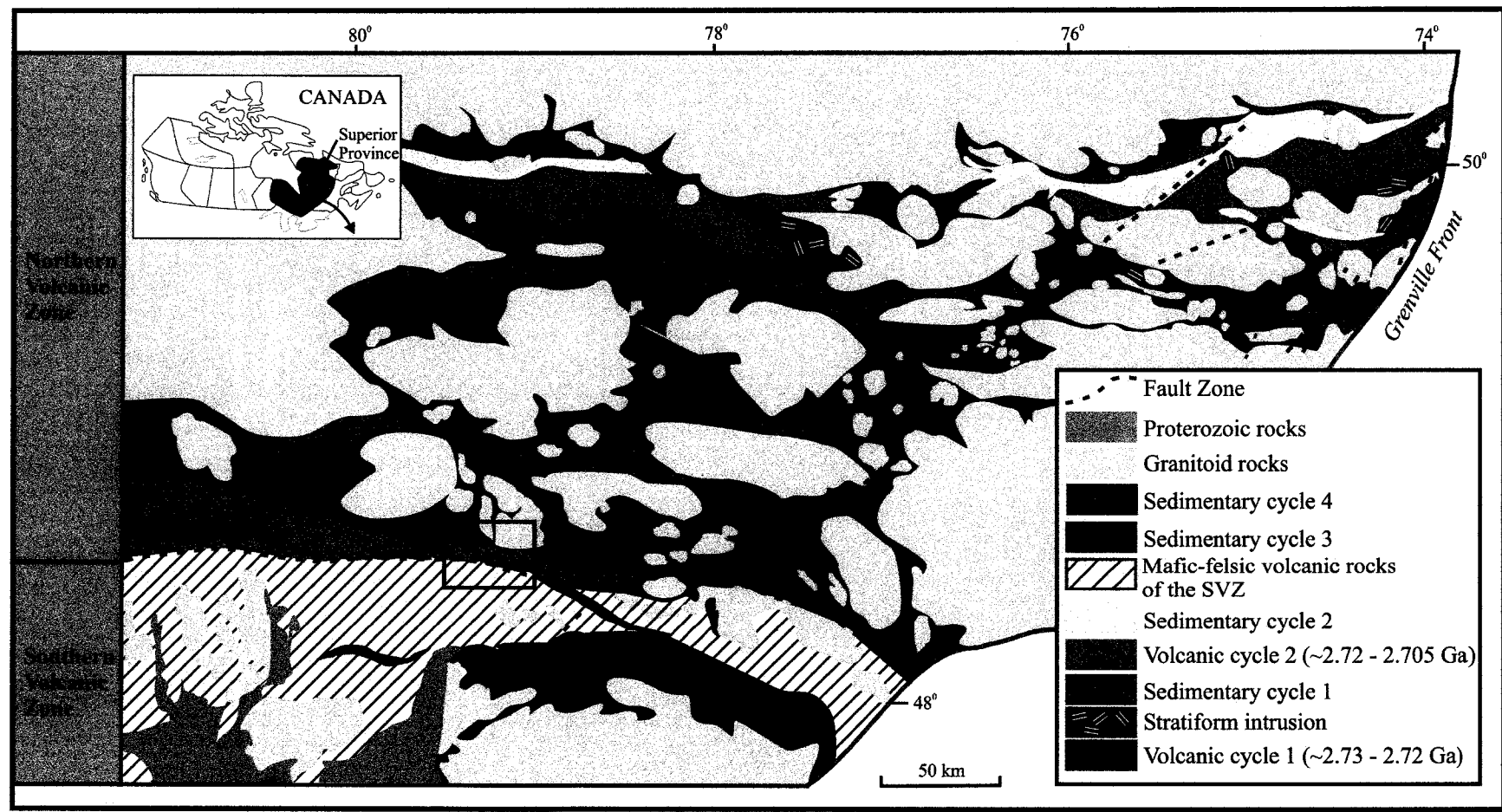
Fig. 7: Subdivision of the Abitibi greenstone belt into Northern Volcanic Zone (NVZ) and Southern Volcanic Zone (SVZ). Further subdivision of

the volcanic and sedimentary cycles is also shown. The location of the study area is outlined. *Modified from Dostal and* Mueller *(1997)*

2.3   The Study Area

The study area (Fig. 7) lies in the southern extremity of the Northern Volcanic Zone that consists of two 1-5 km thick mafic-felsic volcanic cycles, namely:

(i) a Monocyclic Volcanic Segment to the south, made up of an extensive subaqueous basalt plane with scattered felsic volcanic complexes (2730-2725 Ma). It is overlain by and interlayered with elongate volcaniclastic sedimentary basins and intra-arc volcaniclastic turbidites (Chown et al., 1992; Dostal and Mueller, 1997).

(ii) a Polycyclic Volcanic Segment to the north, comprising a second mafic-felsic volcanic cycle (2722-2711 Ma) and a sedimentary assemblage containing local shoshonitic volcanic rocks (Chown et al., 1992).

The Hunter Mine Group — a 4-5 km thick volcanic unit of 2730 Ma; forms part of the monocyclic volcanic segment (Fig. 8). This Group is composed of massive to brecciated rhyolitic lava flows and lobes, and an extensive felsic-dominated dyke swarm (Fig. 8). Mafic dykes (similar to those in the SRG) are as well present in this swarm, signifying a period of prolonged dyke emplacement that involved feeding of the volcanic flows belonging to the SRG (Dostal and Mueller, 1997). Directly above the swarm in the upper 500-1000 m thick transition zone of the Hunter Mine Group is a highly variable association of pyroclastic and volcaniclastic sedimentary rocks, iron formation, mafic to intermediate dykes and sills, and mafic and felsic lava flows. The mafic flow component increases toward the SRG.

24
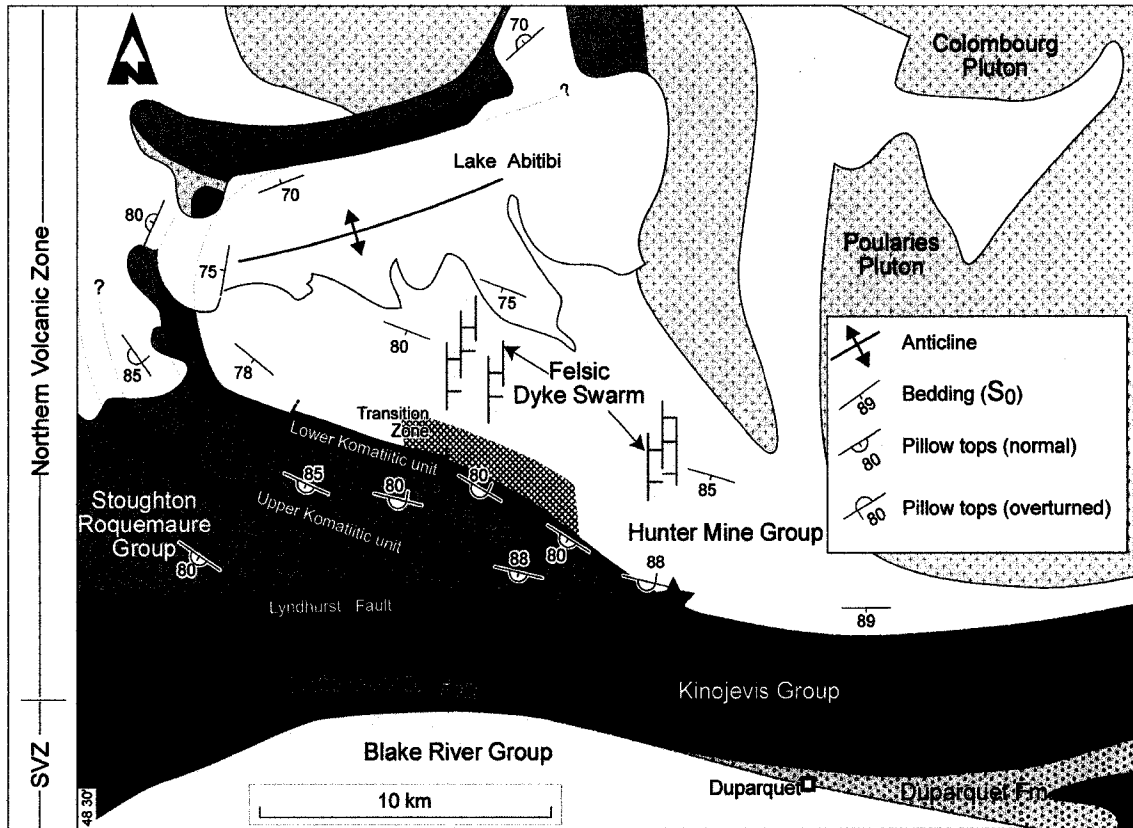
Fig. 8: Geological map of the study area showing the relationship between the Stoughton-Roquemaure Group (SRG) and the Hunter Mine Group. The two komatiite units of the SRG are shown and two sample points are indicated (starred). *Modified from Dostal and Mueller (1997)*

25

In general, the flows are 3-20 m thick and exhibit massive columnar-jointed sections that grade vertically and laterally into pillow breccia and pillowed flows with flows ranging from 20-150 cm in diameter, and displaying centimeter-scale chilled margins and internal polygonal jointing. The pillowed flow facies constitutes the komatiitic basalts and komatiites of the SRG. *In situ* brecciation around pillows is not uncommon but extensive columnar joints range from 10-30 cm in diameter within flows, and are perpendicular to the cooling front. Massive and columnar-jointed mafic dykes represent the youngest phase in the felsic dyke swarm (Dostal and Mueller, 1996).

Immediately above the 4-5 km thick central portion of the Hunter Mine Group is the 200 m thick mafic-ultramafic SRG. To the west, the SRG thickens to 2 km whereas the Hunter Mine Group continues to thin. Both the HMG and SRG are truncated by the Lyndhurst fault (fig. 8). This explains the limited thickness of the SRG above the central part of the Hunter Mine Group (Dostal and Mueller, 1997).

The SRG consists of tholeiitic basalts, with localized komatiites and felsic volcanic rocks. Volcanic rocks of the SRG may represent the start of the polycyclic volcanic segment or may be still part of the monocyclic volcanic segment (Dostal and Mueller, 1997). The narrow age range of 2725-2720 Ma for the SRG indicates that this assemblage was deposited in a relatively short time span (Ayer et al., 2002). Goutier (1993) has identified two lithological units in the SRG, namely, (i) an alternating 50-400 m thick komatiitic unit, and (ii) a 100-1000 m thick basaltic unit. Both units have been traced for several kilometers. The ultramafic flows are probably the lateral along-strike equivalents of the

26

well-documented komatiite flows of Munro Township that lies to the west of the study area.

Rocks of the SRG and the transition zone of the HMG were largely subjected to sub-greenschist facies metamorphism, characterized by the prehnite-chlorite-epidote assemblage. The HMG and SRG are 'locally' overturned strata younging to the south. They trace a large anticline that closes to the west. The sequences dip steeply at 70-90° (Dostal and Mueller, 1997).

CHAPTER 3

PETROGRAPHY

3.1   Komatiite Cooling Units

Ultramafic lavas have distinct features. Arndt et al. (1977) presented sections of 3 types of komatiite flows from the Munro Township (Fig. 9). Spinifex texture is often preserved in the upper parts of such flows. This texture is commonly characterized by randomly oriented skeletal crystals of olivine or pyroxene, and results from relatively rapid *in situ* crystallization of ultramafic or highly mafic liquids (Condie, 1982; Arndt, 1994).

Komatiite cooling units are petrographically and chemically layered (Fig. 9). Layering is a result of gravitative settling of early-formed olivine crystals in the most mafic cooling units and of olivine and pyroxene in the less mafic units (Arndt, 1994). Arndt et al. (1977) showed that layering is not necessarily laterally continuous or of uniform thickness. In moving away from the source of the flow, the spinifex zone (i.e., A_2 unit) may thin out and possibly terminate, leaving only the lower part of the flow (B unit — foliated skeletal olivine and peridotites) covered by the chilled and fractured flow top (A_1 unit) (Fig. 10).

Komatiitic rocks of the SRG display the textural pattern shown in Fig. 9a. It can also be deduced on textural grounds that they belong to the A_2, B_1 and B_2 units of the column. Pyke et al. (1973) subdivided the A_2 unit into upper and lower spinifex zones. Plate 1 illustrates an idealized boundary between the two zones. The upper layer is characterized

28

by short and disoriented clinopyroxenes far less than 30 mm in length, whereas the lower layer comprises of long fan-like clinopyroxene strands of at least 30 mm in length.

Plate 2 shows the boundary between the B_1 unit and overlying A_2 unit. Rocks in the B_1 unit are fine to medium-grained and contain equant and subhedral microphenocrysts of clinopyroxenes showing a weak or skeletal foliation. This observation follows closely those previously made by Pyke et al. (1973), Arndt et al. (1977) and Arndt (1994), for the komatiite flows from Munro Township. The last part of the komatiite flow to remain fluid was the B_1 layer, as shown by flow textures (Arndt, 1986).

The following sections provide general thin section descriptions of four groups of rocks that were collected from the study area by Dostal and Mueller in the years 1995 and 2000. The rocks are: ultramafic komatiites, komatiites, basaltic komatiites and basalts. For this exercise, a total number of 40 slides were selected and examined with the aid of a polarizing microscope.
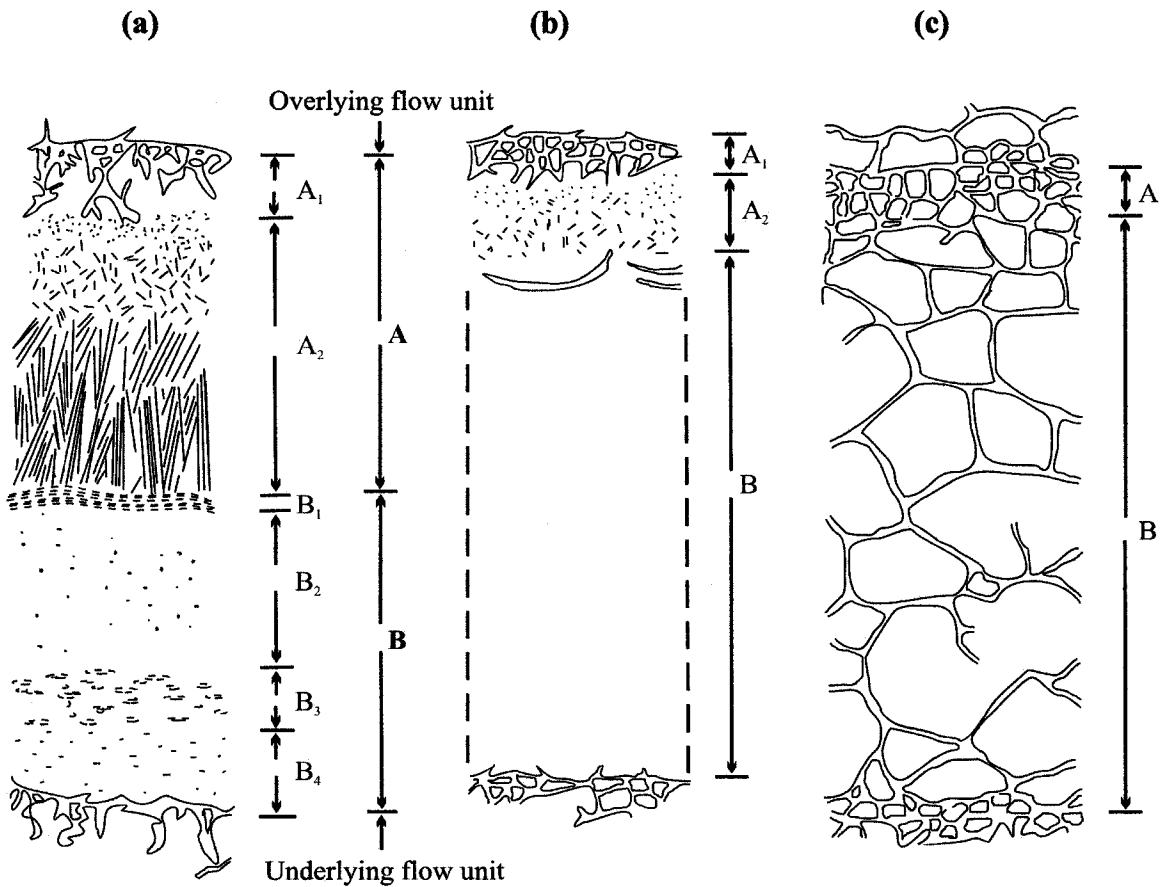
Fig. 9: Diagrammatic sections through three types of komatiite flows from Munro Township, Canada *(Arndt et al., 1977)*.

Description:

(a)

UPPER PART OF FLOW UNIT

A_1: Chilled and fractured flow top.

A_2: Spinifex

LOWER PART OF FLOW UNIT

B_1: Foliated skeletal olivine

$B_2 - B_4$: Medium- to fine-grained
    peridotite.

B_3: Knobby peridotite.

(b)

A_1: Chilled flow top with fine
    polygonal jointing.

A_2: Spinifex

B: Medium- to fine-grained
    peridotite.

(c)

A_1: Chilled flow top with
    Fine polygonal jointing.

B: Main part of flow; medium-
    to fine-grained peridotite with
    coarse polygonal jointing.

30

Chilled and
fractured
flow top (A₁)

Spinifex Zone
(A₂)

Cumulate Zone
(B)

East

West

Direction away from spinifex zone

0   30m
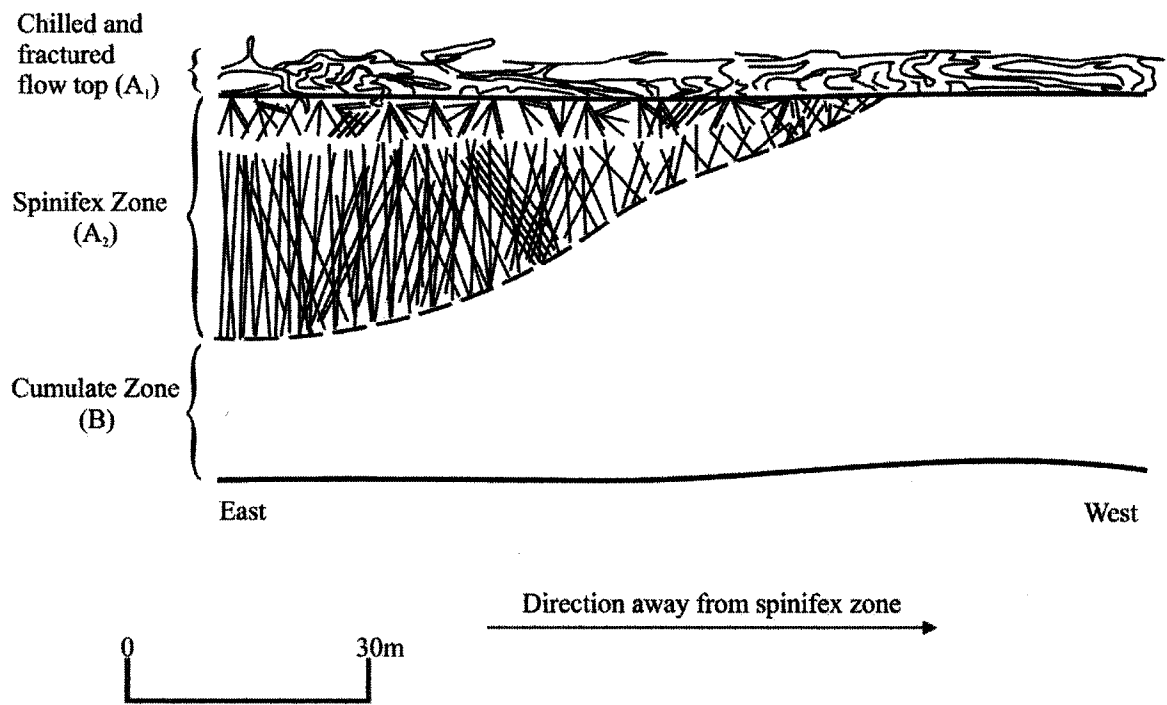
Fig. 10: Thinning of the spinifex zone in a komatiite flow in Munro Township. *Modified after*

Arndt et al. (1977)

31
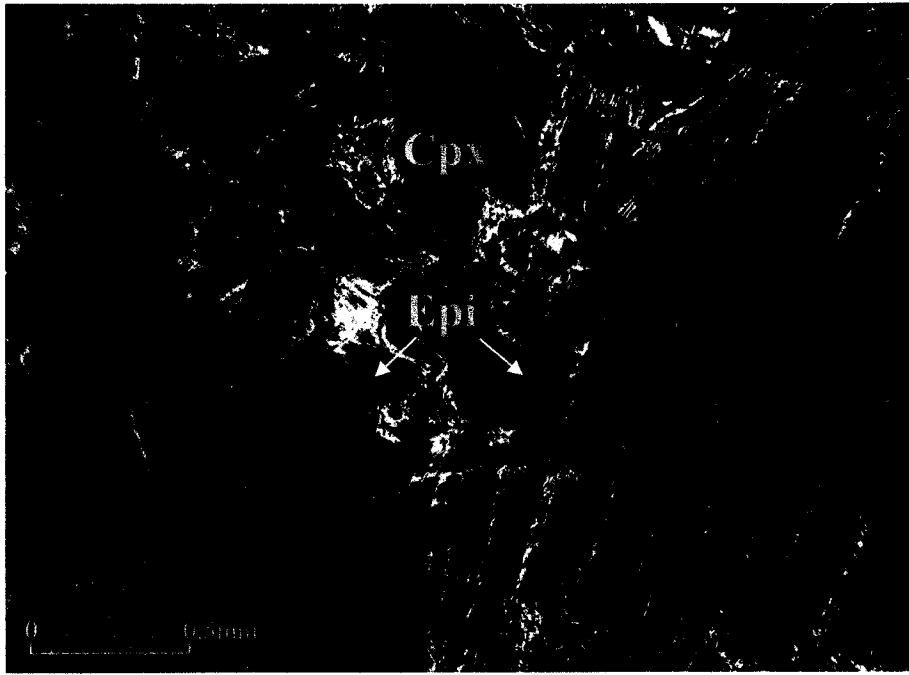
Plate 1: Presumed boundary (broken line) between the upper and lower zones of the A₂ unit. Note the difference in the length of clinopyroxenes in both zones. Cpx = Clinopyroxene; Epi = Epidote. *Sample: ROQ-95-18, x5 crossed polars (xpl).*

Plate 2: Photo showing probable boundary between the A₂ (above) and B₁ (below) units. Note the flow pattern in B₁. *Sample: ROQ-95-8b, x5 plane polars (xpl).*

32

3.1.1 Ultramafic Komatiites

Serpentine and opaque minerals are the essential minerals. The serpentine formed as a result of the alteration of primary olivine. Partially altered olivine phenocrysts retain prominent irregular cracks. Opaque minerals (e.g., magnetite) occur along the edges and cracks of the olivine phenocrysts (Plate 3). Brucite is commonly mixed in with the serpentine alteration products (Shelly, 1993). Hematite occurs as deep red, translucent crystals especially in the cores of grains. These are enclosed by black magnetite, formed at the expense of the hematite. Granular aggregates of chromite crystals are present as inclusions in some olivine plates (Fleet and MacRae, 1975). Clinopyroxenes are observed as minute angular and skeletal crystals. The former show basal sections with extinction angles ranging from 45° to 52°, indicating that they are augites. Some of the skeletal clinopyroxenes exhibit nucleation growth wherein they appear to emanate from a central point (Plate 4).

Chlorite formed through the alteration of either olivine or serpentine and clinopyroxene, commencing from the outer rim and continuing inwards. It shows anomalous interference colours appearing in shades of blue, purple or brown.

33
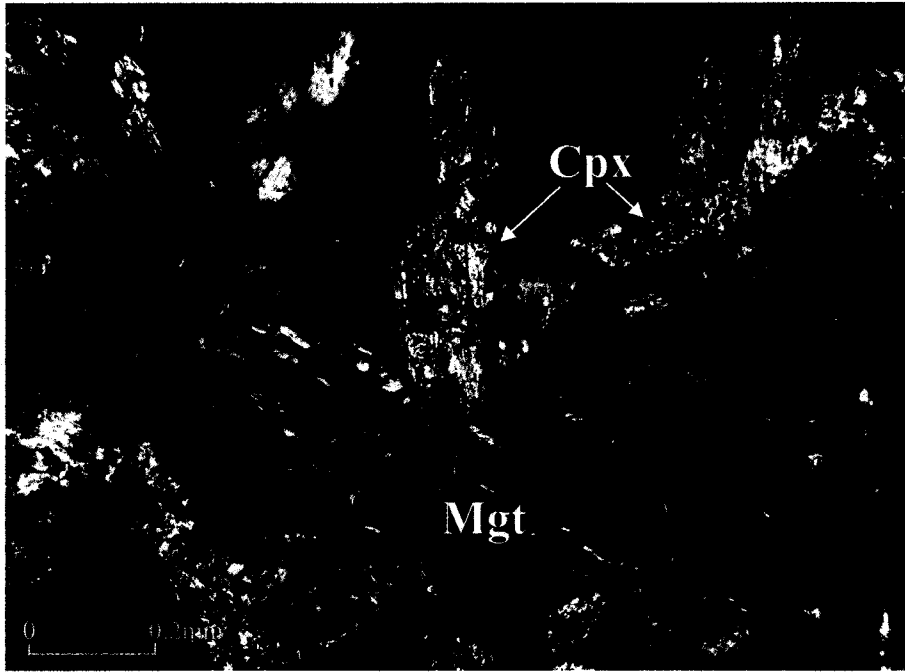
Plate 3: Magnetite (Mgt) aggregates deposited along the edges and cracks of olivine microphenocryst; flanked by clinopyroxenes (Cpx). *Sample: WP-00-15, x10xpl.*
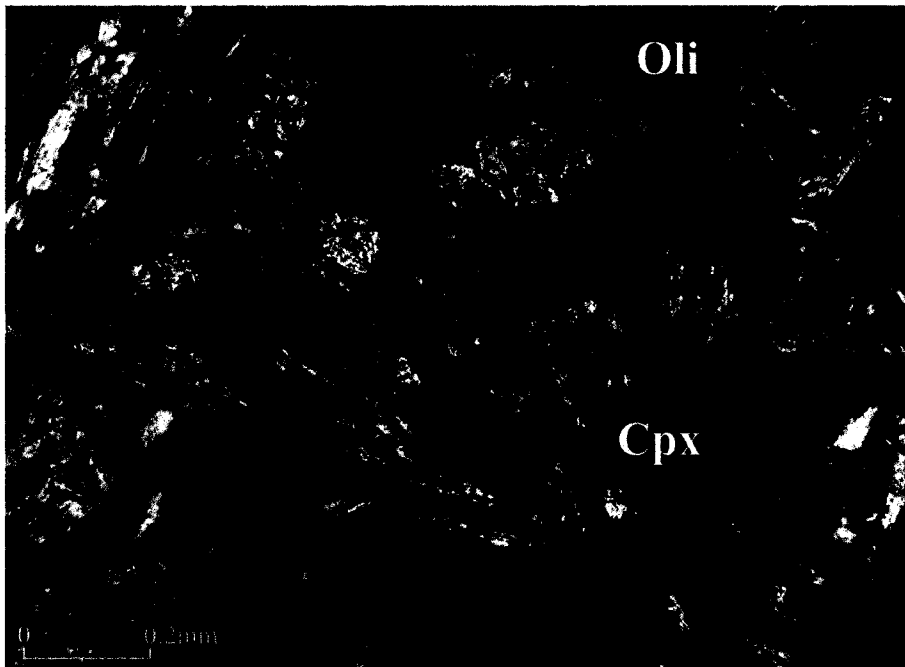
Plate 4: Skeletal clinopyroxenes showing nucleation growth to form a digitating pattern. Oli = olivine. *Sample: WP-00-17, x10xpl.*

34

Plate 5 shows hexagonal serpentine pseudomorphs after olivine, occurring in juxtaposition and aligned parallel to one another in a closely packed manner. The alteration of olivine to serpentine is only partial in this specimen. These might be olivine cumulates and the alignment denotes some amount of flow of the magma.

The ultramafic komatiites occupy the basal portion of the komatiite cooling units. It can be suggested that ultramafic komatiites are distinguished from komatiites by having olivine cumulates; more opaque minerals but no spinifex texture.
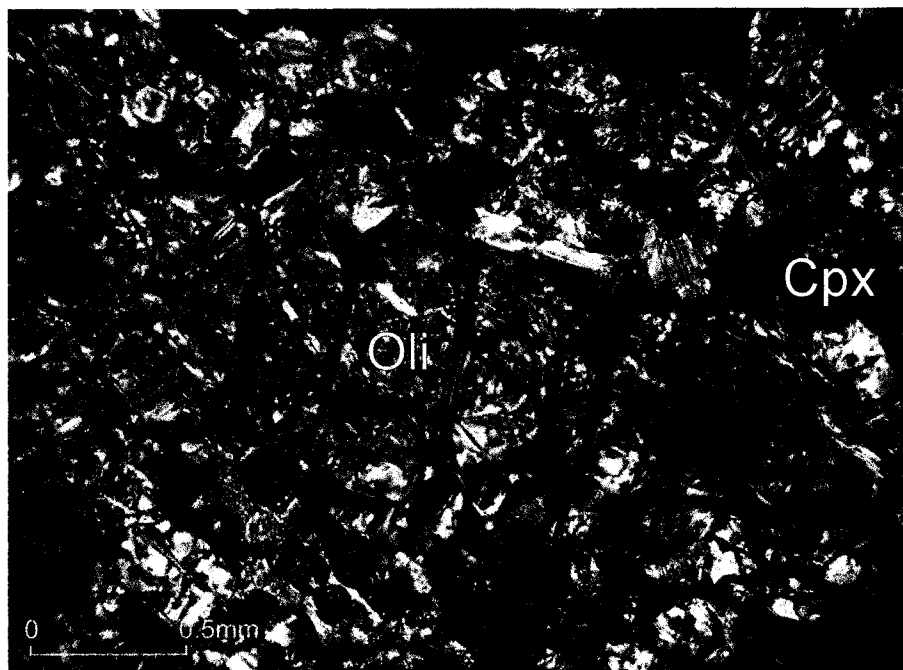
Plate 5: Partially altered olivine cumulates (centre). Note their alignment. Sample: Wp-00-8, x5xpl.

35

3.1.2 Komatiites

The komatiites show several types of spinifex texture. For instance, there is pyroxene spinifex texture with acicular or skeletal clinopyroxene plates ranging from about 0.5 mm to 120 mm in length. Some of these skeletal plates portray 'backbone' (Plate 6) and dendritic structures. In radiating spinifex texture, elongate clinopyroxene phenocrysts assume a fan-like pattern. Furthermore, there is randomly oriented spinifex wherein elongate clinopyroxene phenocrysts are oriented in different directions. Fan-shaped, feathery and aggregates of clinopyroxenes also occur in the fine-grained matrix (Plate 7). Fleet and MacRae (1975) report that as pyroxene grain size decreases, its crystal shape changes from acicular to fan-shaped to bow-tie shape to feathery crystallites. The occurrence of spinifex textures in all the studied komatiite slides suggest that the samples were collected from the A_2 unit.

Chlorite appears to have formed by the alteration of olivine and pyroxene. Also, actinolite seems to have formed by the alteration of clinopyroxenes. Prismatic crystals of orthopyroxenes occur in minor amounts. Some of the pyroxenes are bent, revealing the effect of deformation.

36
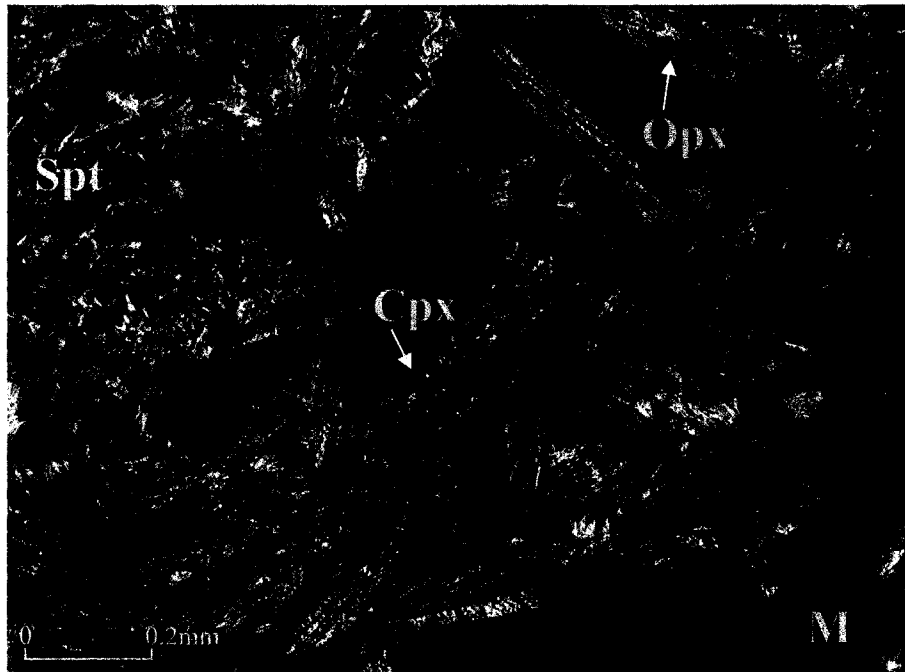
Plate 6: Fibrous serpentine (Spt), skeletal plates of clinopyroxenes and orthopyroxenes (Opx) embedded within a dark brown and glassy matrix (M). The *central* clinopyroxene plate has a 'backbone' structure. *Sample: ROQ-95-15, x10xpl.*
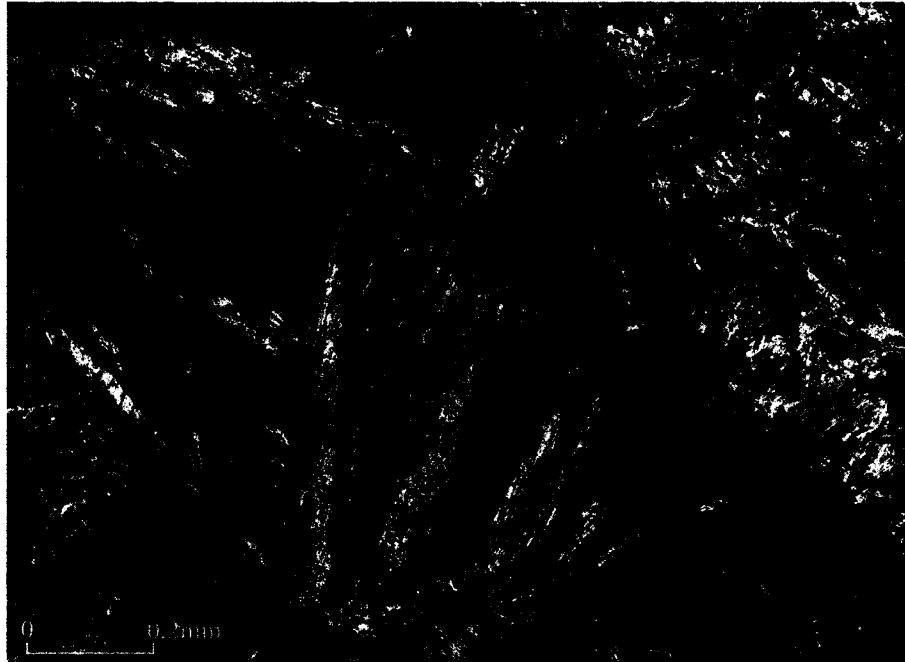
Plate 7: Feathery (centre) and aggregates (top left and right) of clinopyroxenes. *Sample: ROQ-95-15, x10xpl.*

37

3.1.3 Basaltic Komatiites

These rocks consist almost entirely of clinopyroxene, serpentine, actinolite, epidote and locally, partially altered olivine phenocrysts. Clinopyroxene crystals range in size from about less than a millimetre to up to about 20 mm in length (ROQ-95-1), embedded in a groundmass of chlorite and serpentine. Euhedral and subhedral phenocrysts of fresh clinopyroxenes occur (ROQ-95-2) but sometimes, partial alteration to chlorite is evident. As well, clinopyroxenes form fan-like structures (ROQ-95-3) and are pitted (ROQ-95-21A). Clinopyroxene spinifex texture is common in most samples of basaltic komatiites and represents the lower section of the group, close to the underlying komatiite unit (Plate 8). The randomly oriented spinifex portions consist of fibrous serpentine and skeletal plates of clinopyroxenes. They intersect with no preferred orientation and probably represent the top of the A_2 unit of a typical komatiite suite.

Serpentine exhibits a brown mesh-like texture and seems to have been derived from the alteration of olivine and clinopyroxene. Subhedral epidote and euhedral crystals of actinolite occur as well.

The opaque minerals tend to be concentrated in places and are often associated with chlorite. They constitute about 2-15 % by volume of the rock. Plagioclase has largely been deformed and altered to sericite (ROQ-95-19).

Amygdaloidal texture was seen in a few slides (example, ROQ-95-2). In some cases the vesicles have been occupied by quartz (centre), rimmed by minute grains of chlorite,

38

muscovite and clinopyroxene. In other instances (example, ROQ-95-5) the centre is occupied by quartz and pyrite, and rimmed by chlorite.

The basaltic komatiites host secondary veins consisting of plagioclase, quartz, chlorite, ± calcite; ± opaque minerals (Plate 9).
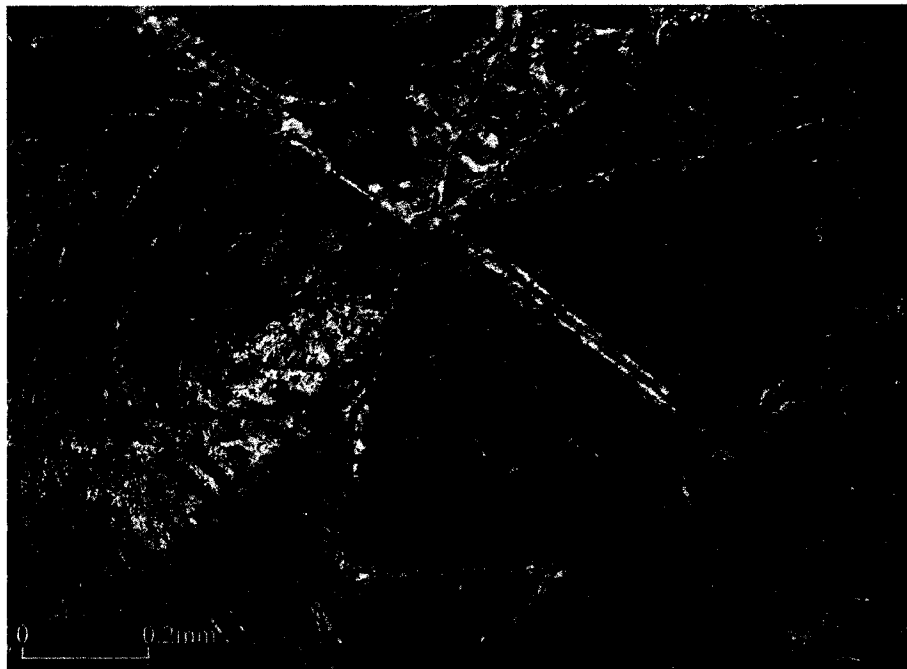
Plate 8: Clinopyroxene plate spinifex texture. The elongated strands of clinopyroxenes in the plates signify that the slide represents the basal end of the unit. *Sample: ROQ-95-18, x10xpl.*

39
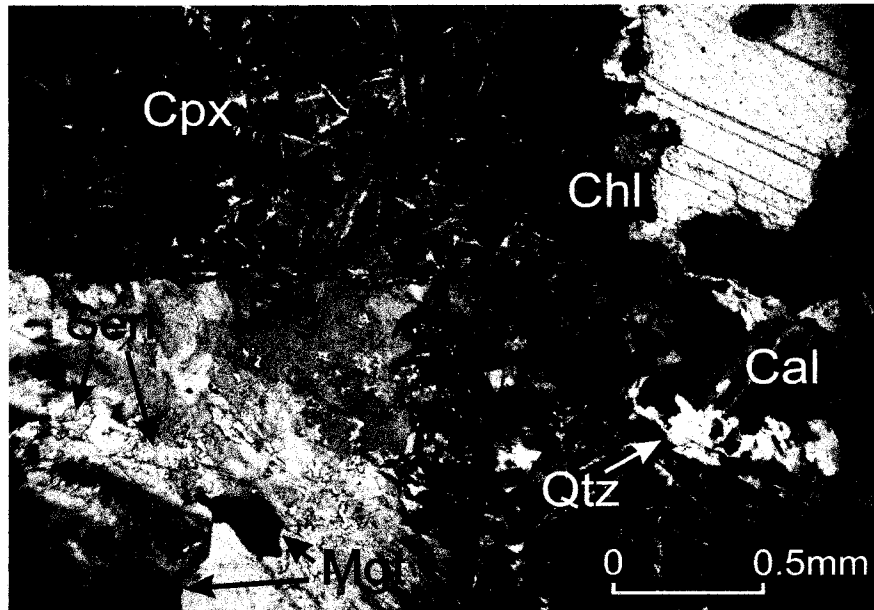
Plate 9: Bifurcating veinlets in clinopyroxene spinifex polygonal plates of basaltic komatiite. Note the alteration of plagioclase (Plg) to sericite (Seri). Chlorite (Chl) occurs at the margins of the veins. Cal = calcite and Qtz = quartz. *Slide: ROQ-95-19, x5xpl.*

3.1.4 Basalts

The basalts are porphyritic. Embedded in the dark, fine-grained matrix are (among others) microphenocrysts of plagioclase and pyroxene. Some of the plagioclase has been partially altered to sericite. Sheaves and spherulites of prehnite (spherulitic texture) are associated with quartz and chlorite (Plate 10).

40
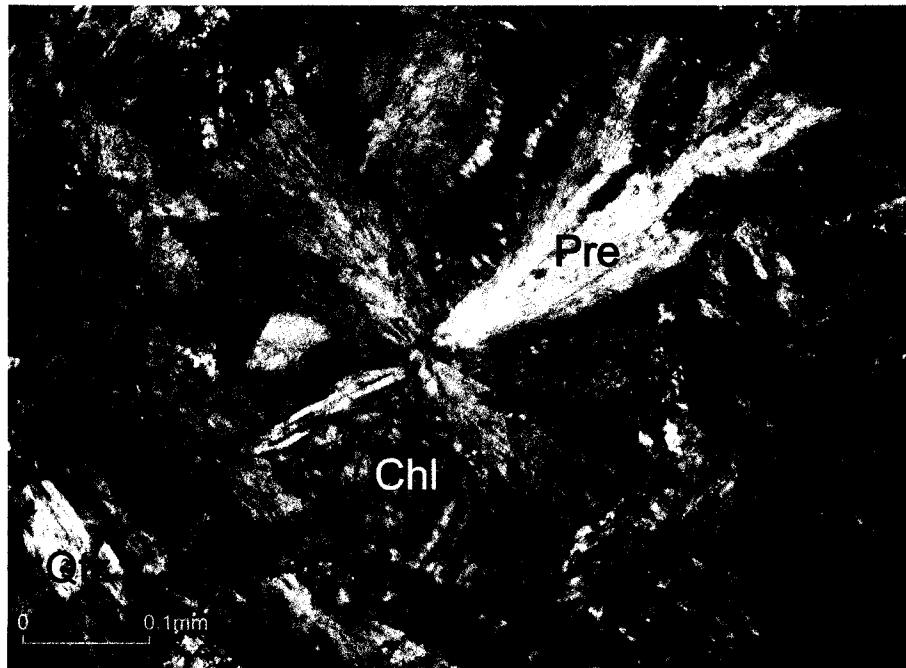
Plate 10: Sheaves and spherulites of prehnite (Pre) in basalt. *Slide: WP-00-13b, x20xpl.*

3.2   Alteration and Metamorphism

Most of the primary minerals in the four groups of rocks have been transformed to secondary minerals via alteration and metamorphism. The vitric groundmass is mostly altered to chlorite, albite, epidote, and Fe-Ti oxides, but quench textures are readily observed (Dostal and Mueller, 1997). The olivine microphenocrysts have been replaced by serpentine, chlorite, magnetite and pyrite. Some of the pyroxenes have been replaced by serpentine, actinolite and chlorite; the plagioclase has transformed to sericite, and in the basalts, to prehnite. These minerals are important metamorphic index minerals, and show that the rocks have been metamorphosed to the sub-greenschist facies.

CHAPTER 4

MINERAL CHEMISTRY

4.1 Introduction

In this chapter, geochemical data obtained on komatiitic rocks from the SRG is discussed. The mineral chemistry of the unaltered clinopyroxenes preserved in the rocks will be utilized to find out the origin of the SRG. Both major and trace elements will be used to determine the original tectonic setting. A first approach will focus on the discrimination diagrams of Nisbet and Pearce (1977), Leterrier et al. (1982) and Beccaluva et al. (1989). The use of such discrimination diagrams may also serve to test their applicability or suitability to rocks of the SRG. The second approach will rely mainly on the systematics shown by the trace elements and rare earth elements (REE).

4.2 Analytical Techniques

Initially, a total of forty thin sections were studied and from these, five thin sections (representative of one ultramafic komatiite, two komatiites, and two basaltic komatiites) were selected on the basis of clinopyroxene freshness and homogeneity. The corresponding hand specimens of the selected slides were located and polished thin sections prepared with a thickness of 0.1 mm. With the aid of a polarizing microscope at Saint Mary's University, at least three clinopyroxene grains were delineated in each slide except for the single ultramafic komatiite slide in which only two grains could be identified.

42

4.2.1 Electron Microprobe Analysis

Electron microprobe analysis is a technique for chemically analyzing small selected areas of solid samples (Reed, 1996). It is principally used for determining the concentrations of the major elements of minerals (Rollinson, 1996). The technique involves exciting the sample with a beam of electrons. The electrons produce secondary X-rays with wavelengths that are characteristic of the elements present in the sample; hence, a qualitative analysis is easy to obtain by identifying the intensities from their wavelengths. By comparing the intensities of these wavelengths with those emitted from standards (pure elements or compounds of known composition), it is also possible to determine the concentrations of the elements (quantitative analysis). Accuracy approaching $\pm$ 1 % (relative) is obtainable and detection limits are typically in the region of 50ppm, though lower values can sometimes be achieved (Reed, 1996).

During fall season of 2005, the clinopyroxene cores were analyzed for major elements using a JEOL JXA-8200 electron microprobe at the Department of Earth Sciences, Dalhousie University, under the expert supervision of Patricia Stoffyn-Egli. The electron beam conditions were 15 kV acceleration voltage, 20 nA current, and minimum beam diameter (~ 1 μm). Sanidine was used as a standard for Si, Al and K; kaersutite for Ti, Ca and Mg; garnet for Fe; pyrolusite for Mn; jadeite for Na; pure nickel metal for Ni; pure chromite metal for Cr; and fluorapatite for P. The count time for each element was 20 seconds on the peak, and 10 seconds for each of the background measurements (one on each side of the peak). Kaersutite was also used as a control to monitor instrument performance. A total of 58 analyses were obtained.

43

4.2.2 Laser ablation (ICP-MS)

Laser ablation (LA) inductively coupled plasma mass spectrometry (ICP-MS) is a versatile technique for solid micro sampling analysis. It provides rapid analysis of small areas on a sample and no lengthy preparations are required. The technique combines the advantage of the in situ micro solid sampling by LA and the high sensitivity multi-element capability by ICP-MS. In analytical atomic spectrometry, free atoms or ions are required for the interaction with light energy. The sampling-generation of such free atoms can be achieved by combination with ICP-MS. The micro amount of the laser-ablated material is transported by a carrier gas to the second excitation process (ICP-MS) in which the ablated materials are evaporated, atomized, and excited. Trace elements and rare earth elements in rock forming minerals, such as pyroxene, olivine and plagioclase can be easily determined.

In early spring of 2006, polished sections of thickness 0.1 mm were sent to the Metals laboratory at the University of Windsor, Windsor, Ontario. The clinopyroxenes were analyzed for trace elements by the expertise of Brian Fryer, using a Thermo Elemental® X7 ICP-MS, coupled with a non-homogenized, high power Continuum solid state ND:YAG laser (wavelength: 266 nm; maximum power: 40 MJ; pulse rate: 20 Hz; primary beam width: 6 mm). To improve ablation characteristics and prevent burning through the thin sections, the laser power was reduced to approximately 2 MJ and the beam diameter to 2 mm, which, when focused onto the sample through a 10x lens, resulted in an ablation spot size of ~ 40 μm. Data acquisition was performed by traversing the laser beam across each grain at a rate of 5 μm/sec. A glass reference

standard (NIST 610) was analyzed before and after every 16 samples (n = 2 replicates before and after), which allowed for subsequent quantification and correction of instrumental drift. This same standard also was used to determine precision ($C_V < 10 \%$ in all cases) in estimating elemental concentrations. The Argon carrier gas (i.e., background) was analyzed for 60 seconds before every sample, allowing limits of detection to be calculated for individual samples. The conversion of the ICP-MS output data (counts/sec) to concentration units ($\mu g/g$) was accomplished using a combination of the X-7 software (Plasma Lab®) to establish integration regions and Microsoft Excel® sheet software for data reduction. Calcium concentrations of the standard and samples were used as an internal standard to correct for ablation yield differences.

4.3   Results

Calculation of pyroxene structural formulae was on the basis of four cations and six oxygens; Fe^{3+} and Fe^{2+} distribution calculated to provide stoichiometric proportions. The calculated cation values range from 3.999 to 4.018, very close to the predicted value. Slightly higher totals for the calculated cations could be as a result of the presence of a small Fe^{3+} occurring in the pyroxene structure as a minor component (Chai and Naldrett, 1994). Table 1 is a report on the clinopyroxene analysis along with calculated structural formulae. Clinopyroxenes of the SRG are (distinctively) Mg-rich augites that merge into the diopside field on a pyroxene quadrilateral (Fig. 11). End-member percentage variations for the three types of rocks are summarized in Table 2. The Ca content is relatively high and varied as seen from the clinopyroxene compositional spread in the

45

quadrilateral plot (Fig. 11); showing that the wollastonite content ($CaSiO_3$) ranges from 34.36 – 45.57 %. The mole fraction of magnesium (X_{Mg}) (= $Mg/[Mg + Fe^{2+}]$) falls within the range of 0.88 – 0.89, 0.76 – 0.87, and 0.81 – 0.86 for the clinopyroxenes, with maximum values decreasing slightly from ultramafic komatiite, komatiites and basaltic komatiites, respectively. In each case the X_{Mg} is > 0.70 and averages beyond 0.80, suggesting that the host rocks are from primary magma. SRG augites have higher wollastonite contents but slightly lower X_{Mg} than those in Barberton komatiites (Fig. 12). From the experimental results of Parman et al. (1997), high wollastonite contents of augite in komatiites indicate crystallization from a water-saturated (hydrous) magma at substantial pressures of ~200 MPa (2 kbars). In addition, crystallization under anhydrous conditions at any pressure cannot produce the high wollastonite contents of the augites.

The SRG augites have lower to moderate concentrations of Al, Ti, Na and other non-quadrilateral components. The number of atoms of Al per formula unit (based on six oxygens) ranges from 0.075 – 0.146, with an average of 0.113 atoms in the clinopyroxenes of ultramafic komatiites. These values are closer to those in komatiite clinopyroxenes (0.069 – 0.138 atoms, average of 0.109 atoms) but slightly lower (only on average) as compared to basaltic komatiite clinopyroxenes (0.058 – 0.202 atoms, average of 0.138 atoms). The average number of atoms of Cr in the ultramafic komatiite clinopyroxenes (0.019 atoms) could also be compared to that in komatiite clinopyroxenes (0.020 atoms). On average, clinopyroxenes in the basaltic komatiites account for the lowest number of atoms of Cr (0.009 atoms). The number of atoms of Ti varies from 0.01 - 0.018 (average of 0.013 atoms) in the clinopyroxenes of ultramafic komatiites; 0.004 –

46

0.016 (average of 0.008 atoms) in the komatiites, and 0.006 – 0.022 (average of 0.014 atoms) in the basaltic komatiite clinopyroxenes. The average number of atoms of Na in all clinopyroxenes of the three rock groups is rather very close— 0.013 atoms in ultramafic komatiites, 0.012 atoms in komatiites, and 0.014 atoms in basaltic komatiites. The same is true for the average concentration of Mn— 0.005 atoms in ultramafic komatiites, 0.007 atoms in komatiites, and 0.006 atoms in clinopyroxenes of basaltic komatiites. The rather uniform number of atoms of non-quadrilateral components could indicate the differentiation of the three groups of rocks from the same parent magma.

Various trends were obtained when Si^{4+} was plotted against certain cations. For example, the plot of Si^{4+} - Al^{3+} gave a negative trend in which number of atoms of Si^{4+} increased relative to Al^{3+} (Fig. 13). Such a pattern might be due to substitution phenomenon during crystallization, wherein, as Si^{4+} decreased in the tetrahedral (T-) site of the pyroxene structure, there was a subsequent increase in the same site by Al^{3+}. A similar negative linear relationship is obtained for the Si^{4+} - Ti^{4+} plot. So, Al^{3+} and Ti^{4+} appear to behave alike with respect to Si^{4+}. The discrepancy of tetrahedral Si^{4+} is compensated by Al^{3+}, but Al^{3+} occupies both tetrahedral and octahedral sites. A negative trend between Ti^{4+} and Si^{4+} may suggest either that Ti^{4+} is more competitive in occupying the octahedral site than Al^{3+} or that replacement of Al^{3+} for Si^{4+} demands an efficient charge balance in the octahedral site of the pyroxene structure (Chai and Naldrett, 1994).

A number of elemental couples illustrate a positive correlation with respect to charge-balance maintenance in the pyroxene structure (Table 3). The most common

47

substitutional pair in all three groups of rocks is $Al^{IV} - Al^{VI}$. Other important substitutional pairs include: $Al^{IV} - Ti$, $Na - Ti$, $Fe^{2+}- Ti$, and $Fe^{2+}- Mn$. $Cr - Na$ and $Cr - Ti$ substitution is important only in ultramafic komatiite clinopyroxenes. Thus, the most significant non-quadrilateral substitutional molecules in all the three groups of pyroxenes are: $CaTiAl_2O_6$, $NaTiSiAlO_6$ and $CaNaMnAlSiO_6$. The first two-named substitutional molecules are in agreement with Beccaluva et al. (1989).

Legend:
● Ultramafic komatiite *(sample WP-00-8)*
◆ Komatiite *(sample ROQ-95-21A)*
◇ Komatiite *(sample ROQ-95-21B)*
■ Basaltic komatiite *(sample ROQ-95-2)*
□ Basaltic komatiite *(sample ROQ-95-12A)*

$CaSiO_3$

$CaMgSiO_3$

$CaFeSiO_3$

40

30

Augite

$MgSiO_3$

$FeSiO_3$
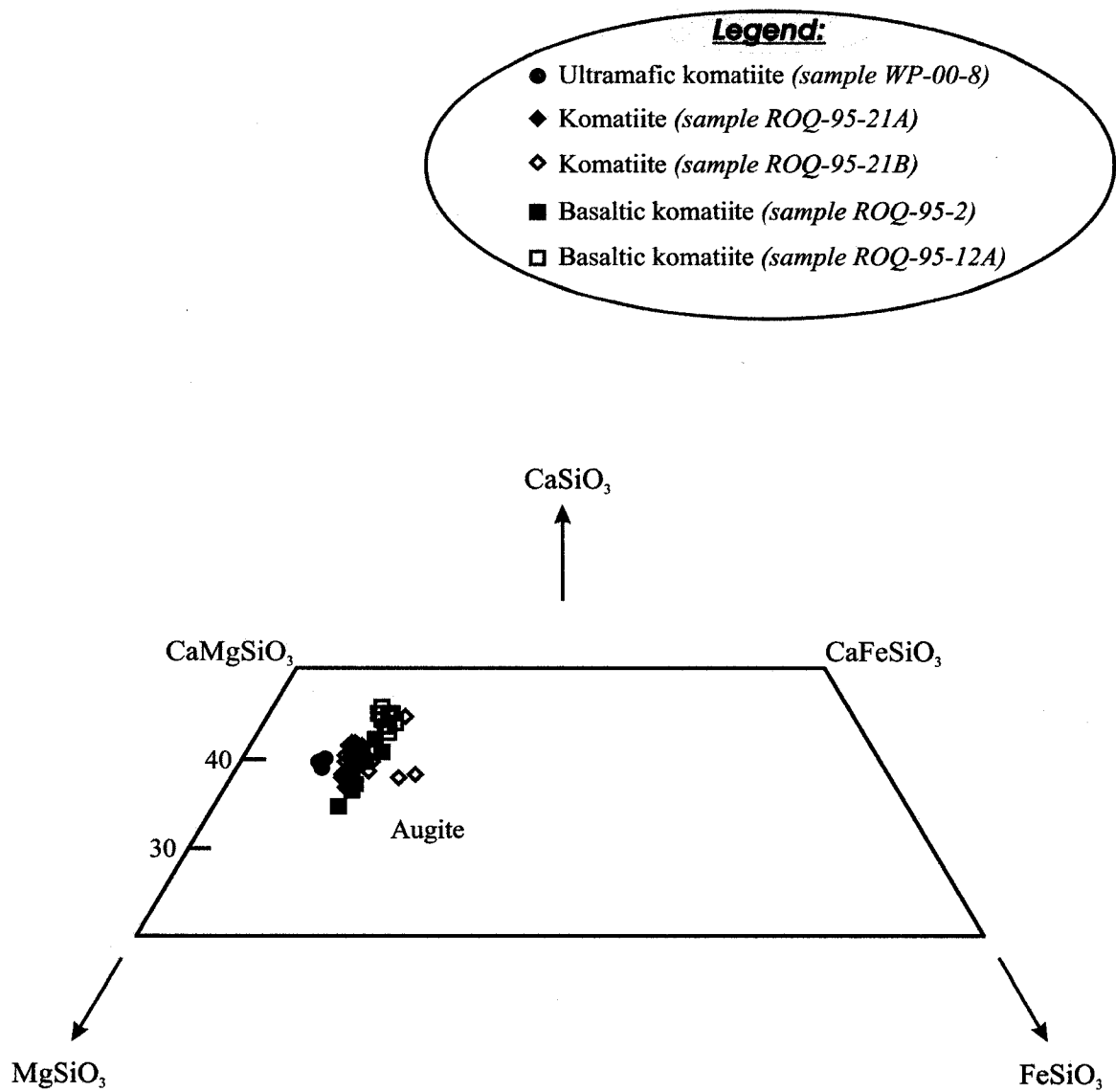
Fig. 11: Clinopyroxene compositions from SRG komatiites and related rocks, plotted on the pyroxene quadrilateral. The clinopyroxenes are Mg-rich augites.

49
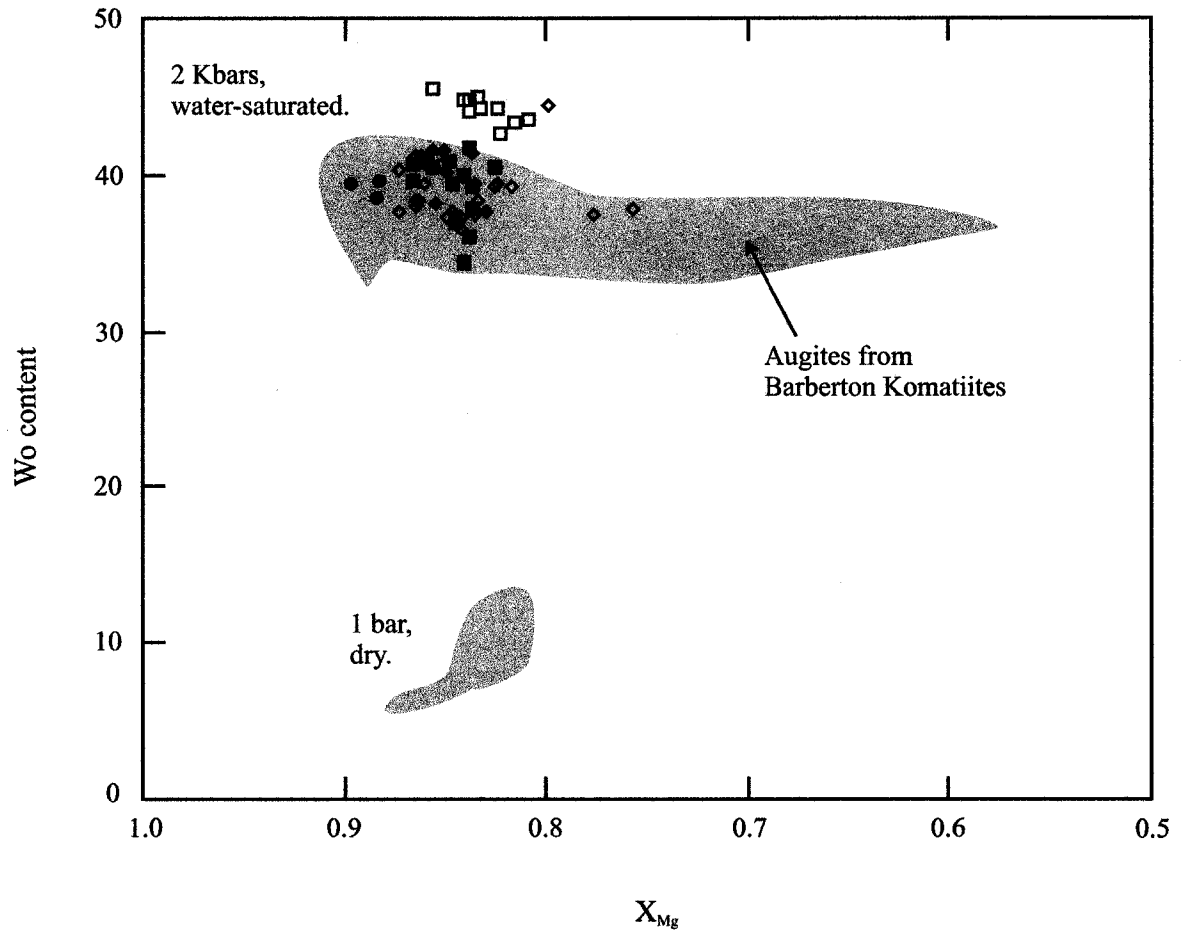
Fig. 12: Wollastonite content (molecular %) versus mole fraction of magnesium (X_{Mg}) (=Mg/[Mg + Fe $^{2+}$]) for clinopyroxenes in SRG komatiitic rocks. The large grey shaded field represents the compositions of augites in Barberton komatiites at high pressure (2 Kilobars). The smaller grey field represents experimentally produced augites at low pressure (1 bar). Refer to Fig. 11 for symbols. *Modified after Parman et al. (1997)*
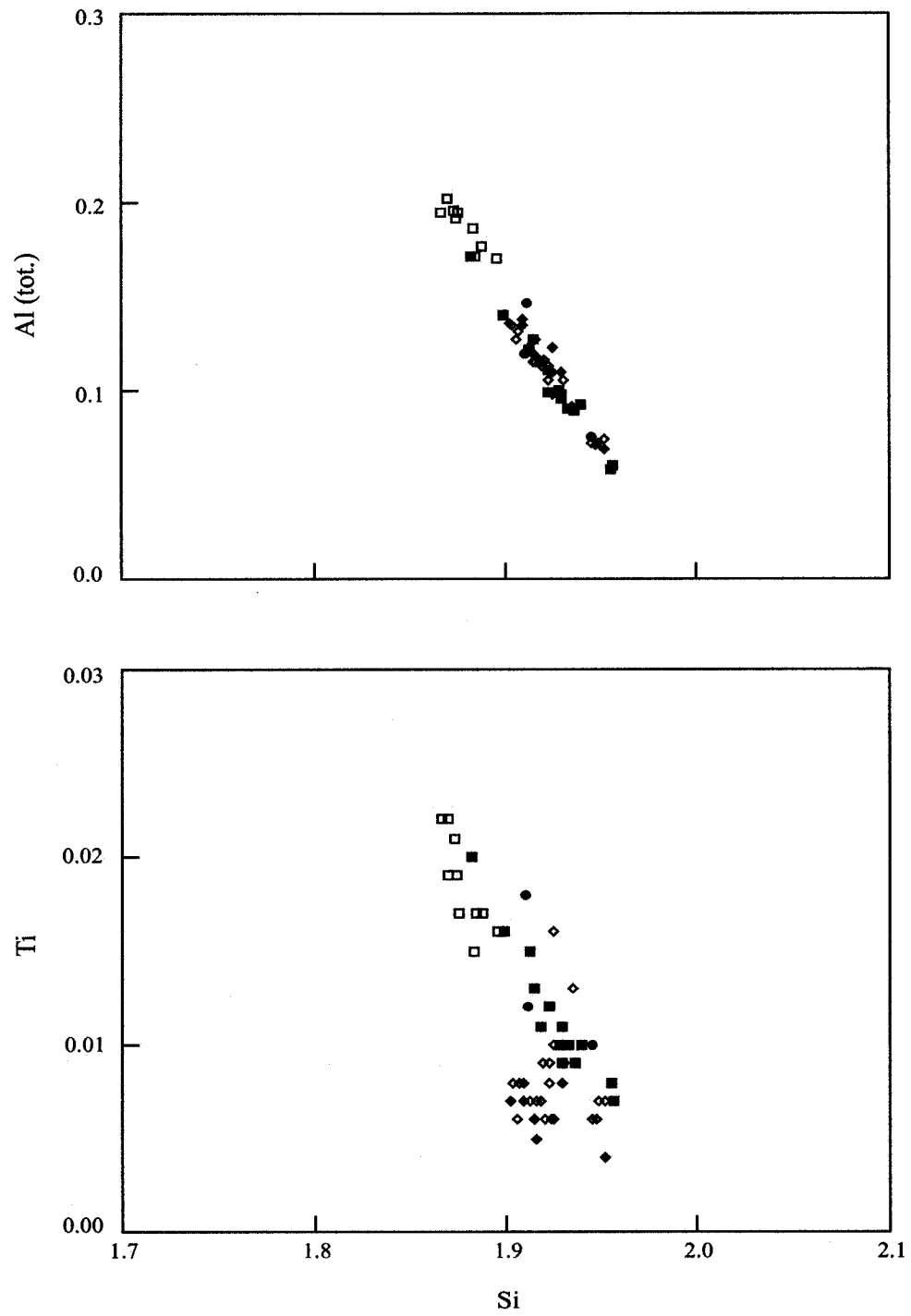
Fig. 13: Plots showing the negative correlation of Al and Ti against Si (atomic proportions) in clinopyroxene.

51

4.4 Clinopyroxene and Original Tectonic Settings

Nisbet and Pearce (1977) reviewed work relating the chemical composition of igneous clinopyroxenes to the nature of their host rocks. The geochemical characteristics of preserved primary clinopyroxenes may be used to identify original magmatic affinities because the composition of these minerals is related to the chemistry of the host lava (Nisbet and Pearce, 1977). A similar approach has been taken by some workers, such as, Leterrier et al. (1982), Beccaluva et al. (1989), Parman et al. (1997), Yaliniz and Goncuoglu (1999), and Shimizu et al. (2005). Consequently, these data help constrain the original tectonic setting(s) of komatiitic rocks.

4.4.1 The Tectonic Discrimination Diagrams of Nisbet and Pearce (1977)

Nisbet and Pearce (1977) investigated the relationship between the composition of calcic clinopyroxenes from basalts of different magma types and tectonic settings. They distinguished between the following magma types:

> Ocean Floor Basalts (OFB) — *These basalts are plume related.*

> Volcanic Arc Basalts (VAB) — *Subduction related.* These basalts are erupted above subduction zones in island arcs or at active continental margins.

> Within Plate Tholeiitic Basalts (WPT) — *plume related.* As the name implies, these basalts are erupted within plates in oceanic islands or continental rifts.

> Within Plate Alkali Basalts (WPA) — *plume related.*

52

WPA magmas are characterized by high concentrations of TiO_2, Al_2O_3 and Na_2O. High-Ti clinopyroxenes typically crystallize from silica-undersaturated magmas. The abundance of Ti and Al in clinopyroxenes reflects that in the magmas from which they crystallized and the proportion of these elements increases from subalkaline through tholeiitic, alkaline to peralkaline magmas. The clinopyroxenes of WPT have higher Ti, Al, Fe and Mn than those in VAB (Nisbet and Pearce, 1977).

The tectonic discrimination diagrams of Nisbet and Pearce (1977) are based on various combinations of: SiO_2, TiO_2, Al_2O_3, FeO (total iron), MnO, MgO, CaO and Na_2O.

4.4.1.1   Observation and Interpretation

The $TiO_2 - MnO - Na_2O$ discrimination diagram (Fig. 14) does not seem to be useful in this study because a greater proportion of the points plot in the 'all' field — D.

Figure 15 shows the relationship between the aluminum content of the SRG clinopyroxenes and the extent of silica saturation of the magma from which the crystals were formed. It can be observed that the clinopyroxenes originated from subalkaline (non-alkaline) magmas. This distinguishes WPA from being the possible magma type for rocks of the SRG. There is an overlap between three magma types (VAB, OFB and WPT) which cannot be conveniently distinguished on the basis of the SiO_2-Al_2O_3 diagram. Nonetheless, perhaps WPT could be eliminated because it has lower SiO_2 and higher Al_2O_3 than VAB. It is, however, important to note from the diagram that

53

clinopyroxenes from one of the two basaltic komatiite samples (*i.e., sample ROQ-95-12A*) appear to be Al-enriched as they plot near the border between subalkaline and alkaline magmas.

The SiO_2-TiO_2 diagram (Fig. 16) helps to discriminate the possible magma type with which clinopyroxenes of the SRG are associated. It reveals that the clinopyroxenes are low in TiO_2 (< 1 wt %) but have comparatively high SiO_2 (> 49 wt %). Hence, WPA magma which contains high TiO_2 and low SiO_2 concentrations is eliminated as a possibility. According to Nisbet and Pearce (1977), WPT magma contains more TiO_2 than VAB magma and so cannot be safely distinguished by this technique. VAB magmas have high SiO_2 and low TiO_2; these criteria are in perfect agreement with the plot. Nonetheless, some of the points overlap with the field of OFB (characterized by a spread from low to high TiO_2 concentrations with simultaneous decreasing SiO_2 concentrations). A similar overlap is reflected in Fig. 17.

One of the techniques of Nisbet and Pearce (1977) employs a statistical approach involving discriminant functions (F1 and F2) containing eigenvectors (Fig. 18). Clinopyroxenes from rocks of the SRG cluster in the VAB/OFB field. Although the diagram could not discriminate between VAB and OFB, it nonetheless eliminates WPA and WPT.

54

4.4.1.2   Summary

Although the discrimination diagrams of Nisbet and Pearce (1977) are of limited use in distinguishing VAB, OFB and WPT magmas; they do link VAB with subduction zones and OFB with plume settings. Unfortunately, overlapping data between the two magma types on the diagrams creates ambiguity, so no firm conclusion can be drawn from Nisbet and Pearce's (1977) plots. Either the diagrams do not effectively discriminate between the two magma types, or both tectonic processes were in fact responsible for emplacement of the SRG rocks. Hence, other tectonic discrimination techniques should be employed.
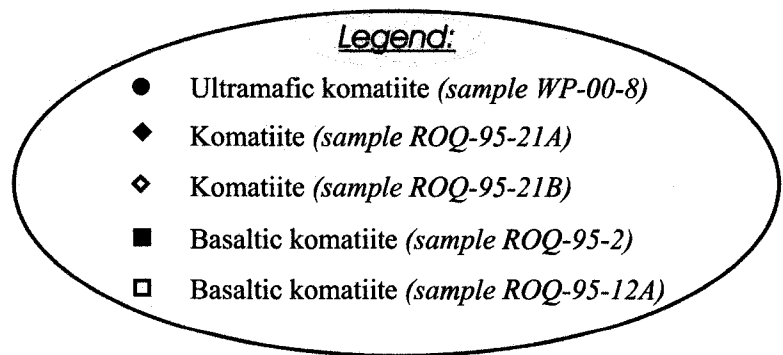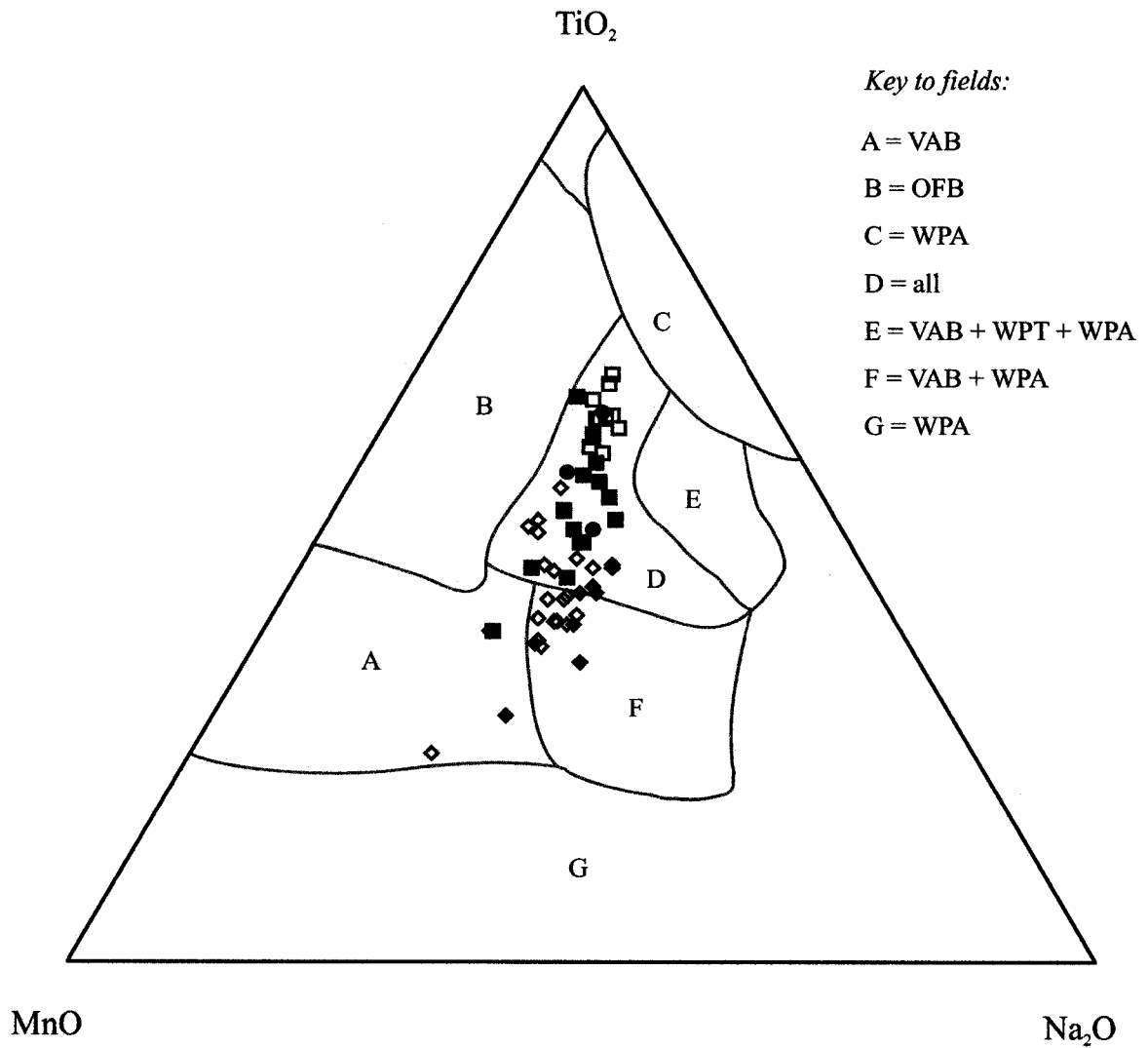
Fig. 14: TiO_2 – MnO – Na_2O (wt %) discrimination diagram using clinopyroxenes of the SRG.

Abbreviations: VAB = volcanic arc basalts; OFB = ocean floor basalts; WPA = within plate alkali

basalts; WPT = within plate tholeiitic basalts. (*Based on Nisbet and Pearce, 1977*)
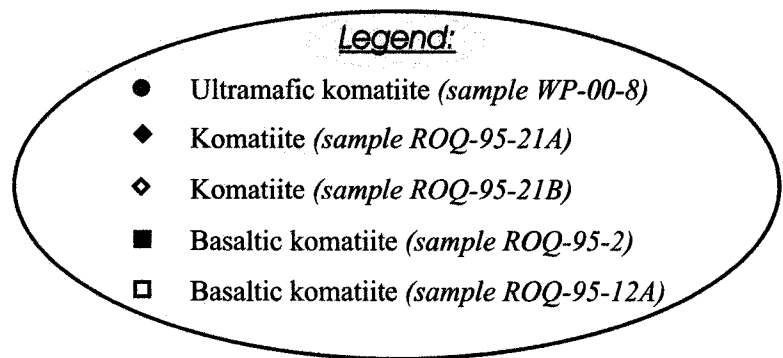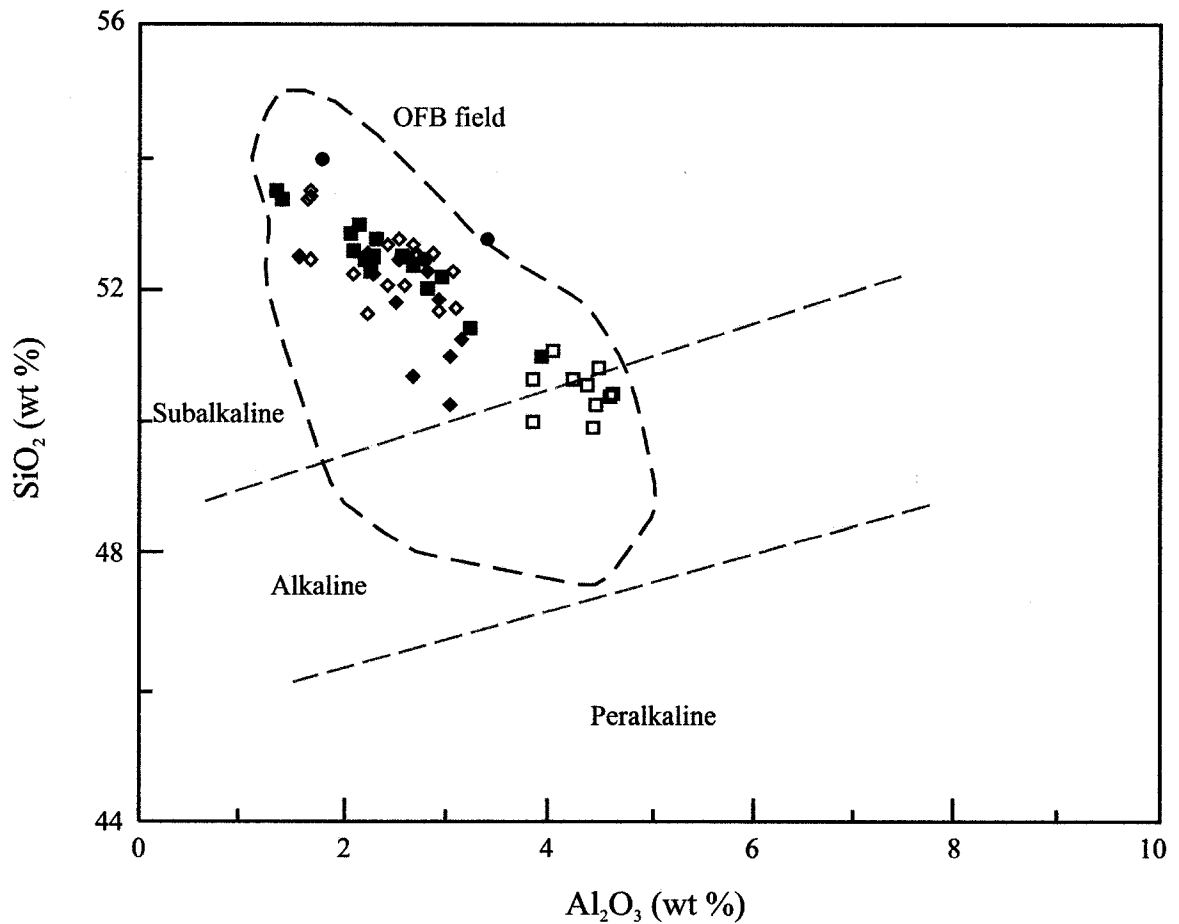
Fig. 15: SiO_2 – Al_2O_3 bivariate plot for discriminating clinopyroxenes from different magma types. Note that most of the clinopyroxenes from the SRG fall into the Subalkaline (non-alkaline) category. *Diagram is modified from Nisbet and Pearce (1977)*.

57
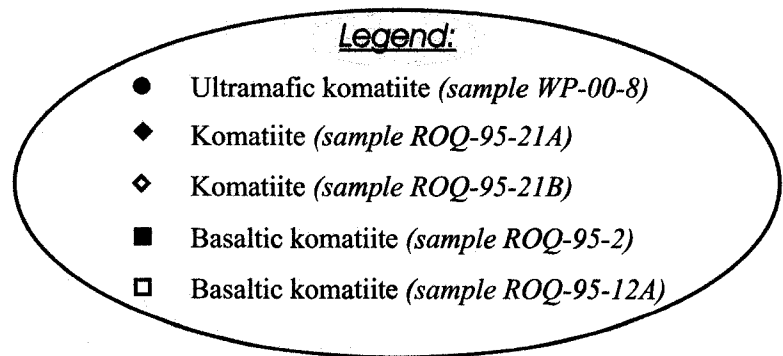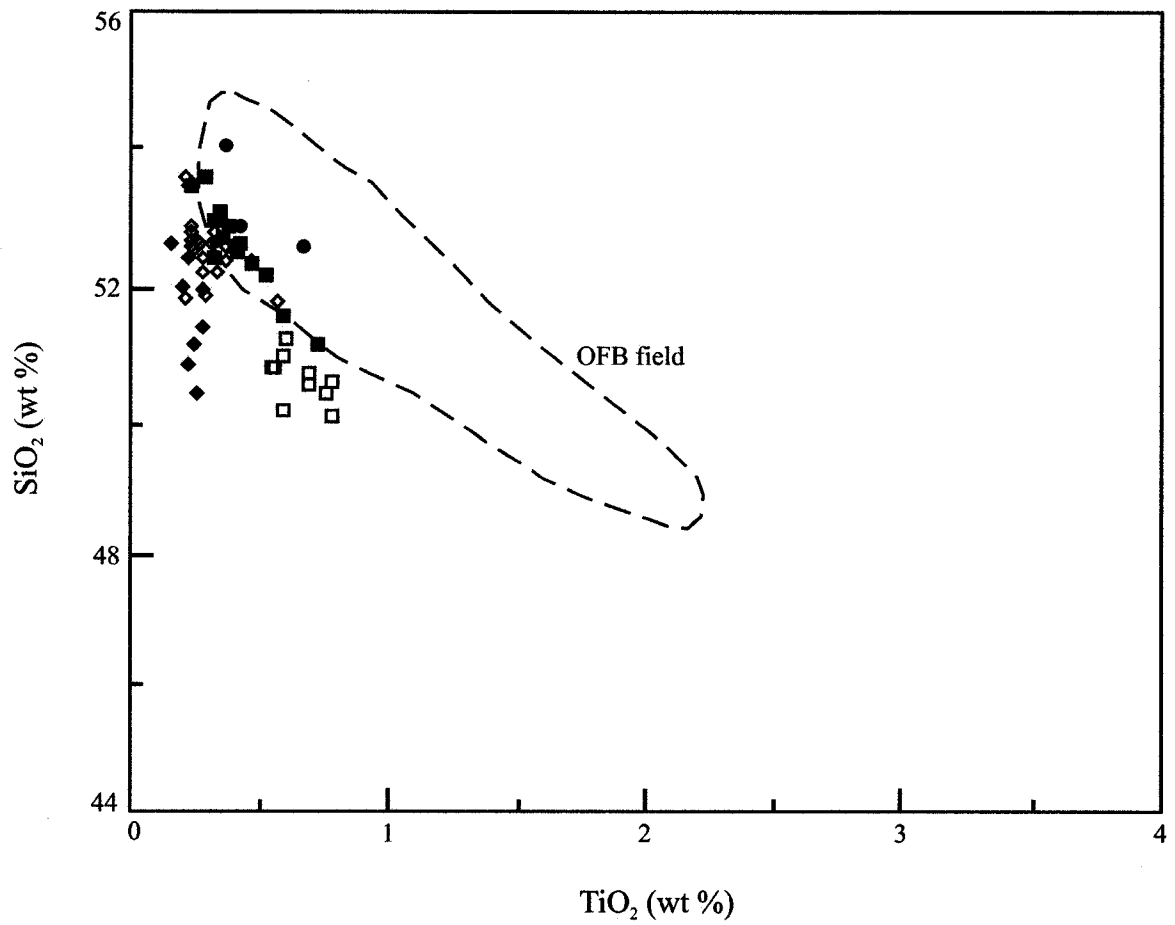
Fig. 16: SiO_2 – TiO_2 bivariate plot for discriminating clinopyroxenes of the SRG. *Diagram is modified from Nisbet and Pearce (1977).*

58
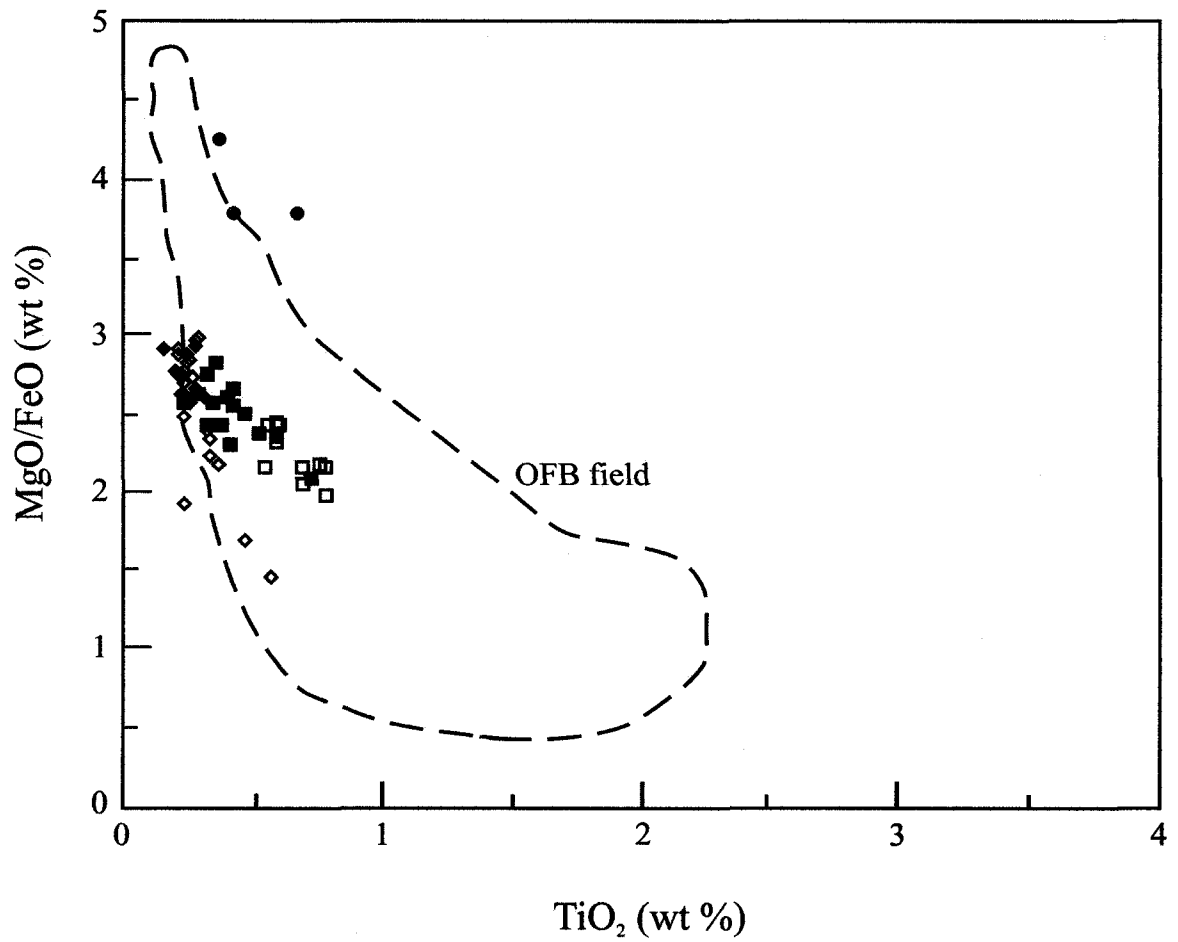
Fig. 17: MgO/FeO – TiO$_2$ discrimination technique employing clinopyroxenes of the SRG. Refer to Fig. 16 for symbols. *This diagram is modified from Nisbet and Pearce (1977).*

59

Fig. 18: F1 – F2 (discriminant functions) plot for clinopyroxenes of the SRG. Refer to Fig. 16 for

symbols. *Abbreviations:* VAB = volcanic arc basalts; OFB = ocean floor basalts; WPT = within

plate tholeiitic basalts; WPA = within plate alkali basalts. (*Based on Nisbet and Pearce, 1977*)
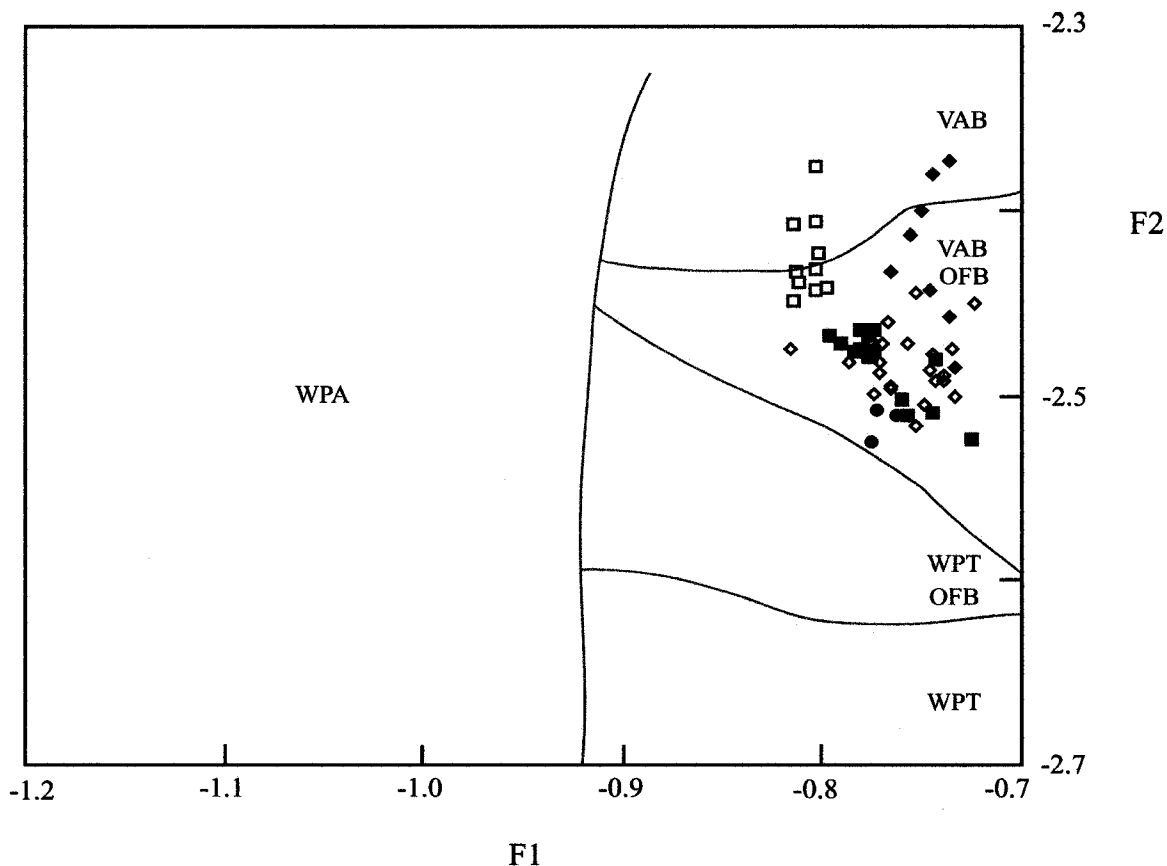
F1= -0.012*SiO_2-0.0807*TiO_2+0.0026*Al_2O_3-0.0012*FeO-0.0026*MnO+0.0087*MgO-0.0128*CaO-0.0419*Na_2O

F2=-0.0469*SiO_2-0.0818*TiO_2-0.0212*Al_2O_3-0.0041*FeO-0.1435*MnO-0.0029*MgO+0.0085*CaO+0.0160*Na_2O

60

4.4.2 The Tectonic Discrimination Diagrams of Leterrier et al. (1982)

By using calcic clinopyroxene phenocrysts from recent basaltic rocks of various magma types, Leterrier et al. (1982) presented a number of discrimination diagrams for use in identifying original tectonic settings irrespective of metamorphic or metasomatic alterations. The discrimination diagrams are based on the Ti, Cr, Ca, Al and Na contents, and give a level of confidence of greater than 80%. The approach of Leterrier et al. (1982) was aimed at attempting to clarify the tectonic discrimination diagrams of Nisbet and Pearce (1977).

Leterrier et al. (1982) distinguished between three basaltic magma types, namely:

➢   Alkali basalts

➢   Non-orogenic tholeiites

➢   Orogenic basalts

This distinction was based on the observation that the composition of clinopyroxenes varies according to the chemistry of their host lavas (e.g., Nisbet and Pearce, 1977; Leterrier et al., 1982).

Alkali basalts are generally low in Si, but have higher Ti, total Al, and Na contents compared to other types of basalts. The group of alkali basalts includes rocks from oceanic and continental intra-plate volcanism (which is the same as WPA and WPT, respectively, of Nisbet and Pearce, 1977).

61

Non-orogenic tholeiites are rich in Ti and Cr. They include oceanic island tholeiites, abyssal tholeiites, back-arc basin tholeiites, continental tholeiites and transitional basalts from rift zones. Non-orogenic tholeiites are formed in spreading zones (*plume related*) and are equivalent to the OFB of Nisbet and Pearce (1977).

Orogenic basalts are low in Ti and Cr when compared to basalts from spreading areas (Leterrier et al., 1982). They include island arc tholeiites and calc-alkali basalts from active continental margins, and island arc shoshonitic lavas. These magmas are subduction-related and could be compared to the VAB of Nisbet and Pearce (1977).

Figures 19, 20 and 21 are the results obtained on inputting the SRG clinopyroxene data into the discrimination diagrams of Leterrier et al. (1982).

4.4.2.1   Observation and Interpretation

Figure 19 shows that rocks of the SRG are not related to alkali basalt magmas, thus, supporting the elimination of oceanic and continental intra-plate volcanism (WPA and WPT) from being the possible tectonic settings of these rocks. This diagram indicates that the host magmas of the samples are either non-orogenic tholeiites (OFB) or orogenic basalts (VAB). Figure 20 indicates clinopyroxenes are from the two families. A tholeiitic character for these clinopyroxenes is apparent in Fig. 21 (note that as a result of an error in the initial formula stated in Leterrier et al. (1982), the regression equation has been amended in this work).

62

4.4.2.2   Summary

Non-orogenic tholeiites of the SRG, which are equivalent to the OFB of Nisbet and Pearce (1977), are of plume origin. In addition, the occurrence of orogenic basalts, which are equivalent to the VAB of Nisbet and Pearce (1977), infers a subduction origin. This, therefore, implies that the tectonic discrimination techniques of Leterrier et al. (1982) are consistent with those of Nisbet and Pearce (1977) in the sense, that the two techniques present results that support both plume and subduction origins for the SRG rocks.

63
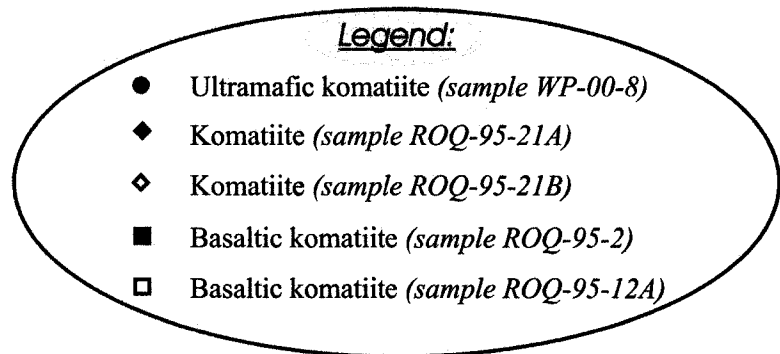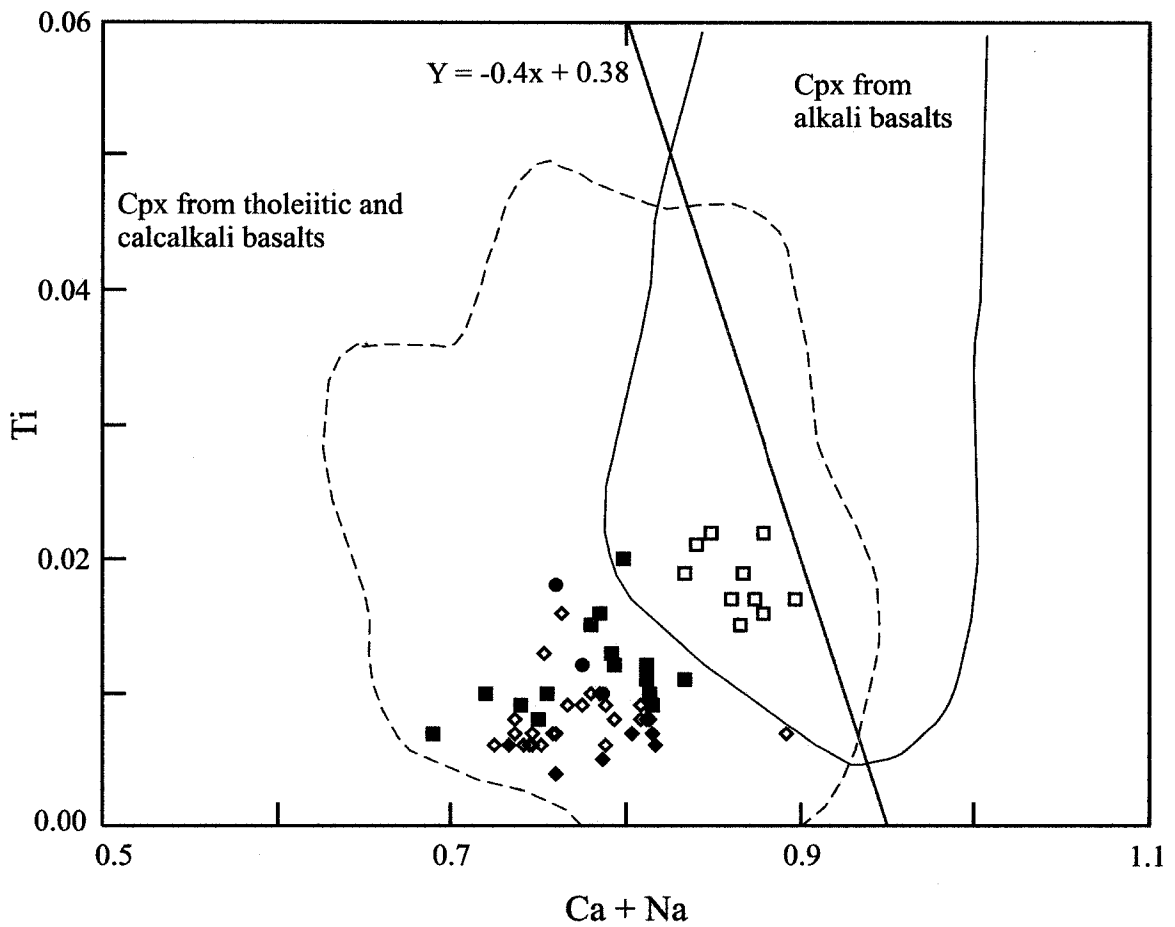
Fig. 19: Ti – Ca + Na (atomic proportions) tectonic discrimination diagram for clinopyroxenes (Cpx) from either alkali basalts or tholeiitic and calcalkali basalts. The line separates the two groups and shows that the last-two-named magma types (non-alkali basalts) are supported for the SRG. *Modified after Leterrier et al. (1982)*

64
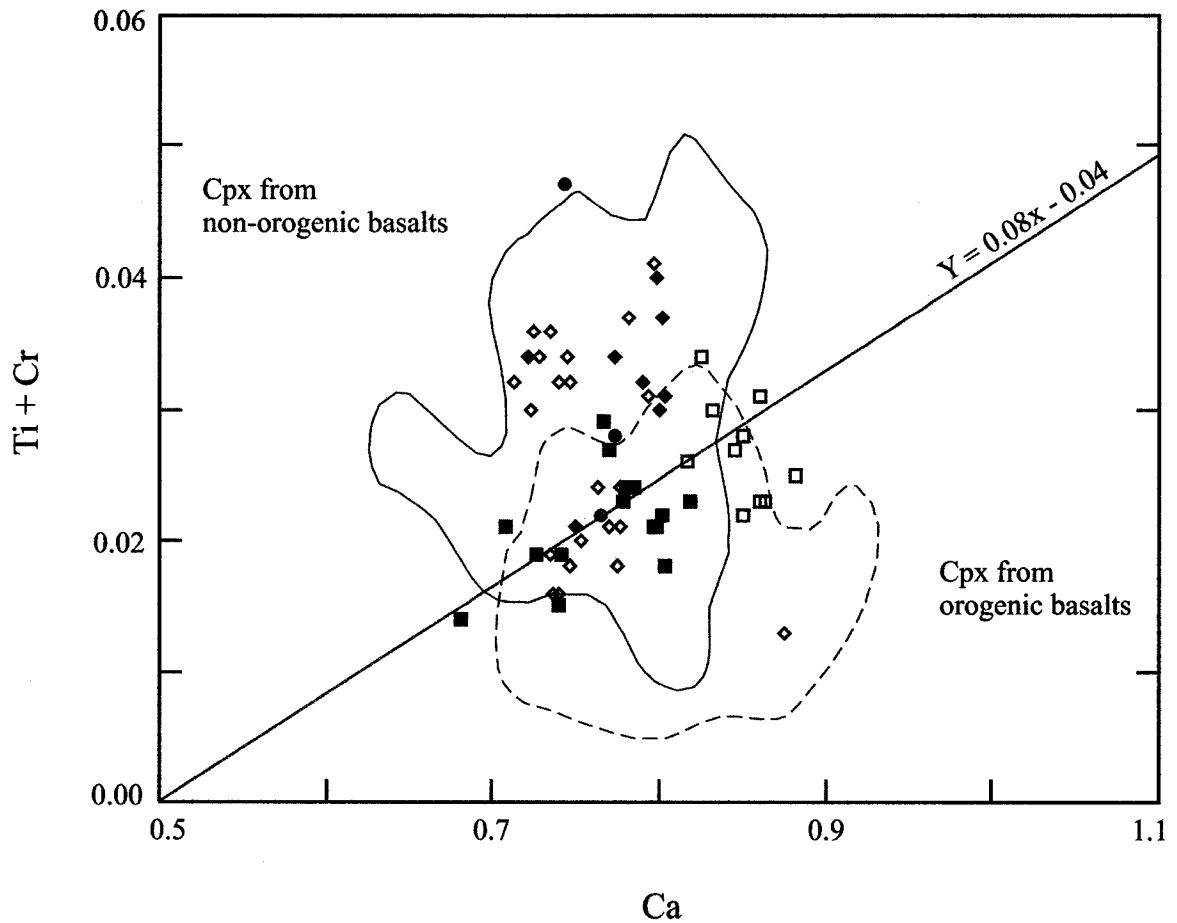
Fig. 20: Ti + Cr – Ca (atomic proportions) tectonic discrimination diagram for non-alkali basalts
between non-orogenic basalts and orogenic basalts. The diagram illustrates that clinopyroxenes of
the SRG are from both non-orogenic and orogenic basalts. *Modified after Leterrier et al. (1982)*
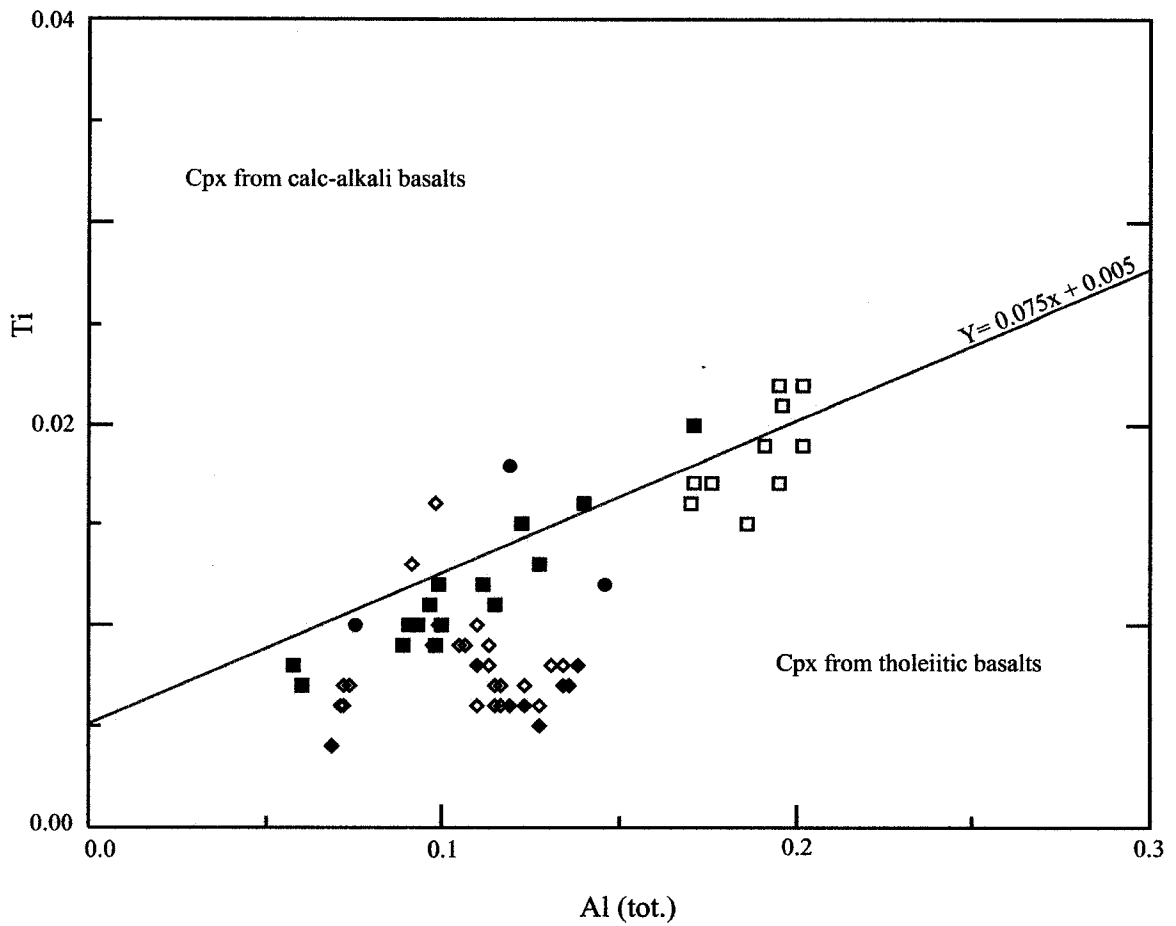
65

Fig. 21: Ti − Al(tot.) (atomic proportions) diagram distinguishing between clinopyroxenes in calc-alkali and tholeiitic basalts. It could be seen that the samples are closely related to the tholeiitic domain. *Modified after Leterrier et al. (1982)*

66

4.4.3 The Tectonic Discrimination Diagrams of Beccaluva et al. (1989)

Beccaluva et al. (1989) assembled over 500 microprobe analyses for igneous calcic-clinopyroxenes in basaltic rocks from various low-Ti to high-Ti ophiolitic complexes. They observed that the composition of clinopyroxenes was related to the host magma type and original tectonic setting. Beccaluva et al. (1989) subdivided ophiolitic basalts into two groups, namely:

➤ Very low-Ti and low-Ti ophiolitic basalts

➤ High-Ti ophiolitic basalts

Very low-Ti and low-Ti ophiolitic basalts have low Al_2O_3, Na_2O and high SiO_2 contents. These basalts are related to island arc tholeiites (IAT) and boninites (BON), respectively, which are generated above subduction zones (Beccaluva et al., 1989). This group of basalts is equivalent to the VAB of Nisbet and Pearce (1977) and the Orogenic basalts of Leterrier et al. (1982).

High-Ti ophiolitic basalts have high Al_2O_3, Na_2O and low SiO_2 contents and are best equated to mid-ocean ridge basalts (MORB) of spreading ridges (Beccaluva et al., 1989). This group is equivalent to the OFB of Nisbet and Pearce (1977) and the Non-orogenic basalts of Leterrier et al. (1982).

The tectonic discrimination diagrams of Beccaluva et al. (1989) are based on various combinations of oxides and cations (Figs. 22 to 27).

4.4.3.1   Observation and Interpretation

A Ca-Mg-Fe diagram was used by Beccaluva et al. (1989) to subdivide ophiolitic basalts into very low-Ti and low-Ti basalts, as well as, high-Ti basalts. Clinopyroxenes from very low-Ti and low-Ti basalts plot around the endiopside-augite boundary, whereas those from high-Ti basalts plot in the augite-to-salite field. Using this diagram, it can be seen from Fig. 22 that the studied clinopyroxenes plot in the endiopside-augite boundary; indicating that they are related to very low-Ti and low-Ti basalts.

The TiO_2-Na_2O-SiO_2 (wt %) diagram in Fig. 23 seems to support both MORB and IAT magma types for rocks of the SRG. With increasing SiO_2 concentrations and decreasing TiO_2 and Na_2O concentrations, clinopyroxenes compare favourably with those of IAT, BON and BA-A (basaltic andesites and andesites). The reverse is the case for clinopyroxenes from MORB and WOPB (within ocean plate basalts). These clinopyroxenes plot within the IAT field. This characteristic pattern is also evident in Figs. 24 and 25. In Figs. 26 and 27, the points plot partly in the fields of IAT, BON and BA-A, all of which are related to subduction origin.

4.4.3.2   Summary

From Fig. 22, positioning of the clinopyroxenes along the endiopside-augite boundary signifies very low- and low-Ti basalts association, which is further revealed in Figs. 25 to 27. Based on the paradigm that the composition of clinopyroxenes reflects the composition of their host magmas (Nisbet and Pearce, 1977; Capedri and Venturelli,

68

1979; Leterrier et al., 1982; Beccaluva et al., 1989; Yaliniz and Goncuoglu, 1999), it could be reasoned (from the results) that rocks of the SRG originated in a subduction zone setting.

The possible affinity with mid-ocean ridge basalts and within ocean plate basalts magmas may be significant (Figs. 23 to 27), even though the points plot in only a narrow zone in some of the diagrams. However, despite the overlaps in the resulting diagrams, the tectonic discrimination techniques of Beccaluva et al. (1989) indicate that rocks of the SRG correspond to island arc tholeiites, boninites, and basaltic andesites and andesites. These three magma types are affiliated with a subduction zone environment.

69
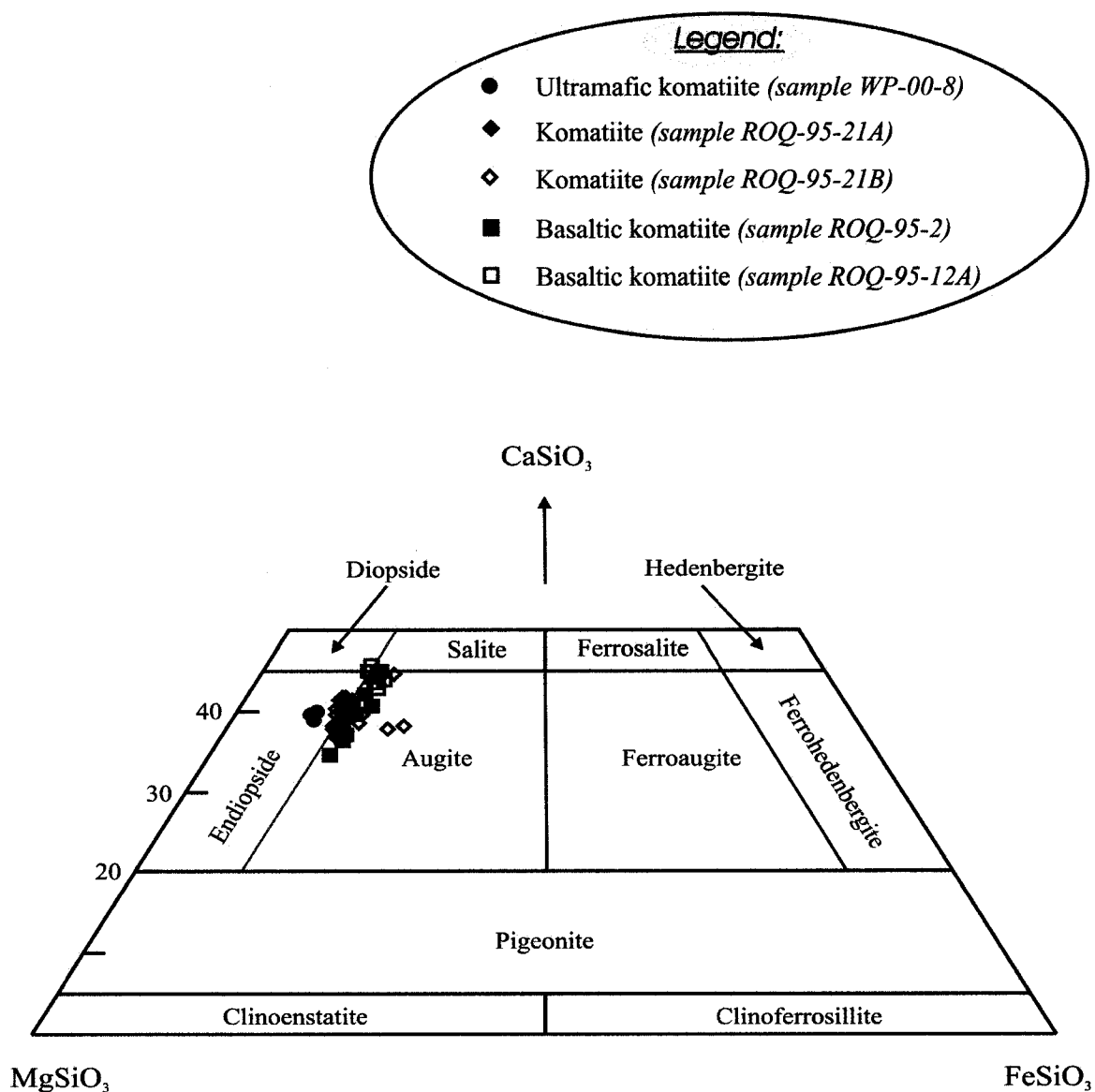
Fig. 22: Classification of clinopyroxenes into (a) very low- and low-Ti, and (b) high-Ti association, based on their positioning in the endiopside-augite and augite-to-salite fields, respectively. Note that the clinopyroxenes plot around the endiopside-augite boundary, indicating their host magma types are very low- and low-Ti basalts. *The diagram is modified after Beccaluva et al. (1989) and Deer et al. (2001)*

70
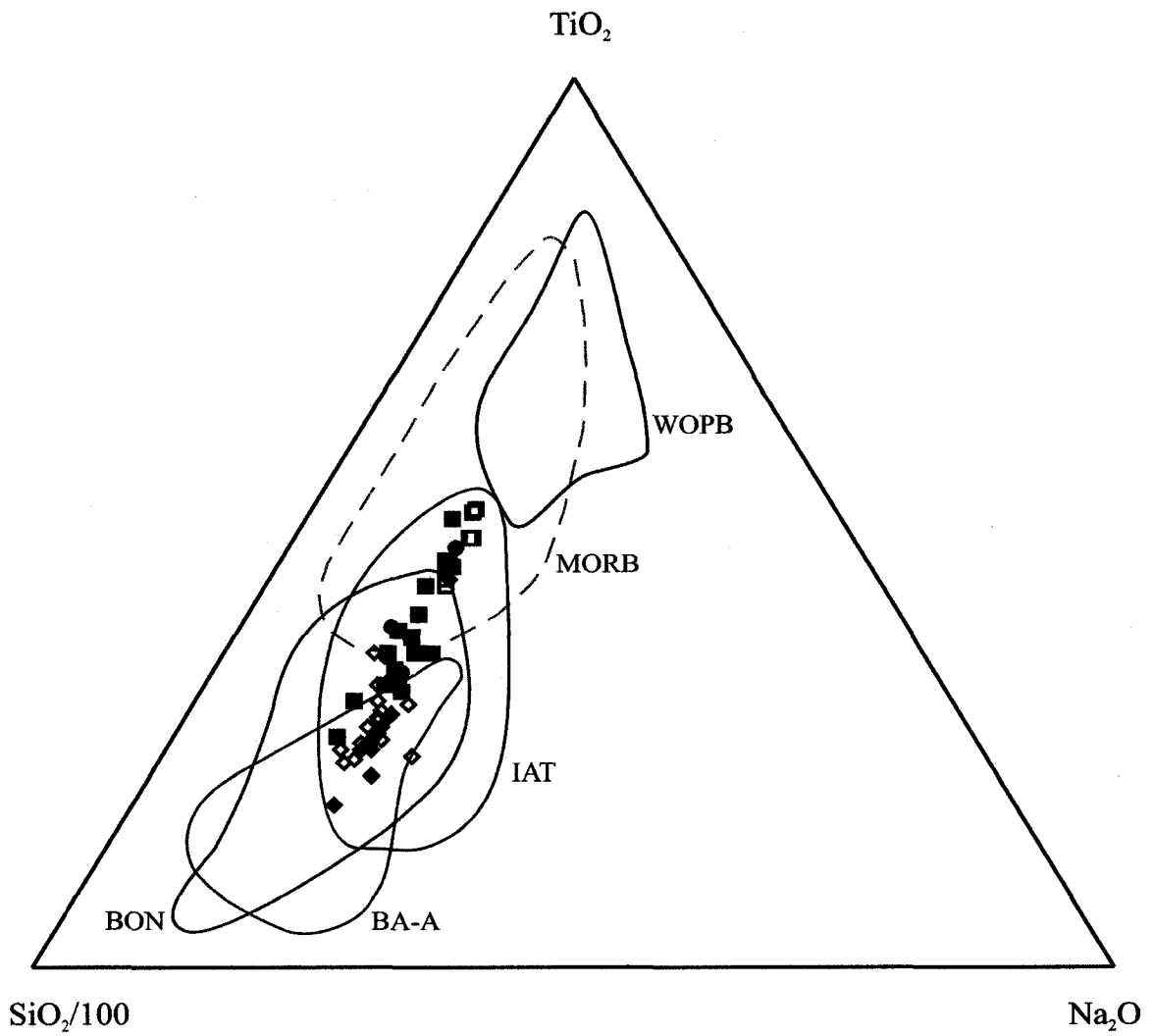
Fig. 23: $TiO_2 - Na_2O - SiO_2$ (wt %) discrimination diagram for clinopyroxenes from basalts of different tectonic settings. *Abbreviations*: WOPB = within ocean plate basalts; MORB = mid-ocean ridge basalts; IAT = island arc tholeiites; BA-A = basaltic andesites and andesites; BON = boninites. Overlaps occur but note the perfection with which clinopyroxenes of the SRG classify as IAT. See Fig. 22 for symbols. *The diagram is modified after Beccaluva et al. (1989).*

71
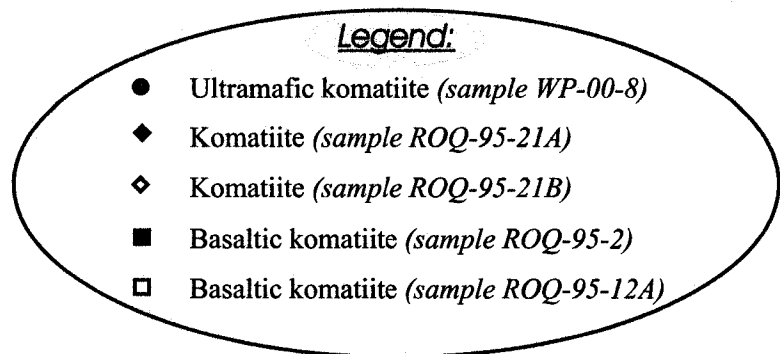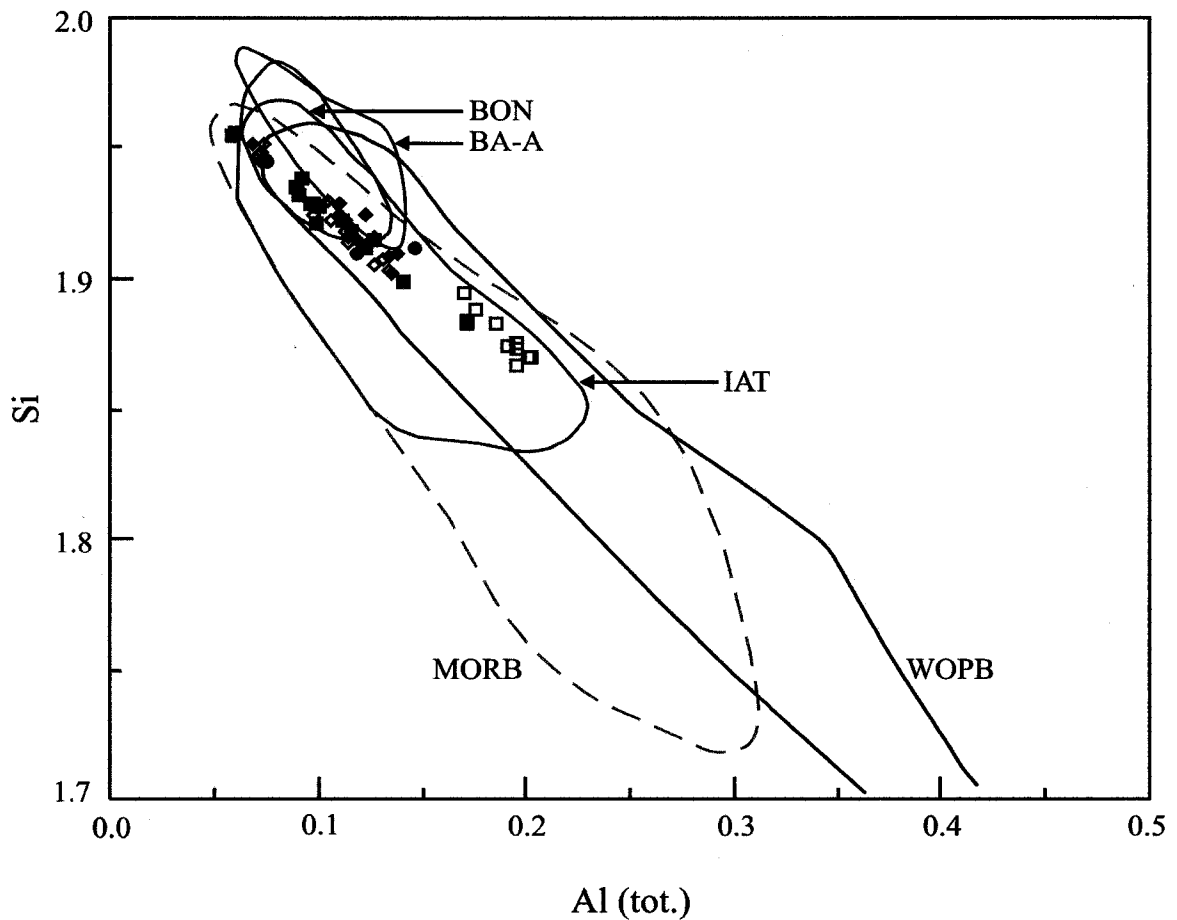
Fig. 24: Si − Al (tot.) (atomic proportions) covariation discrimination technique. There are overlaps but note how the points fit into IAT field. *Abbreviations*: WOPB = within ocean plate basalts; MORB = mid-ocean ridge basalts; IAT = island arc tholeiites; BA-A = basaltic andesites and andesites; BON = boninites. *This diagram is modified after Beccaluva et al. (1989).*
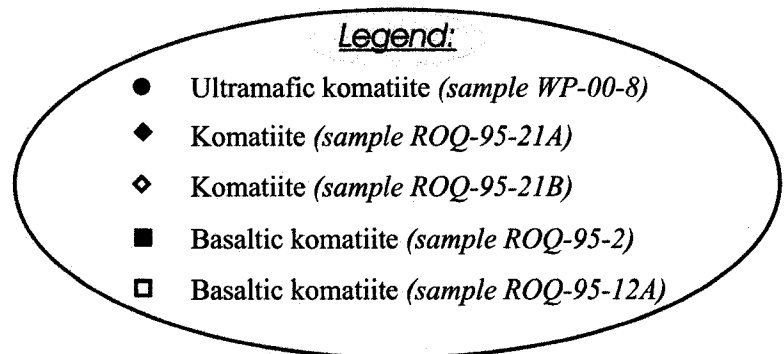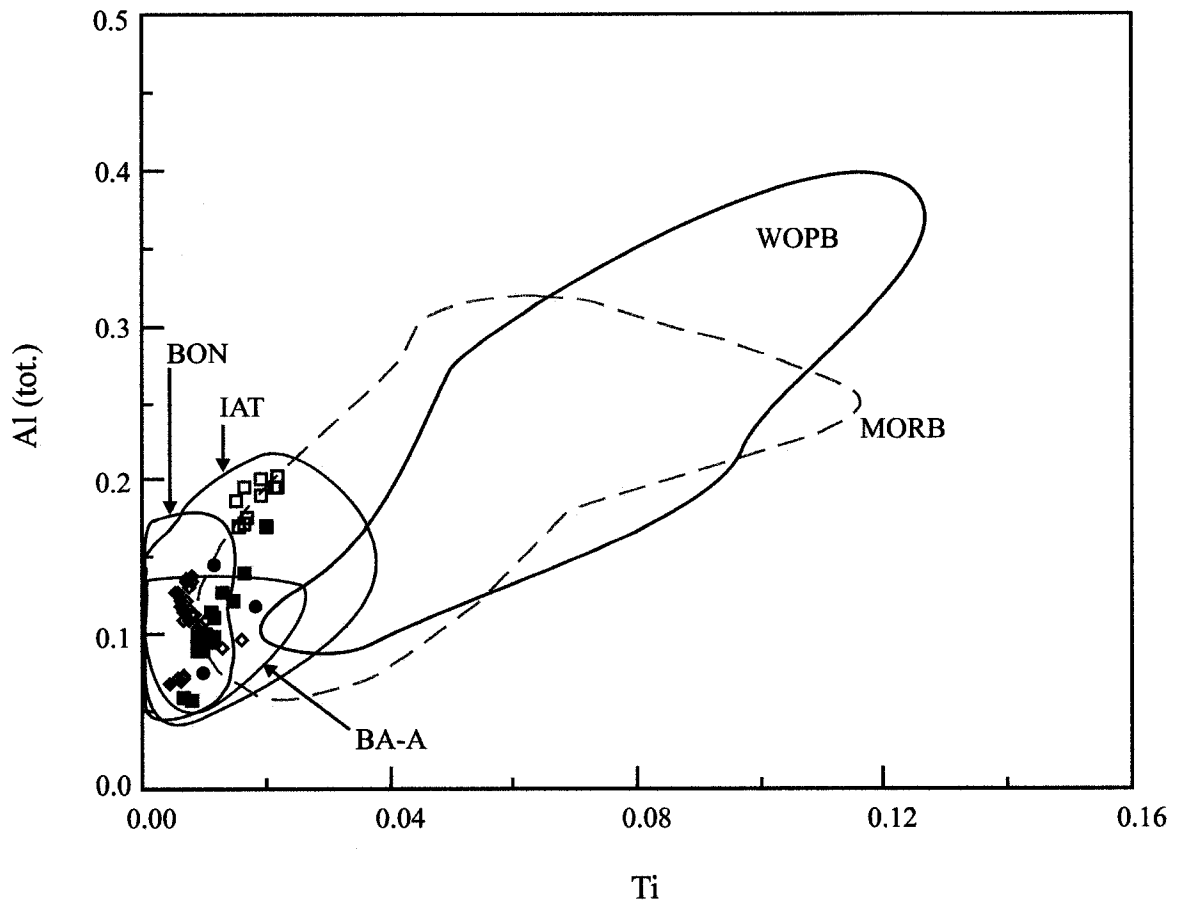
Fig. 25: Al (tot.) – Ti (atomic proportions) for clinopyroxenes of the SRG. Note also how well the points plot in IAT field. Some points plot in a narrow area of the MORB field but none plots within the WOPB field. *Abbreviations*: WOPB = within ocean plate basalts; MORB = mid-ocean ridge basalts; IAT = island arc tholeiites; BA-A = basaltic andesites and andesites; BON = boninites. *Modified after Beccaluva et al. (1989)*
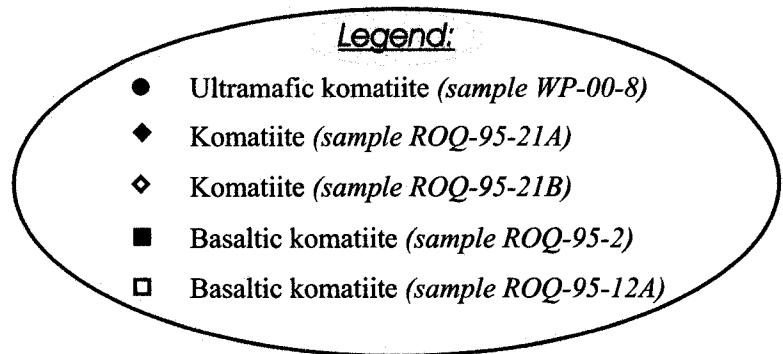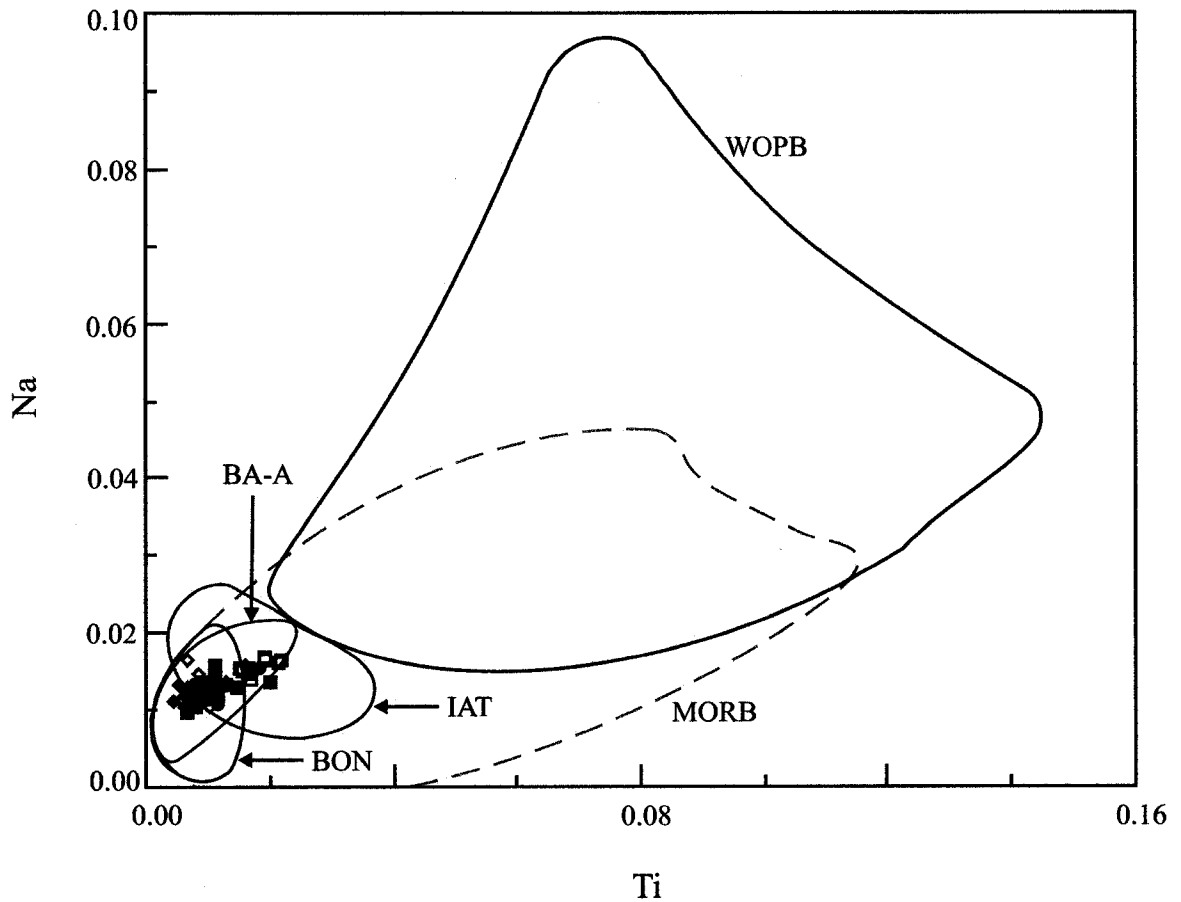
Fig. 26: Na – Ti (atomic proportions) discrimination technique. Affinity with BA-A, BON and

IAT is evident and cluster only within a narrow zone of the MORB field. None of the points plots

in the WOPB field. *Abbreviations*: WOPB = within ocean plate basalts; MORB = mid-ocean

ridge basalts; IAT = island arc tholeiites; BA-A = basaltic andesites and andesites; BON =

boninites. *Modified after Beccaluva et al. (1989)*
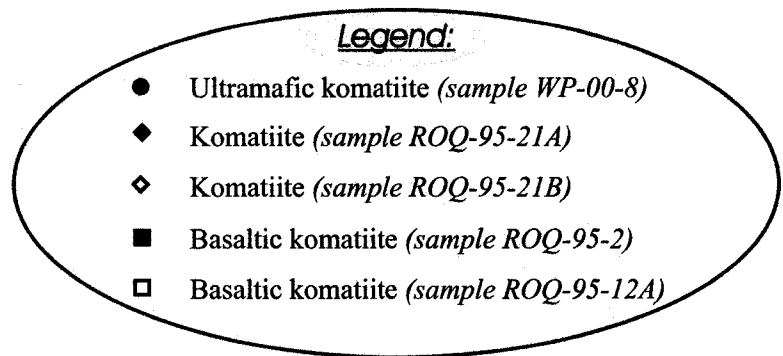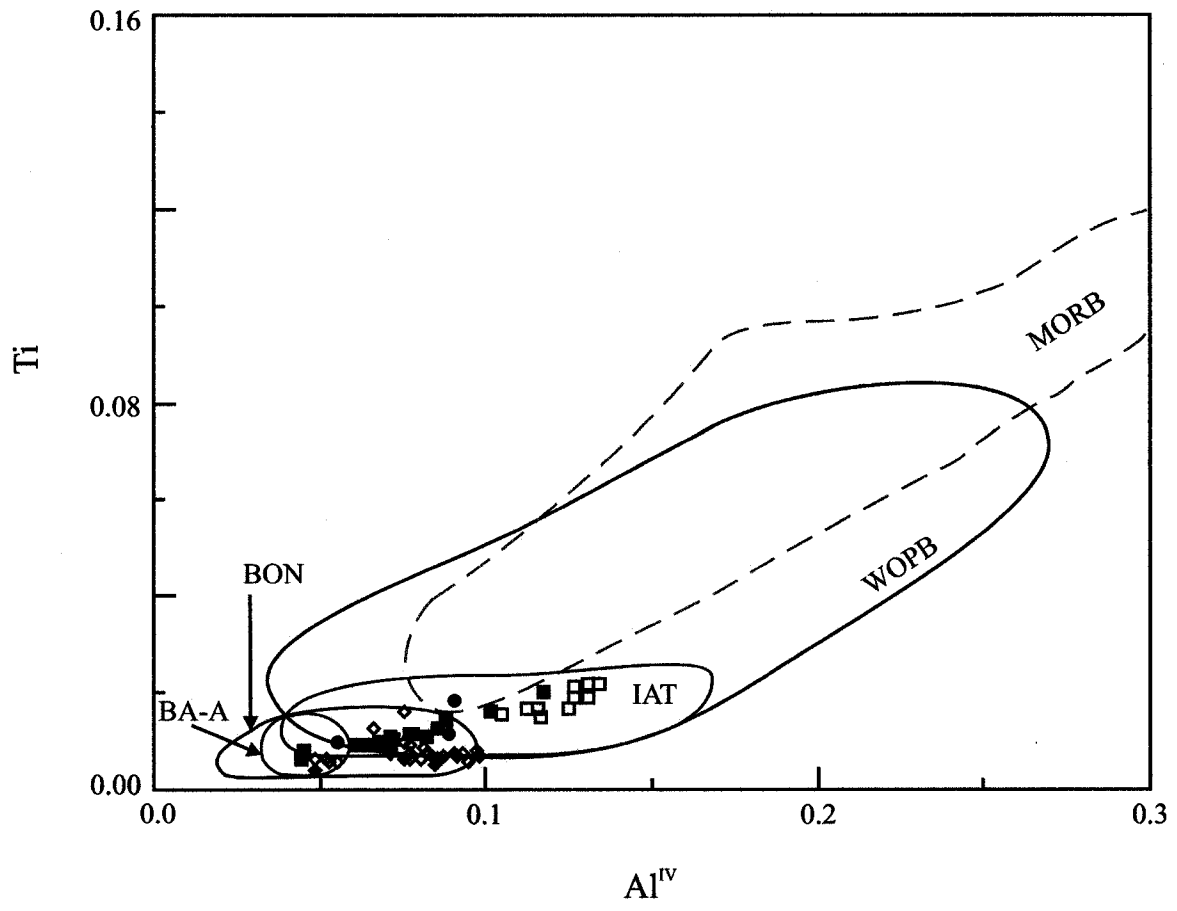
Fig. 27: Ti – Al^{IV} (atomic proportions) covariation discrimination technique. Note that there is no meaningful plot of points within the MORB field. Most points plot in the BON, IAT and WOPB fields. *Abbreviations*: WOPB = within ocean plate basalts; MORB = mid-ocean ridge basalts; IAT = island arc tholeiites; BA-A = basaltic andesites and andesites; BON = boninites. *Modified after Beccaluva et al. (1989)*

4.5   Discussion

Application of the discrimination plots to the SRG rocks provides mixed results but nonetheless places some constraints on the nature of the original tectonic setting of the SRG. It has been seen on one hand that the tectonic discrimination diagrams of Nisbet and Pearce (1977) and Leterrier et al. (1982) favour both processes of plume and subduction origin. The techniques of Beccaluva et al. (1989), on the other hand, point toward a subduction origin. The lack of complete agreement among the three discrimination techniques renders it difficult to advance a general conclusion.

For the purpose of comparison, analyses of clinopyroxenes from the SRG were added to a database containing a total of 32 analyses of calcic clinopyroxenes in komatiites from Barberton Mountainland Greenstone belt, South Africa (Parman et al., 2003); Belingwe Greenstone belt, Zimbabwe (Shimizu et al., 2005); and Gorgona Island, Columbia (Aitken and Echeverria, 1984; Echeverria, 1980) (Table 4).

The resulting discrimination diagrams of Leterrier et al. (1982) show that all the clinopyroxenes from the four localities (including the SRG) are related to tholeiitic basalts (Fig. 28) rather than alkali basalt magma (Fig. 29); and that Gorgona komatiites resemble non-orogenic basalts formed by plumes (Fig. 30). The discrimination diagrams of Beccaluva et al. (1989) further support the idea that Gorgona komatiites are of plume origin, and that Barberton, Belingwe and SRG komatiites are similar in composition because they show close association with boninites, basaltic andesites and andesites, and

76

island arc tholeiites which are thought (Beccaluva et al., 1989; Grove and Parman, 2004) to form in a subduction zone setting (Figs. 31 to 34).

Barberton, Belingwe and SRG clinopyroxenes have lower Al contents when compared to plume-related Gorgona clinopyroxenes (Figs. 31 to 33). The Gorgona clinopyroxenes have relatively high Ti contents (Fig. 34); and they resemble high-Ti basalts as they plot in the augite-to-salite field on a Ca-Mg-Fe diagram (Fig. 35). High-Ti concentrations are common in ocean floor basalts and mid-ocean ridge basalts of plume origin. On the other hand, Barberton, Belingwe and SRG clinopyroxenes straddle the augite-endiopside boundary, consistent with their very low- to low-Ti contents, characteristic of boninites and island arc tholeiites which are generated above subduction zones (Beccaluva et al., 1989).

Clinopyroxenes from Gorgona komatiites are distinguished by having higher concentrations of Al_2O_3 and TiO_2. Gorgona komatiites are reported to have been emplaced by plumes (Arndt et al., 1998; Nna-Mvondo and Martinez-Frais, 2005). Although the origin of Barberton and Belingwe komatiites is still a controversial issue, the compositions of their clinopyroxenes seem to be much closer to SRG clinopyroxenes. The clinopyroxene compositions of Barberton, Belingwe and SRG clinopyroxenes can be better compared to those of boninites, island arc tholeiites and basaltic andesites and andesites formed in subduction zones.

In another similar approach, analyses of clinopyroxenes from the SRG were added to a database containing a total of 46 analyses of calcic clinopyroxenes from rocks of various magma types and localities (Table 5). In every trial plot involving Ti and Na, it could be observed that the SRG clinopyroxenes cluster with those from island arc tholeiites, low-Ti ophiolitic basalts, boninites and basaltic andesites (Figs. 36 to 38). These rocks are known to evolve in a subduction zone setting. Basaltic rocks that could be compared to those from mid-ocean ridges and within ocean plates are clearly distinguished in these diagrams. Clinopyroxenes of the SRG are high in SiO_2 (49.96 - 53.97 wt %), CaO (17.33 - 21.97 wt %), and MgO (14.88 - 19.29 wt %). However, they have low TiO_2 (0.15 - 0.78 wt %) and Na_2O (0.14 - 0.24 wt %) contents compared to alkali basalts, mid-ocean ridge basalts and back-arc basalts (Capedri and Venturelli, 1979; Leterrier et al., 1982; Beccaluva et al., 1989; Lapierre et al., 1992). These geochemical characteristics are synonymous with eastern Mediterranean basalts and the ophiolites of Troodos (Cyprus), Vourinos & Pindos (Greece), Sarikaraman (Turkey); and the basalts of Betts Cove (Newfoundland, Canada), all of which are reported to have island arc affinity (Beccaluva et al., 1989; Yaliniz and Goncuoglu, 1999). Thus, on the basis of such close similarities, it can be argued that rocks of the SRG evolved in a subduction zone environment. This inference can be tested using trace element data for the SRG clinopyroxenes.
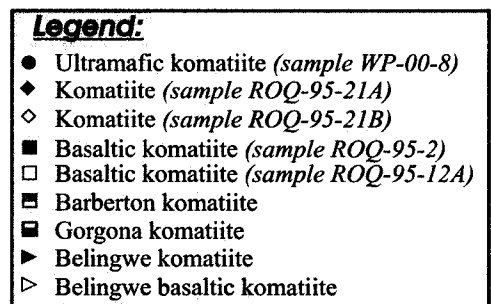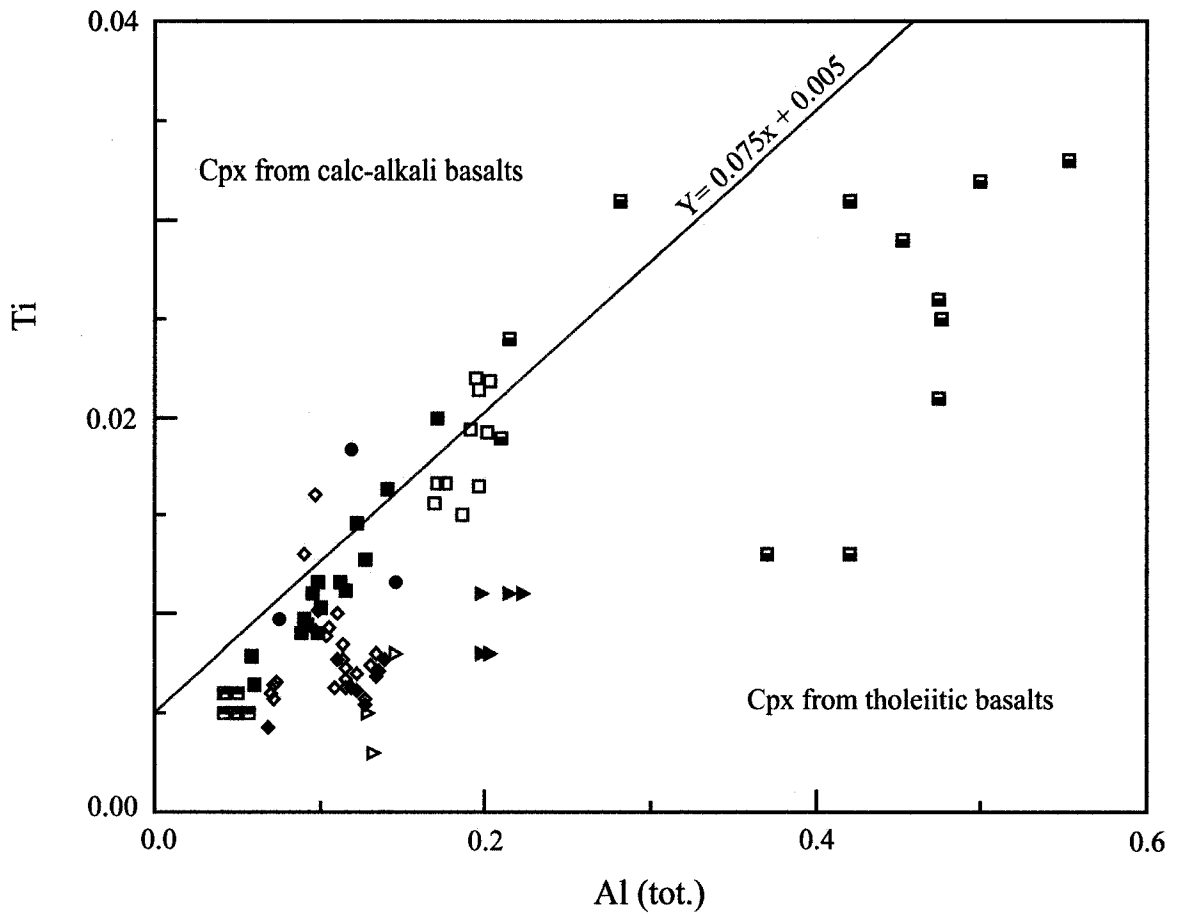
Fig. 28: Ti – Al (tot.) (atomic proportions) diagram distinguishing between clinopyroxenes in calc-alkali and tholeiitic basalts. The figure shows that SRG, Barberton, Belingwe and Gorgona clinopyroxenes are more closely related to tholeiitic basalts than to calc-alkali basalts. *Modified after Leterrier et al. (1982)*
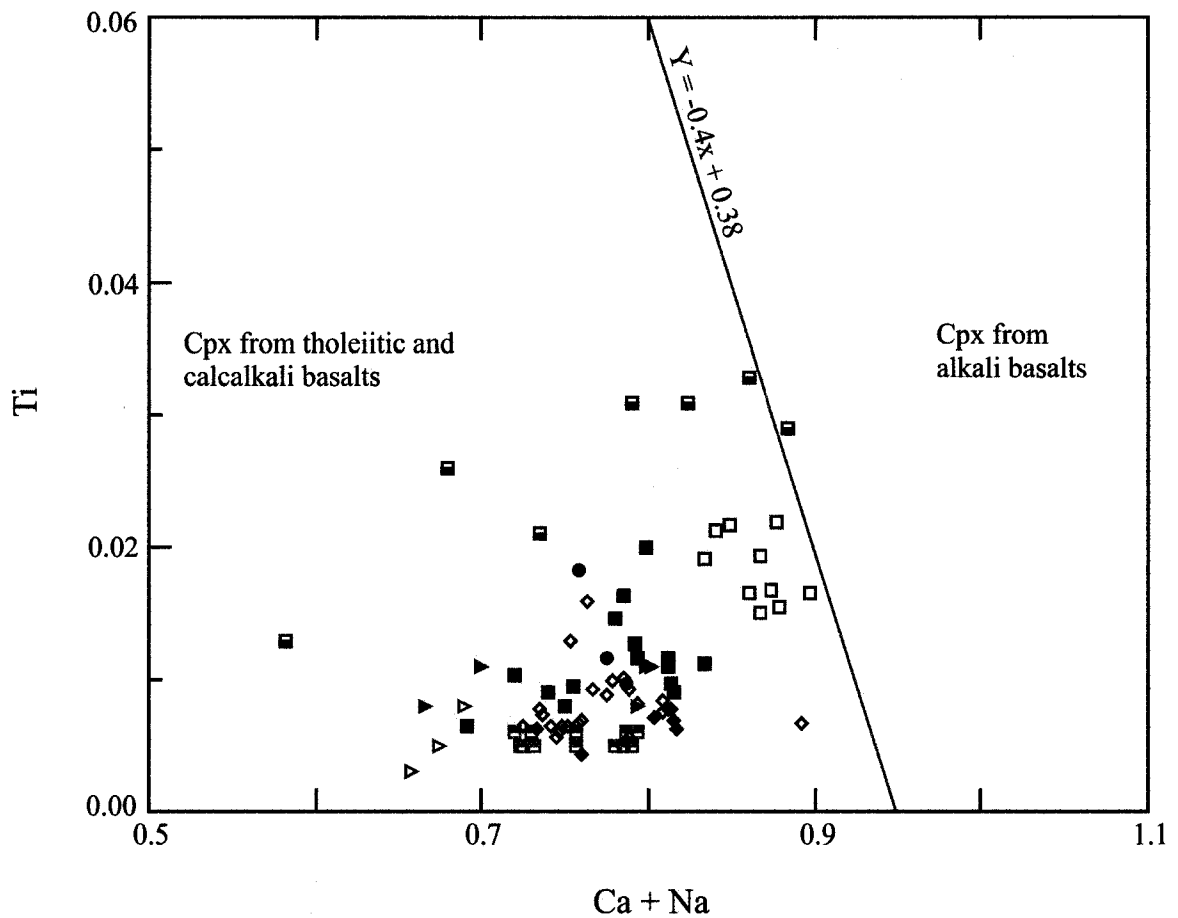
79

0.06

$Y = -0.4x + 0.38$

0.04

Ti

Cpx from tholeiitic and calcalkali basalts

Cpx from alkali basalts

0.02

0.00

0.5　0.7　0.9　1.1

Ca + Na

Legend:
● Ultramafic komatiite *(sample WP-00-8)*
◆ Komatiite *(sample ROQ-95-21A)*
◇ Komatiite *(sample ROQ-95-21B)*
■ Basaltic komatiite *(sample ROQ-95-2)*
□ Basaltic komatiite *(sample ROQ-95-12A)*
▣ Barberton komatiite
▤ Gorgona komatiite
► Belingwe komatiite
▷ Belingwe basaltic komatiite

Fig. 29: Ti − Ca + Na (atomic proportions) diagram comparing clinopyroxenes (Cpx) from the SRG to those from Barberton, Belingwe and Gorgona komatiitic rocks. The line separates two magma types and indicates that the host rocks in all four localities are of tholeiitic and calc-alkali affinity. *Modified after Leterrier et al. (1982)*
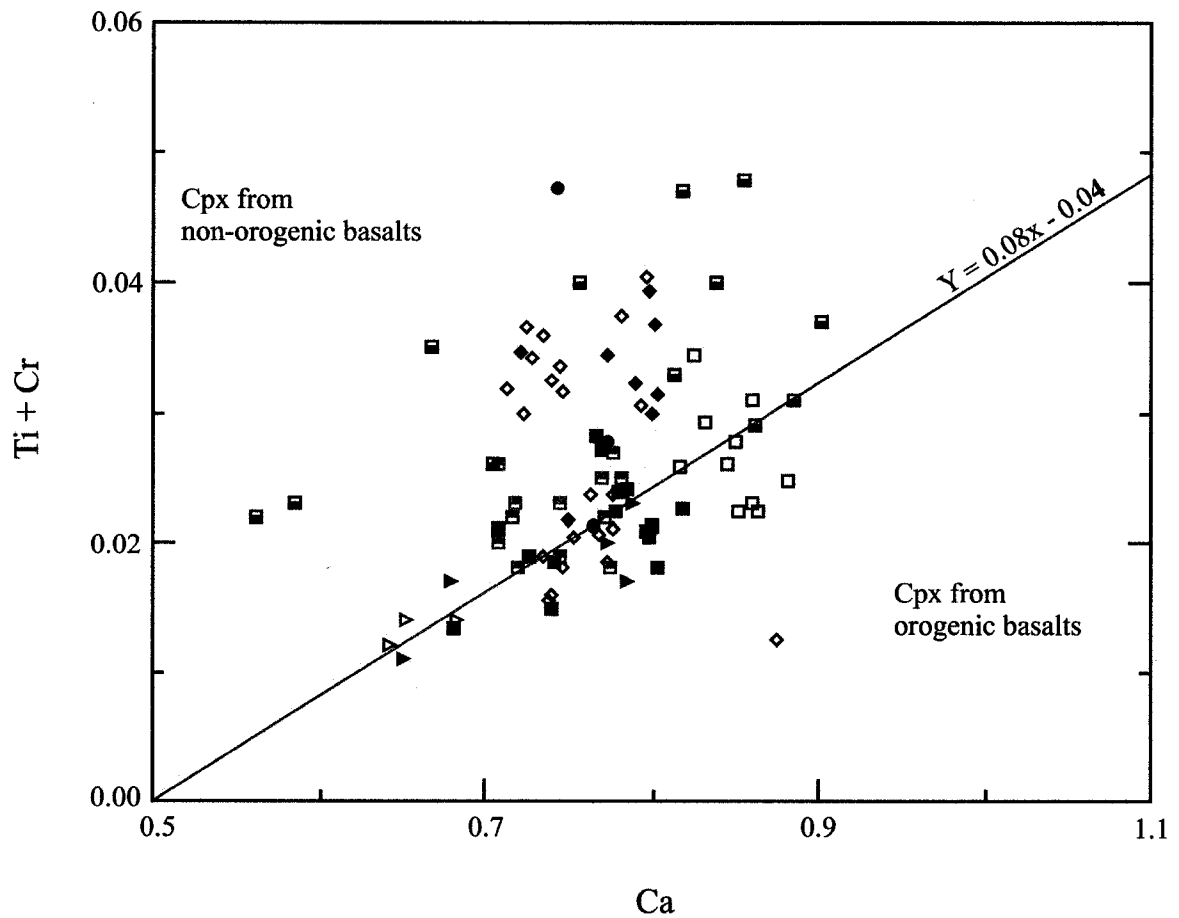
Fig. 30: Tectonic discrimination diagram of Ti + Cr – Ca (atomic proportions) for non-alkali basalts between non-orogenic basalts and orogenic basalts. The SRG, Barberton and Belingwe clinopyroxenes straddle along the line of distinction for which no assertion could be made, but Gorgona clinopyroxenes are clearly from non-orogenic basalts. *Modified after Leterrier et al. (1982)*
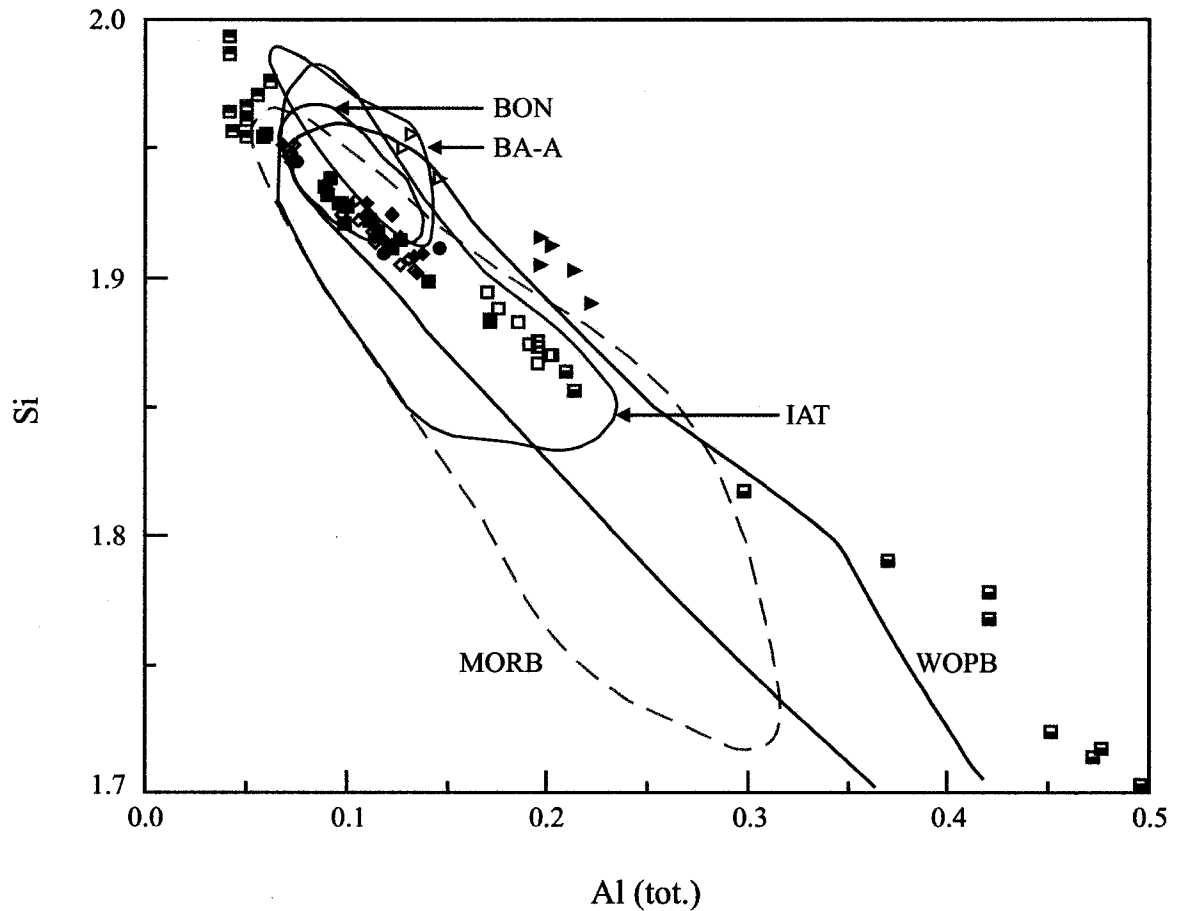
81

Fig. 31: Si – Al (tot.) (atomic proportions) covariation discrimination diagram. Note the parallel relationship between SRG and Belingwe clinopyroxenes. Note also the close relationship and trend of Gorgona clinopyroxenes with the WOPB field. *Abbreviations*: WOPB = within ocean plate basalts; MORB = mid-ocean ridge basalts; IAT = island arc tholeiites; BA-A = basaltic andesites and andesites; BON = boninites. *This diagram is modified after Beccaluva et al. (1989).*

82
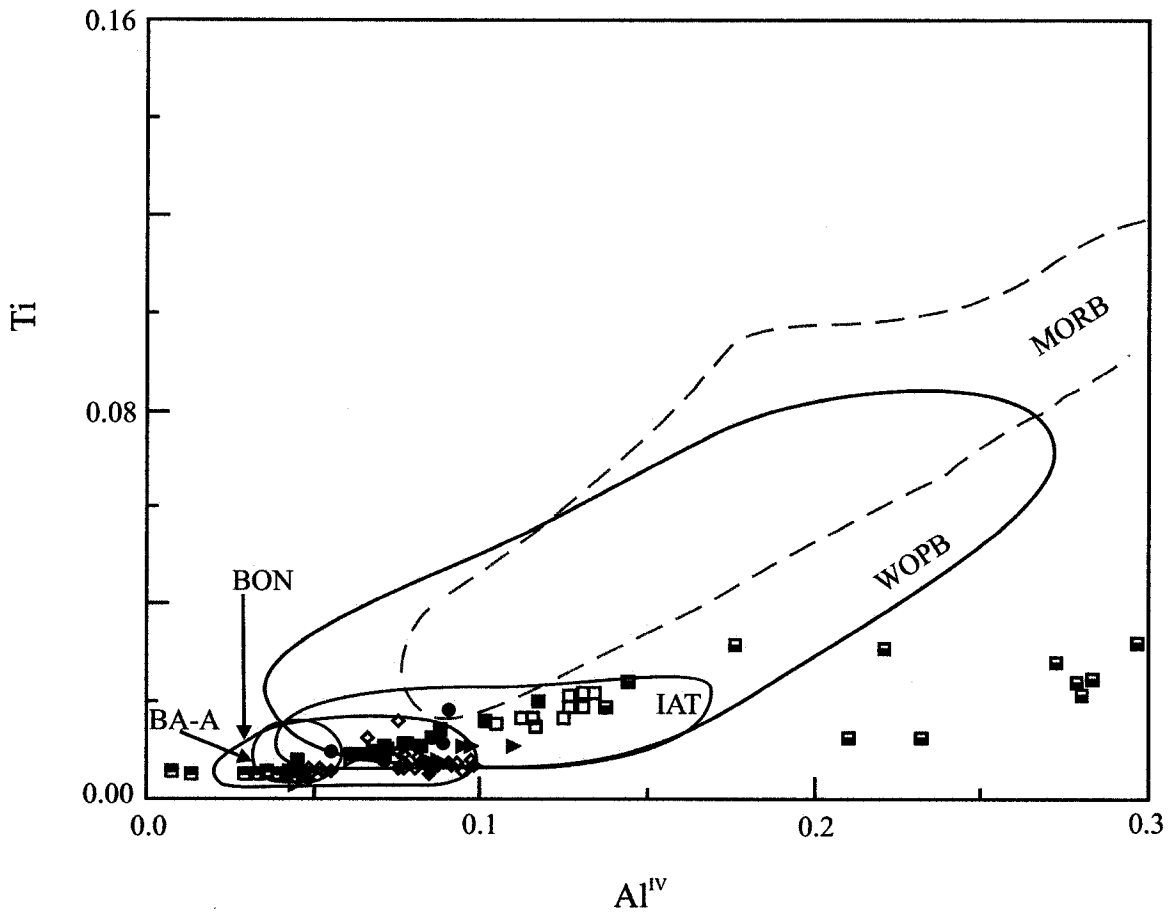
Fig. 32: Ti – Al^{IV} (atomic proportions) covariation discrimination diagram. The figure shows similar character between SRG, Barberton and Belingwe clinopyroxenes to BA-A, BON and IAT. Gorgona clinopyroxenes plot out of these fields. *Abbreviations*: WOPB = within ocean plate basalts; MORB = mid-ocean ridge basalts; IAT = island arc tholeiites; BA-A = basaltic andesites and andesites; BON = boninites. *Modified after Beccaluva et al. (1989)*

83
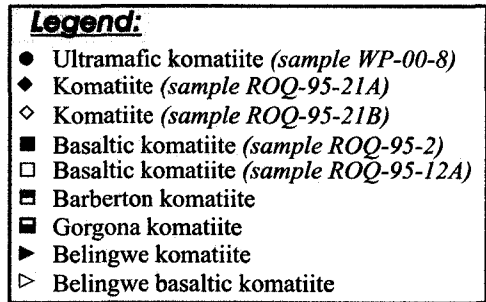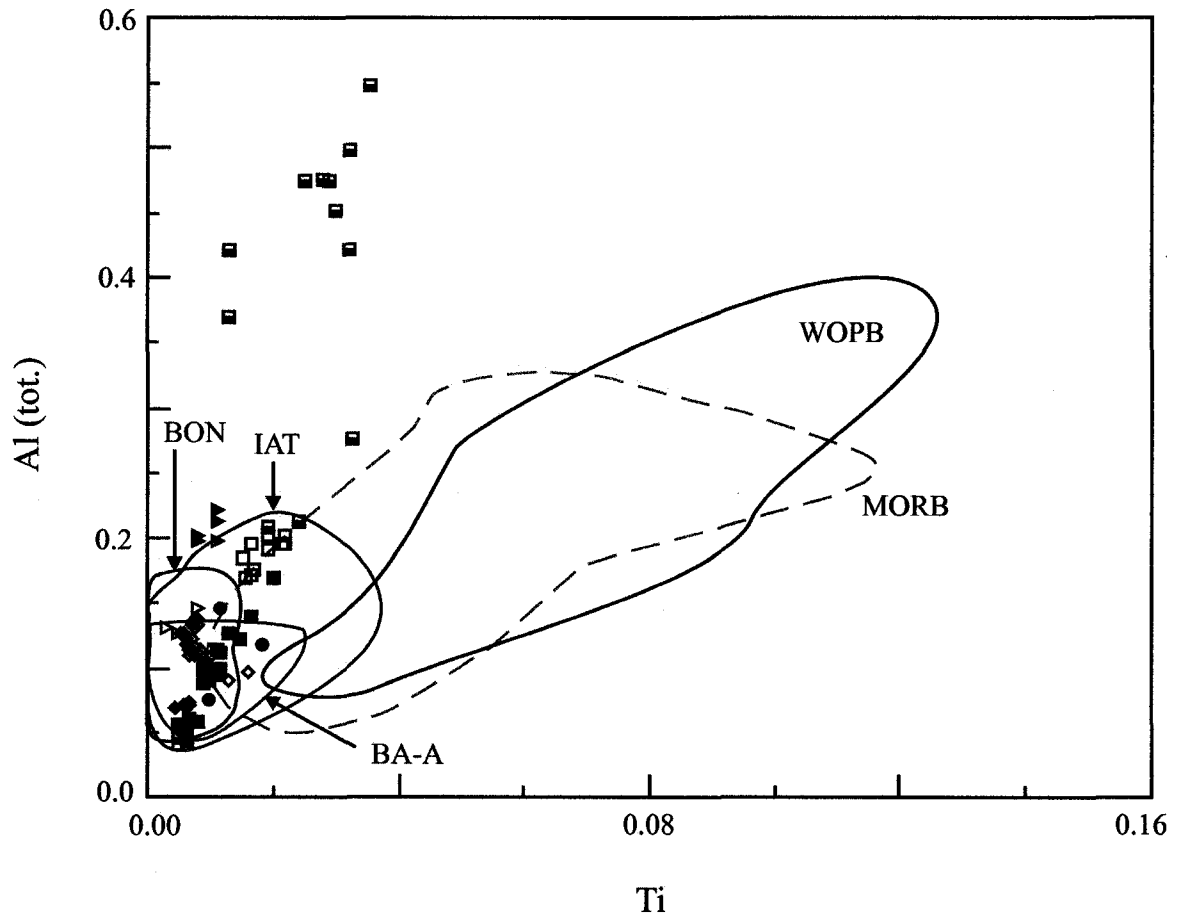
Fig. 33: Al (tot.) – Ti (atomic proportions) discrimination diagram indicating close relationship between SRG, Barberton and Belingwe clinopyroxenes to one another and to BA-A, BON and IAT magmas which are of subduction origin. Gorgona clinopyroxenes plot out of these fields. *Abbreviations*: WOPB = within ocean plate basalts; MORB = mid-ocean ridge basalts; IAT = island arc tholeiites; BA-A = basaltic andesites and andesites; BON = boninites. *Modified after Beccaluva et al. (1989)*

84
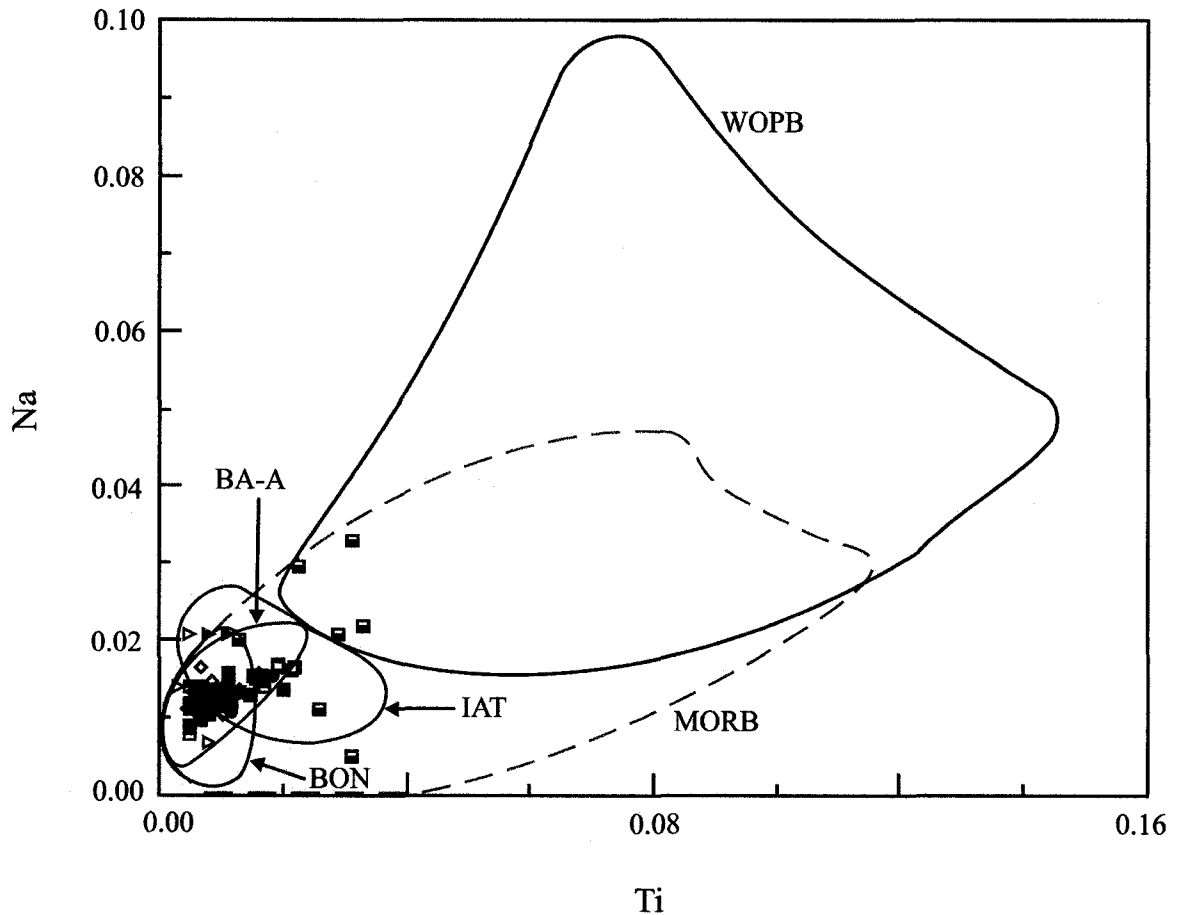
Legend:
- Ultramafic komatiite *(sample WP-00-8)*
- Komatiite *(sample ROQ-95-21A)*
- Komatiite *(sample ROQ-95-21B)*
- Basaltic komatiite *(sample ROQ-95-2)*
- Basaltic komatiite *(sample ROQ-95-12A)*
- Barberton komatiite
- Gorgona komatiite
- Belingwe komatiite
- Belingwe basaltic komatiite

Fig. 34: Na – Ti (atomic proportions) discrimination diagram. Although there is overlap, the affinity of SRG, Barberton and Belingwe clinopyroxenes with BA-A, BON and IAT is evident. On the other hand, Gorgona clinopyroxenes plot well in the MORB and WOPB fields which indicate a plume origin. *Abbreviations*: WOPB = within ocean plate basalts; MORB = mid-ocean ridge basalts; IAT = island arc tholeiites; BA-A = basaltic andesites and andesites; BON = boninites. *Modified after Beccaluva et al. (1989)*

85

Legend:
- ● Ultramafic komatiite *(sample WP-00-8)*
- ◆ Komatiite *(sample ROQ-95-21A)*
- ◇ Komatiite *(sample ROQ-95-21B)*
- ■ Basaltic komatiite *(sample ROQ-95-2)*
- □ Basaltic komatiite *(sample ROQ-95-12A)*
- ▣ Barberton komatiite
- ▤ Gorgona komatiite
- ▶ Belingwe komatiite
- ▷ Belingwe basaltic komatiite
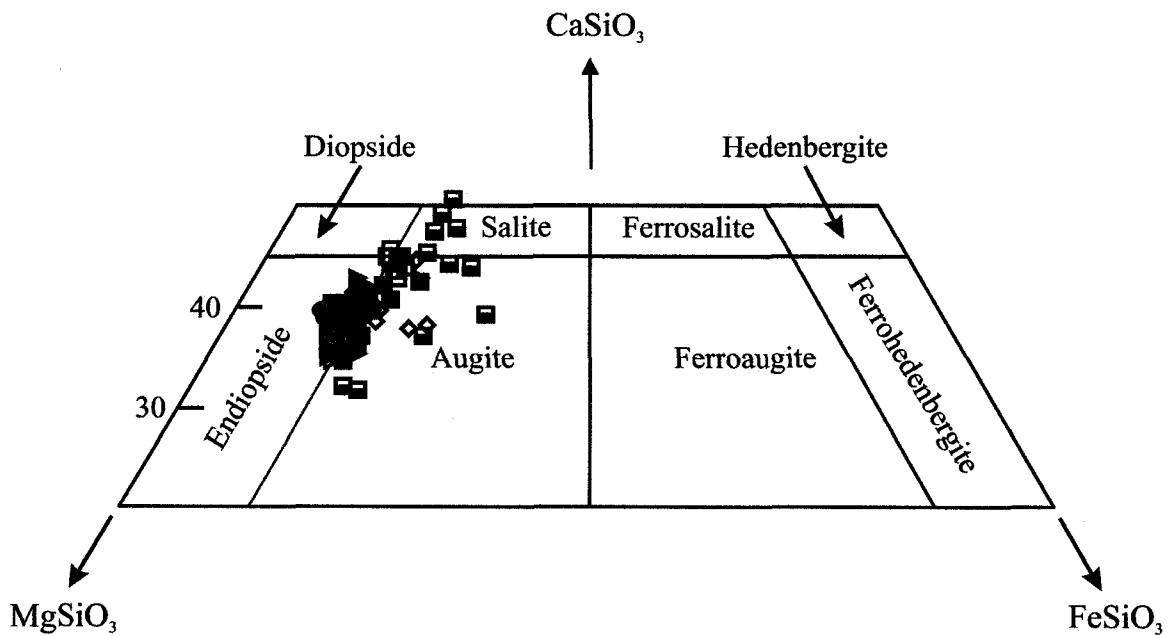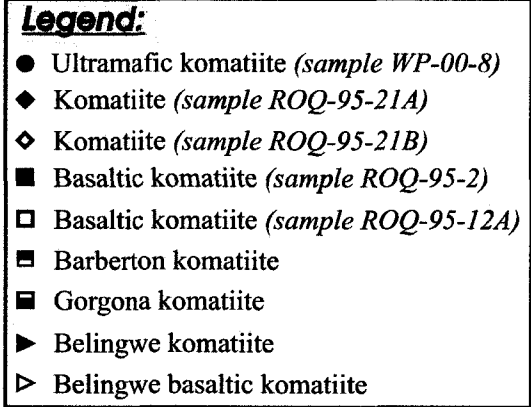
Fig. 35: Classification of clinopyroxenes into (a) very low- and low-Ti, and (b) high-Ti association, based on their positioning in the endiopside-augite and augite-to-salite fields, respectively. SRG clinopyroxenes compare well with Barberton and Belingwe clinopyroxenes because they plot around the endiopside-augite boundary, thus, classifying their host magma types as very low- and low-Ti basalts. Contrarily, Gorgona clinopyroxenes plot in the augite-to-salite field, classifying its host magma type as high-Ti basalts. *The diagram is modified after Beccaluva et al. (1989) and Deer et al. (2001)*

86

Fig. 36: Plots of TiO$_2$ against other oxides in clinopyroxenes from rocks of the SRG and from various localities with basaltic equivalents.

Legend:

	Rock type	Location (examples)	Basaltic equivalent for comparison
▲	Ophiolitic basalts	Mt. Maggiorasca & Mt. Penna-Quatese: Northern Apennines, External Lingurides (Italy).	Mid ocean ridge basalts
△	Ophiolitic basalts	Mt. Bocco-Case Arena & Framura: Northern Apennines, Internal Lingurides (Italy).	Within ocean plate basalts
▼	Alkali basalts	Intracontinental and oceanic islands	„ „ „ „
◑	Ophiolitic basalts	Mathia Mine & Akrounda: Troodos (Cyprus); Krapa Vourino & Pindos (Greece).	Island arc tholeiites
◎	Ophiolitic gabbros	Sarikaraman: Central Anatolia (Turkey).	„ „ „
+	Basalts	Mathiati Mine & Ora: Troodos (Cyprus); Asprokambo Vourinos (Greece).	Boninites
×	Basalts	Grevena District: Pindos (Greece); Betts Cove, Newfoundland (Canada).	Basaltic andesites and andesites
●◆◇■□	Komatiites and related rocks. (*This study*)		

87

Fig. 36 continued:

Legend:

Rock type	Location (examples)	Basaltic equivalent for comparison
▲ Ophiolitic basalts	Mt. Maggiorasca & Mt. Penna-Quatese: Northern Apennines, External Lingurides (Italy).	Mid ocean ridge basalts
△ Ophiolitic basalts	Mt. Bocco-Case Arena & Framura: Northern Apennines, Internal Lingurides (Italy).	Within ocean plate basalts
▼ Alkali basalts	Intracontinental and oceanic islands	" " " "
◑ Ophiolitic basalts	Mathia Mine & Akrounda: Troodos (Cyprus); Krapa Vourino & Pindos (Greece).	Island arc tholeiites
◐ Ophiolitic gabbros	Sarikaraman: Central Anatolia (Turkey).	" " "
+ Basalts	Mathiati Mine & Ora: Troodos (Cyprus); Asprokambo Vourinos (Greece).	Boninites
× Basalts	Grevena District: Pindos (Greece); Betts Cove, Newfoundland (Canada).	Basaltic andesites and andesites
● ♦ ◇ ■ □ Komatiites and related rocks. *(This study)*		

88

Legend:

	Rock type	Location (examples)	Basaltic equivalent for comparison
▲	Ophiolitic basalts	Mt. Maggiorasca & Mt. Penna-Quatese: Northern Apennines, External Lingurides (Italy).	Mid ocean ridge basalts
△	Ophiolitic basalts	Mt. Bocco-Case Arena & Framura: Northern Apennines, Internal Lingurides (Italy).	Within ocean plate basalts
▼	Alkali basalts	Intracontinental and oceanic islands	,, ,, ,, ,,
◑	Ophiolitic basalts	Mathia Mine & Akrounda: Troodos (Cyprus); Krapa Vourino & Pindos (Greece).	Island arc tholeiites
◎	Ophiolitic gabbros	Sarikaraman: Central Anatolia (Turkey).	,, ,, ,,
+	Basalts	Mathiati Mine & Ora: Troodos (Cyprus); Asprokambo Vourinos (Greece).	Boninites
×	Basalts	Grevena District: Pindos (Greece); Betts Cove, Newfoundland (Canada).	Basaltic andesites and andesites
●◆◇■□	Komatiites and related rocks. (This study)		

Fig. 37: Plots of Na$_2$O against other oxides in clinopyroxenes from rocks of the SRG and from various localities with basaltic equivalents.

89

Fig. 37 continued:

Legend:

	Rock type	Location (examples)	Basaltic equivalent for comparison
▲	Ophiolitic basalts	Mt. Maggiorasca & Mt. Penna-Quatese: Northern Apennines, External Lingurides (Italy).	Mid ocean ridge basalts
△	Ophiolitic basalts	Mt. Bocco-Case Arena & Framura: Northern Apennines, Internal Lingurides (Italy).	Within ocean plate basalts
▼	Alkali basalts	Intracontinental and oceanic islands	,, ,, ,, ,,
◑	Ophiolitic basalts	Mathia Mine & Akrounda: Troodos (Cyprus); Krapa Vourino & Pindos (Greece).	Island arc tholeiites
◉	Ophiolitic gabbros	Sarikaraman: Central Anatolia (Turkey).	,, ,, ,,
+	Basalts	Mathiati Mine & Ora: Troodos (Cyprus); Asprokambo Vourinos (Greece).	Boninites
✕	Basalts	Grevena District: Pindos (Greece); Betts Cove, Newfoundland (Canada).	Basaltic andesites and andesites
● ◆ ◇ ■ □	Komatiites and related rocks. (*This study*)		

90

Fig. 38: Plots showing possible combinations of TiO_2 & Na_2O with other oxides.

4.6   Trace Element Investigation

The rare earth element (REE) data of SRG clinopyroxenes have been averaged for each of the three groups of rock types so as to obtain a general picture of the various patterns (Table 6). In order to assess the chemical effects of metamorphism on the samples, the approach of Parman et al. (2003) has been applied. This involves calculating the trace element composition of a hypothetical augite in equilibrium with the melt, and comparing it with the analyzed cores of augite crystals preserved in that sample. The hypothetical augites were calculated using the respective whole-rock compositions (Table 6) and clinopyroxene-melt partition coefficients. Unlike Parman et al. (2003), the partition coefficient values in this work are based on those of tholeiitic basalts as determined by Fujimaki et al. (1984), since the SRG clinopyroxenes are better related to this type of magma (Fig. 21). In komatiitic magmas, olivine and trace amounts of spinel are the only phases to have crystallized before the appearance of augite. The amount of olivine that crystallizes before augite nucleates is ~30 % (Parman et al., 2003). The calculated melt compositions have not been corrected for olivine and spinel addition/subtraction because these minerals have low REE concentrations such that their omission will not have any significant effect on the relative concentrations of the elements (Parman et al., 2003; Shimizu et al., 2005).

REE compositions of augites calculated from the whole-rock compositions of the samples display analogous patterns to the analyzed, averaged augite cores (Fig. 39). Such harmonization indicates that the REE have been immobile in the whole-rock samples (Parman et al., 2003). Agreement is especially displayed by the overlap in the komatiite

92

samples (ROQ-95-21A, ROQ-95-21B) and in one of the two basaltic komatiite samples (ROQ-95-2). The calculated augite composition for the cumulate sample (ultramafic komatiite — WP-00-8) is lower than the others because the melt composition is diluted by the presence of olivine (Parman et al., 2003); this is manifested by the comparatively low REE values for the whole-rock sample (Table 6). There is a general light rare earth element (LREE) depletion and flat heavy rare earth element (HREE) pattern in the analyzed augites (Fig. 39), consistent with known partitioning of trace elements between clinopyroxene and melt. The degree of LREE depletion is similar in the analyzed augites: $(La/Sm)_N = 0.22$ in sample WP-00-8 (ultramafic komatiite); $(La/Sm)_N = 0.20$ in sample ROQ-95-21B (komatiite); 0.24 and 0.25 in the basaltic komatiite samples (ROQ-95-2 and ROQ-95-12A, respectively). Sample ROQ-95-21A (komatiite), however, records the lowest ratio ($[La/Sm]_N = 0.13$); indicating that it is more LREE depleted than the others. Flat HREE pattern is shown in the $(Gd/Y)_N$ ratio, varying almost laterally from 0.80-1.18.

The primitive mantle-normalized (McDonough and Sun, 1995) spidergram shows negative high field strength element (HFSE — Nb, Zr, Ti and Y) anomalies relative to the REEs in all the samples (Fig. 40); indicating that the HFSEs are fractionated with respect to the more incompatible REEs. Sample ROQ-95-21A (komatiite), which has the lowest $(La/Sm)_N$ ratio, also records the greatest depletions in Zr and Ti. Compared to the other HFSEs, the anomaly shown by Y is only subtle. Ta has not been included in the diagram because most of the analyses indicate 'below detection limit'. The fractionation of Zr-Hf in Fig. 40 is particularly striking because these two incompatible HFSEs have the same chemical and geochemical properties. For example, Zr and Hf have the same

93

ionic charge (4+) and very similar ionic radii — 0.072 nm and 0.071 nm in the six fold

coordination, respectively, thus, they are expected to behave similarly (Westrenen et al.,

2001). In this study, Zr/Hf ratios vary between 13.94 and 20.00. Initially, Fujimaki et al.

(1984) stated that Zr-Hf fractionation cannot be usually expected unless under special

circumstances. If the crystallization involves garnet and/or ilmenite, this can be detected

by the Zr and Hf abundance variations in conjunction with the REE.

4.6.1 Discussion

Even in slightly altered rocks, rare earth element (REE) patterns can faithfully represent

the original composition of the unaltered parent (Rollinson, 1996). With respect to trace

element contents, subduction-related lavas are typically enriched in LILE (e.g., Sr, K, Ba,

U, Th) and depleted in the HFSEs (e.g., Nb, Ta, Zr, Hf) relative to mid-ocean ridge

basalts (MORB). The trace element pattern has been interpreted as resulting from

metasomatism of peridotites in the sub-arc mantle, prior to partial melting by a H_2O-rich

component derived from the subducting oceanic lithosphere (Ayers et al., 1997; Johnson,

1998; Gaetani et al., 2003). McDade et al. (2003) similarly suggest that depletion of

HFSEs is attributed to a variety of subduction-related processes, most of which infer

retention of the elements in a titanite (*sphene*, $CaTiSiO_5$) phase in the slab during

dehydration and/or partial melting of the metabasaltic portion of the slab or its

sedimentary cover. Other possible titanium phases could be rutile (TiO_2), ilmenite

($FeTiO_3$), or perovskite ($CaTiO_3$).

94

From the trace element investigation in this study, negative concentration anomalies are observed for Nb, Zr, Ti and Y relative to the REEs (Fig. 40). As noted above, such occurrences are attributed to subduction-related processes; plume-related MORB do not show these anomalies. In Fe-Ti oxides, Ta is more compatible than Nb ($D_{Ta} > D_{Nb}$), meaning, Ta enters the mineral structure more easily than Nb, leaving little (if any) of this component in the melt (Klemme et al., 2006). This behavior is perhaps responsible for the extremely low concentration of Ta in the clinopyroxene analyses.

Recent experimental investigation on clinopyroxene-melt trace element partitioning has shown that clinopyroxene can fractionate Zr and Hf (Lundstrom et al., 1998; Hill et al., 2000; Takawaza et al., 2000; McDade et al., 2003; Carsten et al., 2004). However, negative anomalies for Zr atypical of mid-ocean ridge basalts and ocean island basalts; this suggests that for such basalts, the clinopyroxene effect on Zr is offset by garnet influence, as it appears that garnet has a pronounced positive partitioning anomaly for both Zr and Hf, relative to Sm and Nd (Fujimaki et al., 1984; Green et al., 1989; Sun and McDonough, 1989; Hart and Dunn, 1993).

Trace element investigation in this study is therefore in agreement with assertions made earlier on the basis of major element data. The clinopyroxene trace element systematics support that komatiitic rocks of the SRG are better compared with subduction zone affinity than with those of plumes.
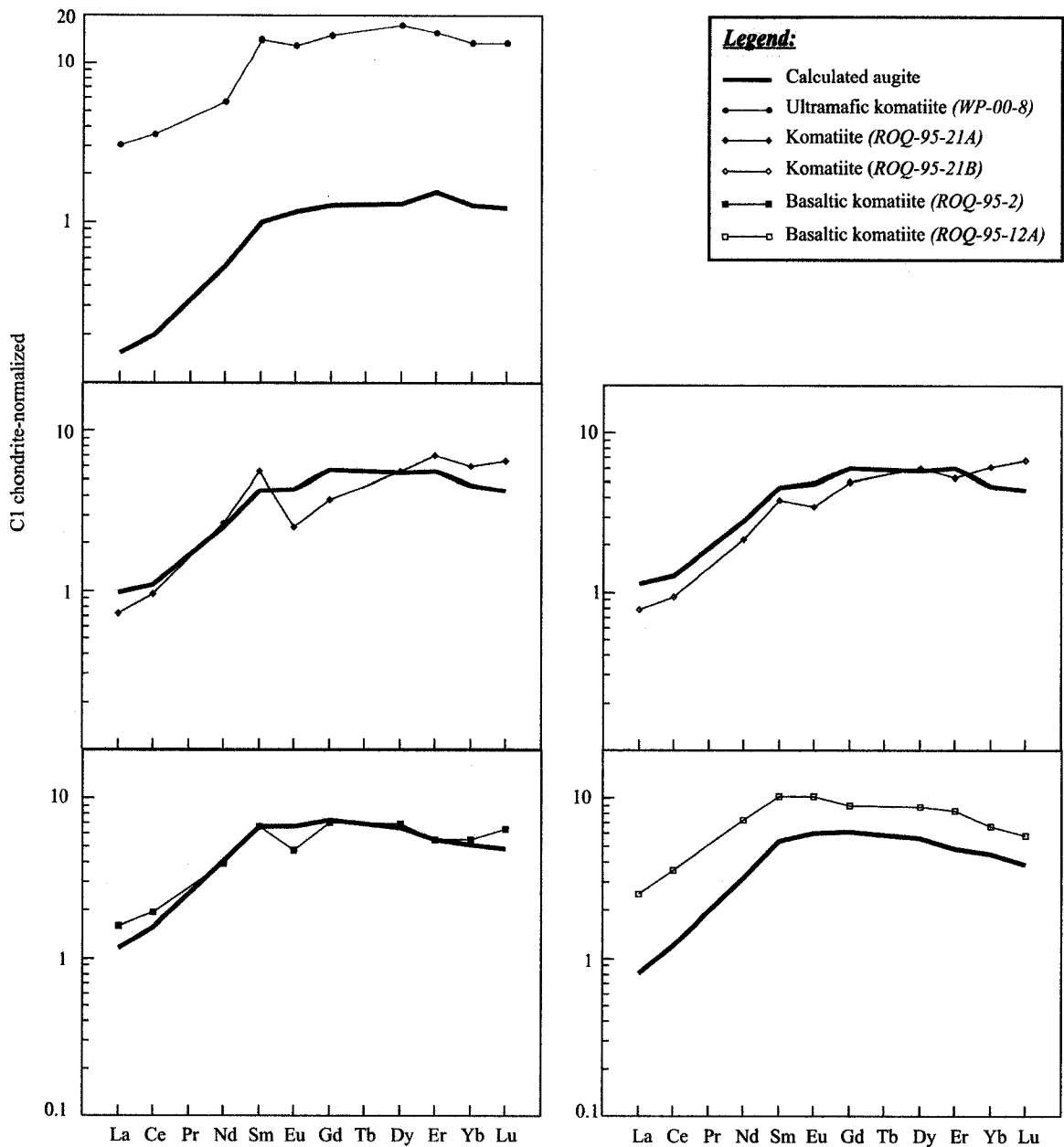
Fig. 39: C1 Chondrite-normalized rare earth element patterns of augite in samples of ultramafic komatiite, komatiite and basaltic komatiite from the SRG. Normalizing values are after McDonough and Sun (1995). Thick solid lines represent the compositions of augite calculated to be in equilibrium with their corresponding whole rock compositions, using the clinopyroxene-melt partition coefficients of Fujimaki et al. (1984).

96
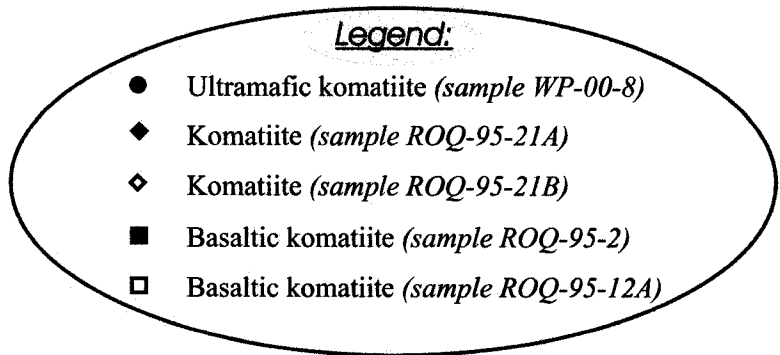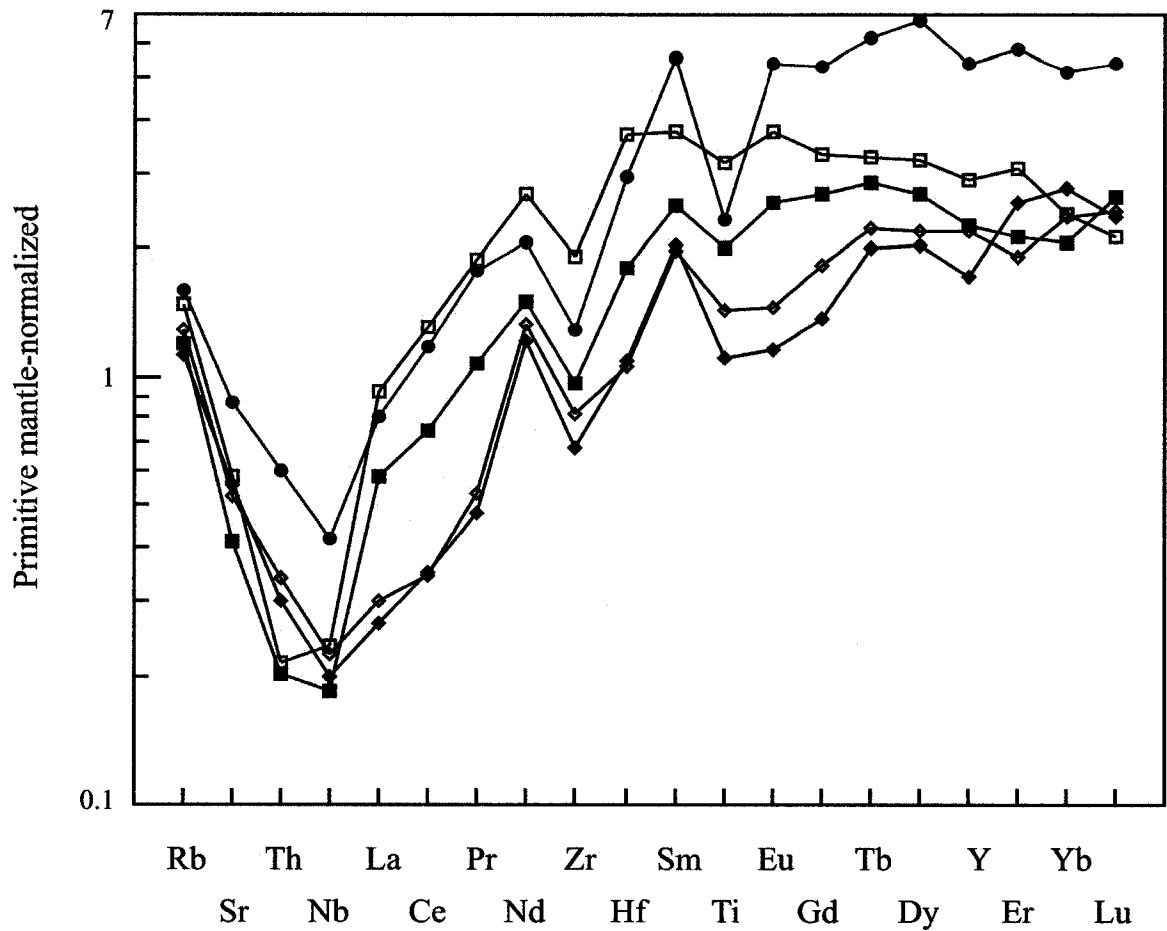
Fig. 40: Primitive mantle-normalized multi-element diagram for clinopyroxenes in komatiitic rocks from the SRG. Normalizing values are those of McDonough and Sun (1995); ordering is according to Pearce (1983). Note the relative enrichment in LILE (Rb, Sr), and depletion in HFSE (Nb, Zr, Ti) relative to the rare earth elements. The pattern is indicative of a subduction origin.

97

CHAPTER 5

CONCLUSIONS

The 'origin of komatiites' has been a subject of research and intense debate over the years. At present, most of the opinions expressed are pivoted on either plumes or subduction processes.

It is of utmost importance to note that the results obtained in this work are exciting on one hand but quite challenging on the next. The tectonic discrimination diagrams of Nisbet and Pearce (1977) and Leterrier et al. (1982) favour both plume and subduction origins for komatiites of the Stoughton-Roquemaure Group. The discrimination diagrams of Beccaluva et al. (1989) support a subduction origin but hints of plume influence are also indicated. Stoughton-Roquemaure Group clinopyroxenes resemble those in Barberton and Belingwe komatiites, and are also associated with very low-Ti and low-Ti ophiolitic basalts, island arc tholeiites, boninites, and basaltic andesites and andesites. This similarity, however, cannot justify a firm subduction zone categorization because the origin of Barberton and Belingwe komatiites still remains controversial. Nevertheless, we have seen that the clinopyroxene compositions of Barberton, Belingwe and Stoughton Roquemaure Group komatiites differ from those of the accepted, plume-generated Gorgona komatiites. The trace element systematics in this study implies that the Stoughton-Roquemaure Group was formed by subduction processes. All these constraints make it cumbersome to pinpoint a single process or activity for emplacement of the Group in question. However, the general geochemical characteristics allow us to purport

98

that there was some plume influence during emplacement of the komatiitic rocks. Whether subduction or mantle plume activity was the main event cannot be distinguished unequivocally, but it seems that more subduction signatures are recorded by clinopyroxenes than are plume. A plausible presumption might be that a rising plume intercepted a subducting slab such that the emplaced lava preserved imprints of both processes.

99

REFERENCES

Abbott, D.H. and Isley, A.E. (2002). *Extraterrestrial influences on mantle plume activity.* Earth and Planetary Science Letters, vol. 205, pp 53-62.

Aitken, B.G. and Echeverria, L.M. (1984). *Petrology and geochemistry of komatiites and tholeiites from Gorgona Island, Columbia.* Contributions to Mineralogy and Petrology, vol. 86, pp 94-105.

Allègre, C.J. (1982). *Genesis of Archaean komatiites in a wet ultramafic subducted plate.* In: Arndt, N.T. and Nisbet, E.G. (eds.), *Komatiites.* Published by George Allen and Unwin, London, pp 495-500.

Anhaeusser, C.R. (1971). *Cyclic volcanicity and sedimentation in the evolutionary development of Archaean greenstone belts of Shield areas.* Geological Society of Australia Special Publication, vol. 3, pp 57-70.

Arndt, N.T., Ginibre, C., Chauvel, C., Albarede, F., Cheadle, M., Herzberg, C., Jenner, G. and Lahaye, Y. (1998). *Were komatiites wet?* Geology, vol. 26, pp 739-742.

Arndt, N.T. (1994). *Archaean Komatiites.* In Condie, K.C. (eds.), *Archaean Crustal Evolution.* Amsterdam: Elsevier, pp 11-44.

Arndt, N.T. (1986). *Spinifex and swirling olivines in a komatiite lava lake, Munro Township, Canada.* Precambrian Research, vol. 34, pp 139-155.

Arndt, N.T. and Nesbitt, R.W. (1982). *Geochemistry of Munro township basalts.* In: Arndt, N.T. and Nisbet, E.G. (eds.), *Komatiites.* Published by George Allen and Unwin, London, pp 309-329.

Arndt, N.T. and Nisbet, E.G. (eds.). (1982). *What is a Komatiite?* In: Arndt, N.T. and Nisbet, E.G. (eds.), *Komatiites.* Published by George Allen and Unwin, London, pp 19-28.

Arndt, N.T., Naldrett, A.J. and Pyke, D.R. (1977). *Komatiites and iron-rich tholeiitic lavas of Munro Township, northeast Ontario.* Journal of Petrology, vol. 18, pp 319-369.

Arndt, N.T. (1976). *Melting relations of ultramafic lavas (komatiites) at 1 atm and high pressure.* Carnegie Institution of Washington Yearbook 75, pp 555-562.

Ayer, J.A, Amelin, Y., Corfu, F., Kamo, S., Ketchum, J., Kwok, K. and Trowell, N. (2002). *Evolution of the southern Abitibi greenstone belt based on U-Pb geochronology: autochthonous volcanic construction followed by plutonism, regional deformation and sedimentation.* Precambrian Research, vol. 115, pp 63-95.

Ayer, J.A., Trowell, N.F., Amelin, Y. and Corfu, F. (1999). *Geological compilation of the Abitibi greenstone belt: toward a revised stratigraphy based on compilation and new geochronology results.* Ontario Geological Survey, Open File Report 6000, pp. 4.4 - 4.14.

Ayers, J.C., Dittmer, S.K. and Layne, G.D. (1997). *Partitioning of elements between peridotite and H_2O at 2.0-3.0 GPa and 900 - 1100°C, and application to models of subduction zone processes.* Earth and Planetary Science Letters, vol. 150, pp 381-398.

Ayres, L.D. and Thurston, P.C. (1985). *Archaean subcrustal sequences in the Canadian Shield. An overview.* In: Thurston, P.C., Card, K.D. and Weber, W. (eds.), *Evolution of Archaean supracrustal sequences.* Geological Association of Canada Special Paper 28, pp 343-380.

Beccaluva, L., Macciotta, G., Piccardo, G.B., and Zeda, O. (1989). *Clinopyroxene composition of ophiolite basalts as petrogenetic indicator.* Chemical Geology, vol. 77, pp165-182.

Brooks, C. and Hart, S.R. (1974). *On the significance of komatiite.* Geology, vol. 2, pp 107 - 110.

Cameron, W.E., Nisbet, E.G. and Dietrich, V.J. (1979). *Boninites, komatiites and ophiolitic basalts.* Nature, vol. 280, pp 550-553.

Campbell, I.H., Griffiths, R.W. and Hill, R.I. (1989). *Melting in an Archaean mantle plume: heads it's basalts, tails it's komatiites.* Nature, vol. 339, pp 697-699.

Capedri, S. and Venturelli, G. (1979). *Clinopyroxene composition of ophiolitic metabasalts in the Mediterranean Area.* Earth and Planetary Science Letters, vol. 43, pp 61-73.

Card, K.D. (1990). *A review of the Superior Province of the Canadian Shield, a product of Archaean accretion.* Precambrian Research, vol. 48, pp 99-156.

Card, K.D. and Ciesielski, A. (1986). *Subdivisions of the Superior Province of the Canadian Shield.* Geoscience Canada, vol. 13, pp 5-13.

Carsten, M., Worner, G., Yogodzinski, G. and Churikova, T. (2004). *Behaviour of high field strength elements in subduction zones: constraints from Kamchatka—Aleutian arc lavas.* Earth and Planetary Science Letters, vol. 224, pp 275-293.

Chai, G. and Naldrett, A.J. (1994). *Pyroxene mineral chemistry of the Jinchuan intrusion, China.* Journal of Mineralogy and Petrology, vol. 51, pp 1-20.

Chown, E.H., Daigneault, R., Mueller, W. and Mortensen, J.K. (1992). *Tectonic evolution of the Northern Volcanic Zone, Abitibi belt, Quebec.* Canadian Journal of Earth Sciences, vol. 29, pp 2211-2225

Condie, K.C. (1982). *Plate tectonics and crustal evolution.* Second Edition. Pergamon Press.

Corfu, F. and Grunsky, E.C. (1987). *Igneous and tectonic evolution of the Batchawana greenstone belt, Superior Province: A U-Pb zircon and titanite study.* Journal of Geology, vol. 95, pp 87-105.

Davis, W.J., Machada, C., Gariepy, C., Sawyer, E.W. and Benn, K. (1994). *U-Pb geochemistry of the Opatica tonalite-gneiss belt and its relationship to the Abitibi greenstone belt, Superior Province, Quebec.* Canadian Journal of Earth Sciences, vol. 3, pp 113-127.

Davis, G.F. (1993). *Cooling the core and mantle by plume and plate flows.* Geophysical Journal International, vol. 115, pp 132-146.

Deer, W.A., Howie, R. A. and Zussman, J. (2001). *Rock-forming Minerals. Single-Chain Silicates.* Second Edition. Published by Geological Society, London.

de Wit, M.J. and Ashwal, L.D. (1997). *Greenstone Belts.* Published by Oxford University Press.

de Wit, M.J. Hart, R.A. and Hart, R.J.(1987). *The Jamestown Ophiolite Complex, Barberton Mountain Belt- a section through 3.5 Ga oceanic-crust.* Journal of African Earth Sciences, vol. 6, pp 681-730.

Donaldson, C.H. (1982). *Spinifex-textured komatiites: a review of textures, compositions and layering.* In: Arndt, N.T. and Nisbet, E.G. (eds.), *Komatiites.* Published by George Allen and Unwin, London. pp 211-244.

Dostal, J. and Mueller, W.U. (1997). *Komatiite flooding of a rifted Archaean rhyolitic arc complex: Geochemical signature and tectonic significance of the Stoughton-Roquemaure Group, Abitibi Greenstone belt, Canada.* Journal of Geology, vol. 105, pp 545-563.

Eakins, P.R. (1972). *Roquemaure Township, Abitibi-West County.* Quebec Department of Natural Resources, Geological Report 150, p 69.

Easton, R.M. (2000). *Metamorphism of the Canadian Shield, Ontario, Canada. 1. The Superior Province.* The Canadian Mineralogist, vol. 38, pp 287-317.

Echeverria, L. M. and Aitken, B. G. (1986). *Pyroclastic rocks; another manifestation of ultramafic volcanism on Gorgona Island, Columbia.* Contributions to Mineralogy and Petrology, vol. 92, pp 428-436.

Echeverria, L.M. (1980). *Tertiary or Mesozoic komatiites from Gorgona Island, Columbia — Field relations and geochemistry.* Contributions to Mineralogy and Petrology, vol. 73, pp 253-266.

Fleet, M.E. and MacRae, N.D. (1975). *A spinifex rock from Munro Township, Ontario.* Canadian Journal of Earth Sciences, vol. 12, pp 923-39.

Fujimaki, H., Tatsumoto, M. and Aoki, K. (1984). *Partition coefficients of Hf, Zr, and REE between phenocrysts and groundmasses.* In: Proceedings of the Fourteenth Lunar and Planetary Science Conference, Part 2. Journal of Geophysical Research, vol. 89, supplement, pp B662-B672.

104

Fyfe, W.S. (1978). *The evolution of the Earth's crust: Modern plate tectonics to ancient hot spot tectonics.* Chemical Geology, vol. 23, pp 89-114.

Fyon, J.A. and Green, A.H. (1991). *Geology and ore deposits of the Timmins district, Ontario (Field Trip 6).* Geological Survey of Canada Open File Report 2161.

Gaetani, G.A., Kent, A.J.R., Grove, T.L., Hutcheon, I.D. and Stolper, E.M. (2003). *Mineral/melt partitioning of trace elements during hydrous peridotite partial melting.* Contributions to Mineralogy and Petrology, vol. 145, pp 391-405.

Gibson, H., Richardson, D., Hannington, M., Gibbins, S., Dewolfe, M. and Duff, D. (2003). *The Kidd Creek volcanologenic massive sulphide deposits: A growing giant, after forty years of mining, exploration, and research.* The Gangue, G.A.C. Mineral Deposits Division, Issue 78.

Glikson, A.Y. (1971). *Primitive Archaean element distribution patterns: Chemical evidence and geotectonic significance.* Earth and Planetary Science Letters, vol. 12, pp 309-320.

Goodwin, A.M. (1996). *Principles of Precambrian Geology.* Academic Press Limited.

Goodwin, A.M. (1991). *Precambrian Geology.* Academic Press, London.

Goodwin, A.M. and Ridler, R. (1970). *The Abitibi Orogenic Belt.* In: Baer, A.J. (ed.), *Symposium on Basins and Geosynclines of the Canadian Shield.* Geological Survey of Canada, Paper 70-40, pp 1-30.

Goutier, J. (1993). *Porcupine-Destor 5.* Quebec Department of Natural Resources Report on Activity 93 (DV-93-02), 60p.

Green, D.H., Sie, S.H., Ryan, C.G. and Cousens, D.R. (1989). *Proton microprobe-determined partitioning of Nb, Ta, Zr, Sr and Y between garnet, clinopyroxene and basaltic magma at high pressure and temperature.* Chemical Geology, vol. 74, pp 201-216.

Green, D.H. (1975). *Genesis of Archaean peridotitic magmas and constraints on Archaean geothermal gradients and tectonics.* Geology, vol. 3, pp15-18.

Green, D.H. (1972). *Archaean greenstone belts may include terrestrial equivalents of lunar maria?* Earth and Planetary Science Letters, vol. 15, pp 263-270.

Grove, T.L. and Parman, S.W. (2004). *Thermal evolution of the Earth as recorded by komatiites.* Earth and Planetary Science letters, vol. 219, pp 173-187.

Hall, C.J., Gurnis, M., Sdrolias, M., Lavier, L.L. and Muller, R.D. (2003). *Catastrophic initiation of subduction following forced convergence across fracture zones.* Earth and Planetary Science Letters, vol. 212, pp 15-30.

Hanski, E.J. (1992). *Petrology of the Pechenga ferropicrites and cogenetic, Ni-bearing gabbro-wehrlite intrusion, Kola Peninsula, Russia.* Geological Survey of Finland Bulletin, vol. 367, 192pp.

Hart, S.R. and Dunn, T. (1993). *Experimental cpx/melt partitioning of 24 trace elements.* Contributions to Mineralogy and Petrology, vol. 133, pp 60-68.

Herzberg, C. (1995). *Generation of plume magmas through time: An experimental perspective.* Chemical Geology, vol. 126, pp 1-16.

Hill, E., Wood, B.J. and Blundy, J.D. (2000). *The effect of Ca-Tschermaks component on trace element partitioning between clinopyroxene and silicate melt.* Lithos, vol. 53, pp 205-217.

Hollings, P., Wyman, D. and Kerrich, R. (1999). *Komatiite-basalt-rhyolite volcanic associations in northern Superior Province greenstone belt; significance of plume-arc interaction in the generation of the proto continental Superior Province.* Lithos, vol. 46, pp 137-161.

Inoue, T., Rapp, R.P., Zhang, J., Gasparik, T., Weidner, D.J., and Irifune, T. (2000). *Garnet fractionation in a hydrous magma ocean and the origin of Al-depleted komatiites: melting experiments of hydrous pyrolite with REEs at high pressure.* Earth and Planetary Science Letters, vol. 177, pp 81-87.

Jackson, S.L., Fyon, J.A. and Corfu, F. (1994). *Review of Archaean supracrustal assemblages of the Southern Abitibi greenstone belt in Ontario, Canada: product of microplate interaction within a large-scale plate-tectonic setting.* Precambrian Research, vol. 65, pp 183-205.

Jackson, S.L. and Fyon, J.A. (1991). *The Western Abitibi Subprovince in Ontario.* In: Thurston, P.C., Williams, H.R., Sutcliffe, R.H. and Scott, G.M. (eds.), *Geology of Ontario.* Ontario Geological Survey Special, vol. 4, Part I, pp 405-82.

Jensen, L.S. and Langford, F.F. (1985). *Geology and Petrogenesis of the Archaean Abitibi belt in the Kirkland Lake Area, Ontario.* Ontario Geological Survey, Miscellaneous Paper 123, 130p.

Jensen, L.S. (1978). *Geology of Stoughton and Marriott Townships, District of Cochrane.* Ontario Geological Survey, Geological Report 173, 73p.

Johnson, K.T.M. (1998). *Experimental determination of partition coefficients for rare earth and high-field-strength elements between clinopyroxene, garnet, and basaltic melt at high pressures.* Contributions to Mineralogy and Petrology, vol. 133, pp 60-68.

Koizumi, K. and Ishiwatari, A. (2006). *Oceanic plateau accretion inferred from Late Palaeozioc greenstones in the Jurassic Tamba accretionary complex, Southwest Japan.* Island Arc, vol. 15, pp 58-83.

Kerr, A.C., Marriner, G.F., Arndt, N.T. and Tarney, J. (1996). *The petrogenesis of Gorgona komatiites, picrites and basalts: new field petrographic and geochemical constraints.* Lithos, vol. 37, pp 245-260.

107

Kerrich, R., Wyman, D., Fan, J. and Bleeker, W. (1998). *Boninite series; low Ti-tholeiite associations from the 2.7 Ga Abitibi greenstone belt.* Earth and Planetary Science Letters, vol. 164, pp 303-316.

Klemme, S., Gunther, D., Hametner, K., Prowatke, S. and Zack, T. (2006). *The partitioning of trace elements between ilmenite, ulvospinel, armalcolite and silicate melts with implications for the early differentiation of the moon.* Chemical Geology, vol. 234, pp 251-263.

Kroner, G.R., Byerly, G.R. and Lowe, D.R. (1991). *Chronology of early Archaean granite-greenstone evolution in the Barberton Mountain Land, South Africa, based on precise dating by single zircon evaporation.* Earth and Planetary Science Letters, vol. 103, pp 41-54.

Lapierre, H., Taylor, R.N., Rouer, O. and Chaisemartin, H. (1992). *Mineral chemistry of forearc volcanic rocks from the izu-Bonin arc. Holes 792E and 793B.* Proc. Ocean Drilling Program Sci. Res., vol. 126, pp 431-447.

Le Bas, M.J. and Streckeisen, A.L. (1991). *The IUGS systematics of igneous rocks.* Journal of the Geological Society, London, vol. 148, pp 825-833.

Leterrier, J., Maury, R.C., Thonon, P., Girard, D. and Marchal, M. (1982). *Clinopyroxene composition as a method of identification of the magmatic affinities of paleo-volcanic series.* Earth and Planetary Science Letters, vol. 59, pp 139-154.

Lopez-Martinez, M., York, D. and Hanes, J.A. (1992). *An Ar-40/Ar-39 Geochronological study of komatiites and komatiitic basalts from the Lower Onverwacht Volcanics, Barberton Mountain Land, South Africa.* Precambrian Research, vol. 57, pp 91-119.

Lumbers, S.B. (1963). *Geology of the South Patten River area.* Ontario Department of Mines, Geological Report 14, 40p.

Lumbers, S.B. (1962). *Geology of Steele, Bonis, and Scapa Townships.* Ontario Department of Mines, Geological Report 8, 50p.

Lundstrom, C.C., Shaw, H.F., Ryerson, F.J., Williams, Q. and Gill, J. (1998). *Crystal chemical control of cpx-melt partitioning in the Di-Ab-An system: Implications for elemental fractionations in the depleted mantle.* Geochim. Cosmochim. Acta., vol. 62, pp 2849-2862.

McDade, P., Blundy, J.D., and Wood, B.J. (2003). *Trace element partitioning between mantle wedge peridotites and hydrous MgO-rich melt.* American Mineralogist, vol. 88, pp 1825-1831.

McDonough, W.F. and Sun, S.-s. (1995). *The composition of the Earth.* Chemical Geology, vol. 120, pp 223-253.

Nesbitt, R.W. (1971). *Skeletal crystal form in the ultramafic rocks of the Yilgarn Block, Western Australia: evidence for an Archaean ultramafic liquid.* Geological Society of Australia Special Publication, vol. 3, pp 331-347.

Nisbet, E. G. and Pearce, J. A. (1977). *Clinopyroxene composition in mafic lavas from different tectonic settings.* Contributions to Mineralogy and Petrology, vol. 63, pp 149-160.

Nna-Mvondo, D. and Martinez-Frais, J. (2005). *Komatiites: From Earth's Geological Settings to Planetary and Astrobiological Contexts.* Earth, Moon and Planets, 53p.

Parman, S.W., Grove, T.L., Dann, J. C. and de Wit, M.J. (2004). *A subduction origin for komatiite and cratonic lithospheric mantle.* South African Journal of Geology, vol. 107, pp 107-118.

Parman, S.W., Shimizu, N., Grove, T.L. and Dann, J.C. (2003). *Constraints on the pre-metamorphic trace element composition of Barberton komatiites from ion probe analyses of preserved clinopyroxene.* Contributions to Mineralogy and Petrology, vol. 144, pp 383-396.

Parman, S.W., Grove, T. L. and Dann, J.C. (2001). *The production of Barberton komatiites in an Archaean subduction zone.* Geophysical Research Letters, vol. 28, pp 2513-2516.

Parman, S. W., Dann, J. C., Grove, T. L. and de Wit M. J. (1997). *Emplacement conditions of komatiite magmas from the 3.49 Ga Komati Formation, Barberton Greenstone Belt, South Africa.* Earth and Planetary Science Letters, vol. 150, pp 303-323.

Pearce, J.A. (1983). *Role of sub-continental lithosphere in magma genesis at active continental margins.* In: Hawkesworth, C.J. and Norry, M.J. (eds.), *Continental basalts and mantle xenoliths.* Shiva, Nantwich, pp 230-248.

Poidevin, J.L. (1994). *Boninite-like rocks from the Palaeoproterozoic greenstone belt of Bogoin, Central African Republic; geochemistry and petrogenesis.* Precambrian Research, vol. 68, pp 97-113.

Pyke, D.R., Naldrett, A.J. and Eckstrand, O.R. (1973). *Archaean ultramafic flows in Munro Township, Ontario.* In: Arndt, N.T. and Nisbet, E.G. (eds.), *Komatiites.* Published by George Allen and Unwin, London.

Reed, S.J.B. (1996). *Electron Microprobe Analysis and Scanning Electron Microscopy in Geology.* Published by Cambridge University Press.

Rollinson, H. (1996). *Using geochemical data: evaluation, presentation, interpretation.* Published by Longman Press.

Rollinson, H. (1999). *Petrology and geochemistry of metamorphic komatiites and basalts from the Sula Mountains greenstone belt, Sierra Leone.* Contributions to Mineralogy and Petrology, vol. 134, pp 86-101.

Shelley, D. (1993). *Igneous and Metamorphic rocks under the microscope: classification, textures, microstructures and mineral preferred orientations.* Published by Chapman and Hall.

Shimizu, K., Nakamura, E. and Maruyama, S. (2005). *The Geochemistry of Ultramafic to Mafic Volcanics from the Belingwe Greenstone Belt, Zimbabwe: Magmatism in an Archaean Continental Large Igneous Province.* Journal of Petrology, vol. 46, pp 2367-2394.

110

Smith, I.E.M. and Williams, J.G. (1980). *Geochemical variety among Archaean granitoids in Northwestern Ontario.* In: Strangway, D.W. (ed.). *The Continental Crust and its Mineral Deposits.* Geological Association of Canada Special Paper 20, pp 181-192.

Sproule, R.A., Lesher, C.M., Houlé, M.G., Keays, R.R., Ayer, J.A. and Thurston, P.C. (2002a). *Geochemistry, Petrogenesis, and Metallogenesis of komatiites in the Abitibi greenstone belt, Canada.* In: 9th International Platinum Symposium, Billings, Montana: 439-432.

Sproule, R.A., Lesher, C.M., Ayer, J.A., Thurston, P.C. and Herzberg, C.T. (2002b). *Spatial and temporal variations in the geochemistry of komatiites and komatiitic basalts in the Abitibi greenstone belt.* Precambrian Research, vol. 115, pp 153-186.

Stern, R.J. and Bloomer, S.H. (1992). *Subducton zone infancy; examples from the Eocene Izu-Bonin-Mariana and Jurassic California arcs.* Geological Society of America Bulletin, vol. 104, pp 1621-1636.

Stern, R.A., Hanson, G.N. and Shirey, S.B. (1989). *Petrogenesis of mantle-derived, LILE-enriched Archaean monzodiorites and trachyandesites (sanukitoids).* Canadian Journal of Earth Sciences, vol. 26, pp 1688-1712.

Stone, W.E., Deloule, E., Larson, M.S. and Lesher, C.M. (1997). *Evidence for hydrous high-MgO melts in the Precambrian.* Geology, vol. 25, pp 143-146.

Sun, S-s., and McDonough, W.F. (1989). *Chemical and isotopic systematics of oceanic basalts: implications for Mantle Composition and Processes.* In: Saunders, A.D. and Norry, M.J. (eds.). *Magmatism in the Ocean Basins.* Geological Society Special Publication, London, pp 313-345.

Sun, S-s., Nesbitt, R.W. and McCulloch, M.T. (1989). *Geochemistry and petrogenesis of Archaean and early Proterozoic siliceous high-magnesian basalts.* In: Crawford A.J. (Ed.). *Boninites and Related Rocks.* Published by Unwin and Hyman, London, pp 148-173.

Takawaza, E., Frey, F.A., Shimizu, N. and Obata, M. (2000). *Whole rock compositional variations in an upper mantle peridotite (Horoman, Hokkaido, Japan): Are they consistent with a partial melting process?* Geochim. Cosmochim. Acta., vol. 64, pp 695-716.

Thurston, P.C. (1994). *Archaean volcanic patterns.* In: Condie, K.C. (Ed.), Archaean Crustal Evolution. Elsevier, New York, pp 45-84.

Thurston, P.C. (1991). *Archaean geology of Ontario; introduction.* In: Thurston, P.C. (ed.), *Geology of Ontario.* Geological Survey Special, vol. 4, pp 73-78.

Thurston, P.C. and Chivers, K.M. (1990). *Secular variations in greenstone sequence development emphasizing Superior Province, Canada.* Precambrian Research, vol. 46, pp 21-58.

Tomlinson, K.Y., Hughes, D.J., Thurston, P.C. and Hall, R.P. (1998). *Plume magmatism and crustal growth at 2.9 to 3.0 Ga in the Steep Rock and Lumby Lake area, Western Superior Province.* Lithos, vol. 46, pp 103-136.

Viljoen, M.J. and Viljoen, R.P. (1969). *The geology and geochemistry of the lower ultramafic unit of the Onverwacht Group and a proposed new class of igneous rocks.* Special Publication, Geological Society of South Africa, vol. 2, pp 55-85.

Westrenen, W.V., Blundy, J.D. and Wood, B.J. (2001). *High field strength element/rare earth element fractionation during partial melting in the presence of garnet: Implications for identification of mantle heterogeneities.* Geochemistry, Geophysics, Geosystems (G ^{3}). An Electronic Journal of the Earth Sciences. Published by AGU and the Geochemical Society, vol. 2, ISSN 1525-2027.

Wilson, A.H. (2003). *A new class of silica enriched, highly depleted komatiites in the southern Kaapvaal Craton, South Africa.* Precambrian Research, vol. 127, pp 125-141.

Wilson, A.H. and Versfeld, J.A. (1994). *The early Archaean Nondweni greenstone belt, southern Kaapvaal Craton, South Africa; Part II, Characteristics of the volcanic rocks and constraints on magma genesis.* Precambrian Research, vol. 67, pp 277-320.

Wyman, D.A., Kerrich, R. and Polat, A. (2002). *Assembly of Archaean cratonic mantle lithosphere and crust: plume-arc interaction in the Abitibi-Wawa subduction-accretion complex.* Precambrian Research, vol. 115, pp 37-62.

Yaliniz, M.K. and Goncuoglu, M.C. (1999). *Clinopyroxene composition of the isotropic gabbros from the Sarikaraman Ophiolite: New evidence on supra-subduction zone type magma genesis in Central Anatolia.* Turkish Journal of Earth Sciences, vol. 8, pp 103-111.

* * * * *

APPENDICES

114

Table 1a: Electron Microprobe analyses of clinopyroxenes in ultramafic komatiite.

Oxides (wt %)	WP-00-8-1	WP-00-8-2a	WP-00-8-2b	Average
SiO2	52.76	52.46	53.97	53.06
TiO2	0.42	0.67	0.36	0.48
Al2O3	3.42	2.78	1.77	2.66
Cr2O3	0.34	1.01	0.63	0.66
FeO*	4.87	4.96	4.51	4.78
MnO	0.18	0.18	0.18	0.18
MgO	18.46	18.70	19.17	18.78
CaO	19.68	19.05	20.02	19.59
Na2O	0.16	0.22	0.19	0.19
K2O	0.01	0.00	0.00	0.00
Total	100.30	100.02	100.81	100.38
Wo	39.68	38.51	39.48	39.23
En	51.81	52.60	52.61	52.34
Fs	7.95	8.09	7.21	7.75
Ac	0.57	0.80	0.69	0.69

Table 1b: Electron Microprobe analyses of clinopyroxenes in komatiites.

Oxides (wt %)	ROQ9521A1a	ROQ9521A1b	ROQ9521A2	ROQ9521A3	ROQ9521A4a1	ROQ9521A4a2	ROQ9521A4b	ROQ9521A5	ROQ9521B1a1	ROQ9521B1a2	ROQ9521B1b1
SiO2	51.03	50.72	52.52	51.84	52.32	51.86	50.29	51.27	51.76	51.68	52.09
TiO2	0.25	0.22	0.15	0.27	0.22	0.20	0.25	0.28	0.29	0.21	0.28
Al2O3	3.04	2.68	1.57	2.51	2.83	2.92	3.05	3.15	3.09	2.92	2.60
Cr2O3	1.01	0.84	0.59	0.75	0.98	1.00	0.84	1.07	1.01	1.04	0.76
FeO*	5.78	6.02	6.20	6.23	6.52	6.18	6.44	5.67	5.84	6.31	6.83
MnO	0.16	0.18	0.23	0.19	0.22	0.19	0.16	0.15	0.17	0.21	0.22
MgO	16.63	16.62	18.14	16.64	17.83	17.20	16.58	16.65	17.51	18.21	17.99
CaO	20.01	19.87	18.82	20.08	18.28	19.54	19.49	20.02	19.85	18.58	18.27
Na2O	0.18	0.17	0.15	0.19	0.17	0.19	0.17	0.18	0.17	0.16	0.18
K2O	0.00	0.00	0.01	0.00	0.00	0.00	0.00	0.00	0.00	0.00	0.00
Total	98.09	97.33	98.39	98.70	99.37	99.26	97.28	98.44	99.68	99.32	99.22
Wo	41.59	41.28	38.13	41.34	37.58	40.06	40.60	41.65	40.34	37.70	37.20
En	48.12	48.04	51.15	47.66	50.98	49.08	48.06	48.21	49.53	51.42	50.96
Fs	9.63	10.03	10.16	10.31	10.82	10.17	10.69	9.45	9.51	10.28	11.19
Ac	0.66	0.65	0.57	0.69	0.62	0.69	0.65	0.69	0.61	0.59	0.65

* Total Fe analysed as FeO.

Table 1b continued:

Oxides (wt %)	ROQ9521B1b2	ROQ9521B2a1	ROQ9521B2a2	ROQ9521B2b1	ROQ9521B2b2	ROQ9521B3a1	ROQ9521B3a2	ROQ9521B3b1	ROQ9521B3b2	ROQ9521B4a1	ROQ9521B4a2
SiO2	52.70	52.24	52.69	52.08	52.47	52.57	52.75	53.49	52.57	52.54	52.28
TiO2	0.24	0.37	0.32	0.34	0.24	0.33	0.23	0.21	0.23	0.25	0.27
Al2O3	2.69	2.28	2.42	2.44	1.68	2.24	2.55	1.68	2.70	2.86	3.06
Cr2O3	0.91	0.29	0.51	0.38	0.20	0.41	0.89	0.62	0.96	0.86	1.14
FeO*	6.60	7.79	7.20	7.76	7.69	7.37	6.99	6.24	6.70	6.36	5.80
MnO	0.20	0.22	0.23	0.23	0.52	0.23	0.20	0.20	0.19	0.19	0.16
MgO	18.35	16.98	17.32	17.33	14.88	17.27	18.42	18.17	18.14	18.18	17.29
CaO	19.01	19.56	19.44	19.05	21.97	19.73	18.23	19.95	18.61	19.15	20.38
Na2O	0.17	0.16	0.16	0.19	0.23	0.17	0.17	0.16	0.18	0.17	0.17
K2O	0.00	0.00	0.00	0.00	0.00	0.00	0.00	0.00	0.00	0.01	0.01
Total	100.86	99.88	100.30	99.79	99.89	100.32	100.41	100.73	100.28	100.58	100.56
Wo	37.91	39.34	39.18	38.32	44.39	39.47	36.64	39.48	37.56	38.42	41.26
En	50.93	47.54	48.57	48.51	41.84	48.08	51.51	50.04	50.95	50.74	48.72
Fs	10.54	12.54	11.67	12.49	12.92	11.83	11.25	9.93	10.85	10.23	9.39
Ac	0.62	0.58	0.59	0.68	0.85	0.62	0.60	0.56	0.64	0.61	0.63

Oxides (wt %)	ROQ9521B4b1	ROQ9521B4b2	ROQ9521B4c1	ROQ9521B4c2	ROQ9521B5a1	ROQ9521B5a2	ROQ9521B5b1	ROQ9521B5b2	Average
SiO2	51.67	52.24	52.53	52.45	52.53	52.48	53.38	53.40	52.21
TiO2	0.57	0.47	0.27	0.25	0.31	0.36	0.22	0.24	0.28
Al2O3	2.22	2.09	2.70	2.67	2.63	2.55	1.65	1.68	2.50
Cr2O3	0.07	0.10	1.01	0.92	0.76	0.37	0.45	0.31	0.70
FeO*	10.73	9.72	6.64	6.39	6.58	7.79	7.03	7.34	6.89
MnO	0.27	0.28	0.20	0.19	0.17	0.21	0.19	0.25	0.21
MgO	15.71	16.48	18.25	18.15	17.20	17.02	18.52	18.28	17.40
CaO	18.71	18.63	18.51	19.05	20.26	19.56	18.82	18.86	19.34
Na2O	0.22	0.19	0.18	0.18	0.21	0.15	0.15	0.14	0.17
K2O	0.01	0.00	0.00	0.01	0.00	0.00	0.00	0.00	0.00
Total	100.18	100.19	100.28	100.26	100.65	100.48	100.41	100.51	99.72
Wo	37.79	37.49	37.35	38.27	40.67	39.33	37.28	37.37	39.17
En	44.14	46.16	51.24	50.76	48.03	47.62	51.06	50.41	49.00
Fs	17.26	15.67	10.76	10.30	10.55	12.52	11.15	11.72	11.19
Ac	0.81	0.69	0.65	0.67	0.76	0.53	0.52	0.50	0.64

* Total Fe analysed as FeO.

116

Table 1c: Electron Microprobe analyses of clinopyroxenes in basaltic komatiites.

Oxides (wt %)	ROQ95-2-1	ROQ95-2-2	ROQ95-2-3a	ROQ95-2-3b	ROQ95-2-3c	ROQ-95-2-4	ROQ95-2-5	ROQ95-2-6a1	ROQ95-2-6a2	ROQ95-2-6b1	ROQ95-2-6b2
SiO2	52.59	51.03	53.36	52.06	52.40	52.48	52.86	52.29	52.51	52.21	52.50
TiO2	0.36	0.72	0.24	0.53	0.41	0.40	0.33	0.32	0.42	0.46	0.42
Al2O3	2.08	3.93	1.39	2.82	2.67	2.21	2.06	2.26	2.29	2.94	2.58
Cr2O3	0.40	0.14	0.23	0.47	0.40	0.34	0.31	0.34	0.42	0.33	0.30
FeO*	6.21	7.76	7.47	7.21	7.16	6.63	6.34	7.39	6.67	6.85	6.68
MnO	0.19	0.20	0.25	0.17	0.17	0.15	0.18	0.22	0.16	0.16	0.17
MgO	17.54	16.27	19.29	17.25	16.50	17.32	17.47	18.07	17.80	17.20	17.16
CaO	20.34	19.87	17.33	19.47	20.86	20.25	20.47	18.38	19.88	19.81	20.36
Na2O	0.18	0.19	0.14	0.18	0.22	0.20	0.17	0.19	0.19	0.19	0.17
K2O	0.00	0.00	0.00	0.00	0.00	0.00	0.00	0.00	0.00	0.00	0.00
Total	99.87	100.10	99.69	100.17	100.78	99.98	100.19	99.46	100.35	100.15	100.34
Wo	40.65	40.51	34.36	39.29	41.79	40.51	40.80	36.90	39.53	39.99	40.83
En	48.77	46.17	53.22	48.45	45.98	48.22	48.46	50.51	49.24	48.31	47.88
Fs	9.94	12.62	11.93	11.59	11.42	10.56	10.11	11.88	10.55	11.02	10.69
Ac	0.64	0.70	0.50	0.67	0.81	0.71	0.63	0.70	0.68	0.68	0.61

Oxides (wt %)	ROQ95-2-6c1	ROQ95-2-6c2	ROQ95-2-6d1	ROQ95-2-6d2	ROQ95-12A1a	ROQ95-12A1b	ROQ95-12A1c	ROQ95-12A1d	ROQ95-12A2a	ROQ95-12A2b	ROQ95-12A2c
SiO2	52.98	51.42	53.51	52.76	50.01	50.28	50.68	50.66	50.83	50.41	51.09
TiO2	0.34	0.59	0.29	0.38	0.59	0.76	0.54	0.55	0.60	0.69	0.60
Al2O3	2.15	3.22	1.34	2.33	3.86	4.47	4.25	3.85	4.49	4.61	4.04
Cr2O3	0.31	0.37	0.24	0.37	0.27	0.45	0.25	0.23	0.33	0.22	0.22
FeO*	7.00	7.18	7.06	7.55	6.12	6.96	6.94	6.21	6.61	7.43	6.30
MnO	0.18	0.18	0.21	0.19	0.15	0.16	0.18	0.14	0.20	0.19	0.17
MgO	18.03	17.06	18.54	18.48	14.99	15.17	15.04	15.15	15.40	15.35	15.41
CaO	18.90	19.47	18.91	18.09	21.86	20.67	21.38	21.53	21.37	20.56	21.71
Na2O	0.19	0.21	0.15	0.16	0.21	0.22	0.21	0.21	0.22	0.23	0.20
K2O	0.00	0.00	0.00	0.00	0.00	0.00	0.00	0.00	0.00	0.00	0.01
Total	100.08	99.70	100.24	100.31	98.05	99.14	99.46	98.54	100.03	99.71	99.76
Wo	37.87	39.48	37.34	36.09	45.57	43.31	44.33	44.91	44.07	42.60	44.72
En	50.25	48.14	50.97	51.29	43.50	44.22	43.38	43.98	44.20	44.25	44.16
Fs	11.21	11.61	11.17	12.03	10.16	11.62	11.49	10.32	10.93	12.29	10.38
Ac	0.68	0.76	0.52	0.59	0.77	0.85	0.80	0.79	0.80	0.86	0.74

* Total Fe analysed as FeO.

Table 1c continued:

Oxides (wt %)	ROQ95-12A3a	ROQ95-12A3b	ROQ95-12A3c	Average
SiO2	49.9566	50.4516	50.5635	51.6757
TiO2	0.7793	0.782	0.693	0.5110
Al2O3	4.428	4.6268	4.3707	3.1711
Cr2O3	0.3091	0.2549	0.2901	0.3120
FeO*	6.8829	7.4757	6.9834	6.9224
MnO	0.156	0.2021	0.183	0.1803
MgO	14.8778	14.9366	15.0952	16.6154
CaO	21.5009	20.9463	21.418	20.2132
Na2O	0.2275	0.2293	0.2368	0.1963
K2O	0.0073	0	0	0.0007
Total	99.1255	99.9054	99.8337	99.7981
Wo	44.71	43.53	44.23	41.12
En	43.05	43.19	43.38	46.93
Fs	11.38	12.42	11.51	11.23
Ac	0.86	0.86	0.88	0.72

* Total Fe analysed as FeO.

Table 1d: Clinopyroxene formulae on the basis of six oxygens (ultramafic komatiite).

	WP-00-8-1	WP-00-8-2a	WP-00-8-2b	Average
Si	1.912	1.910	1.945	1.922
Al (iv)	0.088	0.090	0.055	0.078
Al (vi)	0.057	0.029	0.020	0.035
Fe (3+)	0.014	0.017	0.017	0.016
Cr	0.010	0.029	0.018	0.019
Ti	0.012	0.018	0.010	0.013
Fe (2+)	0.133	0.133	0.119	0.129
Mn	0.005	0.005	0.005	0.005
Mg	0.997	1.015	1.030	1.014
Ca	0.764	0.743	0.773	0.760
Na	0.011	0.016	0.014	0.013
K	0.001	0.000	0.000	0.000
Total	4.005	4.006	4.005	4.005

Table 1e: Clinopyroxene formulae on the basis of six oxygens (komatiites).

	ROQ9521A1a	ROQ9521A1b	ROQ9521A2	ROQ9521A3	ROQ9521A4a1	ROQ9521A4a2	ROQ9521A4b	ROQ9521A5	ROQ9521B1a1	ROQ9521B1a2	ROQ9521B1b1
Si	1.909	1.915	1.951	1.928	1.925	1.916	1.902	1.909	1.903	1.906	1.923
Al (iv)	0.091	0.085	0.049	0.072	0.075	0.084	0.098	0.091	0.097	0.094	0.077
Al (vi)	0.043	0.034	0.020	0.039	0.047	0.043	0.038	0.048	0.037	0.032	0.036
Fe (3+)	0.025	0.039	0.021	0.013	0.000	0.022	0.050	0.014	0.039	0.047	0.025
Cr	0.030	0.025	0.017	0.022	0.028	0.029	0.025	0.032	0.029	0.030	0.022
Ti	0.007	0.006	0.004	0.008	0.006	0.005	0.007	0.008	0.008	0.006	0.008
Fe (2+)	0.155	0.150	0.171	0.180	0.201	0.168	0.153	0.163	0.140	0.146	0.186
Mn	0.005	0.006	0.007	0.006	0.007	0.006	0.005	0.005	0.005	0.006	0.007
Mg	0.928	0.935	1.005	0.923	0.978	0.947	0.935	0.924	0.960	1.001	0.990
Ca	0.802	0.804	0.749	0.800	0.721	0.773	0.790	0.799	0.782	0.734	0.723
Na	0.013	0.013	0.011	0.013	0.012	0.013	0.013	0.013	0.012	0.011	0.013
K	0.000	0.000	0.000	0.000	0.000	0.000	0.000	0.000	0.000	0.000	0.000
Total	4.008	4.013	4.007	4.004	3.999	4.007	4.016	4.004	4.012	4.015	4.008

Table 1e continued:

	ROQ9521B1b2	ROQ9521B2a1	ROQ9521B2a2	ROQ9521B2b1	ROQ9521B2b2	ROQ9521B3a1	ROQ9521B3a2	ROQ9521B3b1	ROQ9521B3b2	ROQ9521B4a1	ROQ9521B4a2
Si	1.914	1.929	1.930	1.923	1.951	1.929	1.923	1.945	1.920	1.913	1.907
Al (iv)	0.086	0.071	0.070	0.077	0.049	0.071	0.077	0.055	0.080	0.087	0.093
Al (vi)	0.030	0.028	0.035	0.029	0.025	0.026	0.033	0.017	0.036	0.036	0.038
Fe (3+)	0.043	0.040	0.020	0.048	0.032	0.040	0.026	0.030	0.025	0.038	0.029
Cr	0.026	0.008	0.015	0.011	0.006	0.012	0.026	0.018	0.028	0.025	0.033
Ti	0.006	0.010	0.009	0.009	0.007	0.009	0.006	0.006	0.006	0.007	0.007
Fe (2+)	0.156	0.200	0.200	0.191	0.207	0.186	0.187	0.160	0.179	0.155	0.147
Mn	0.006	0.007	0.007	0.007	0.016	0.007	0.006	0.006	0.006	0.006	0.005
Mg	0.994	0.935	0.946	0.954	0.825	0.945	1.001	0.985	0.987	0.986	0.940
Ca	0.740	0.774	0.763	0.753	0.875	0.776	0.712	0.777	0.728	0.747	0.796
Na	0.012	0.011	0.011	0.013	0.017	0.012	0.012	0.011	0.012	0.012	0.012
K	0.000	0.000	0.000	0.000	0.000	0.000	0.000	0.000	0.000	0.001	0.000
Total	4.014	4.012	4.006	4.015	4.010	4.013	4.008	4.009	4.008	4.012	4.009

	ROQ9521B4b1	ROQ9521B4b2	ROQ9521B4c1	ROQ9521B4c2	ROQ9521B5a1	ROQ9521B5a2	ROQ9521B5b1	ROQ9521B5b2	Average
Si	1.925	1.934	1.918	1.916	1.919	1.925	1.947	1.948	1.923
Al (iv)	0.075	0.066	0.082	0.084	0.081	0.075	0.053	0.052	0.077
Al (vi)	0.022	0.025	0.034	0.031	0.032	0.035	0.018	0.021	0.032
Fe (3+)	0.053	0.038	0.026	0.039	0.038	0.030	0.030	0.028	0.032
Cr	0.002	0.003	0.029	0.027	0.022	0.011	0.013	0.009	0.020
Ti	0.016	0.013	0.007	0.007	0.008	0.010	0.006	0.006	0.008
Fe (2+)	0.279	0.262	0.176	0.156	0.163	0.208	0.184	0.195	0.180
Mn	0.008	0.009	0.006	0.006	0.005	0.006	0.006	0.008	0.007
Mg	0.872	0.910	0.993	0.989	0.936	0.930	1.007	0.994	0.955
Ca	0.747	0.739	0.724	0.745	0.793	0.768	0.735	0.737	0.764
Na	0.016	0.014	0.013	0.013	0.015	0.010	0.010	0.010	0.012
K	0.000	0.000	0.000	0.000	0.000	0.000	0.000	0.000	0.000
Total	4.016	4.012	4.008	4.012	4.012	4.009	4.010	4.009	4.010

Table 1f: Clinopyroxene formulae on the basis of six oxygens (basaltic komatiites).

	ROQ95-2-1	ROQ95-2-2	ROQ95-2-3a	ROQ95-2-3b	ROQ95-2-3c	ROQ-95-2-4	ROQ95-2-5	ROQ95-2-6a1	ROQ95-2-6a2	ROQ95-2-6b1	ROQ95-2-6b2
Si	1.932	1.883	1.956	1.912	1.918	1.929	1.936	1.929	1.922	1.915	1.923
Al (iv)	0.068	0.117	0.044	0.088	0.082	0.071	0.064	0.071	0.078	0.085	0.077
Al (vi)	0.022	0.054	0.016	0.034	0.034	0.025	0.025	0.027	0.021	0.042	0.034
Fe (3+)	0.041	0.050	0.028	0.037	0.045	0.043	0.036	0.044	0.053	0.032	0.035
Cr	0.012	0.004	0.007	0.014	0.011	0.010	0.009	0.010	0.012	0.010	0.009
Ti	0.010	0.020	0.006	0.015	0.011	0.011	0.009	0.009	0.012	0.013	0.012
Fe (2+)	0.149	0.188	0.200	0.184	0.173	0.160	0.157	0.183	0.150	0.177	0.169
Mn	0.006	0.006	0.008	0.005	0.005	0.005	0.005	0.007	0.005	0.005	0.005
Mg	0.961	0.895	1.054	0.945	0.900	0.949	0.954	0.994	0.971	0.940	0.937
Ca	0.801	0.785	0.680	0.766	0.818	0.797	0.803	0.726	0.780	0.778	0.799
Na	0.013	0.014	0.010	0.013	0.016	0.014	0.012	0.014	0.013	0.013	0.012
K	0.000	0.000	0.000	0.000	0.000	0.000	0.000	0.000	0.000	0.000	0.000
Total	4.013	4.016	4.009	4.012	4.014	4.014	4.012	4.014	4.017	4.010	4.011

	ROQ95-2-6c1	ROQ95-2-6c2	ROQ95-2-6d1	ROQ95-2-6d2	ROQ95-12A1a	ROQ95-12A1b	ROQ95-12A1c	ROQ95-12A1d	ROQ95-12A2a	ROQ95-12A2b	ROQ95-12A2c
Si	1.939	1.899	1.955	1.928	1.884	1.873	1.883	1.895	1.875	1.870	1.888
Al (iv)	0.061	0.101	0.045	0.072	0.116	0.127	0.117	0.105	0.125	0.130	0.112
Al (vi)	0.031	0.039	0.013	0.028	0.055	0.069	0.069	0.065	0.070	0.071	0.064
Fe (3+)	0.023	0.051	0.030	0.036	0.051	0.027	0.038	0.026	0.040	0.046	0.033
Cr	0.009	0.011	0.007	0.011	0.008	0.013	0.007	0.007	0.009	0.007	0.006
Ti	0.009	0.016	0.008	0.010	0.017	0.021	0.015	0.016	0.017	0.019	0.017
Fe (2+)	0.191	0.170	0.186	0.194	0.141	0.189	0.177	0.168	0.163	0.183	0.161
Mn	0.006	0.006	0.006	0.006	0.005	0.005	0.006	0.005	0.006	0.006	0.005
Mg	0.983	0.939	1.010	1.006	0.842	0.842	0.833	0.845	0.847	0.849	0.849
Ca	0.741	0.770	0.740	0.708	0.882	0.825	0.851	0.863	0.844	0.817	0.860
Na	0.013	0.015	0.010	0.012	0.015	0.016	0.015	0.015	0.015	0.017	0.014
K	0.000	0.000	0.000	0.000	0.000	0.000	0.000	0.000	0.000	0.000	0.000
Total	4.007	4.016	4.009	4.011	4.016	4.008	4.012	4.008	4.013	4.015	4.010

121

Table 1f continued:

	ROQ95-12A3a	ROQ95-12A3b	ROQ95-12A3c	Average
Si	1.866	1.870	1.874	1.906
Al (iv)	0.134	0.130	0.126	0.094
Al (vi)	0.061	0.072	0.065	0.044
Fe (3+)	0.054	0.036	0.047	0.039
Cr	0.009	0.007	0.008	0.009
Ti	0.022	0.022	0.019	0.014
Fe (2+)	0.160	0.195	0.168	0.173
Mn	0.005	0.006	0.006	0.006
Mg	0.829	0.825	0.834	0.913
Ca	0.861	0.832	0.850	0.799
Na	0.016	0.016	0.017	0.014
K	0.000	0.000	0.000	0.000
Total	4.017	4.011	4.015	4.012

Table 2: Synopsis of clinopyroxene end-member percent ranges for rocks of the SRG.

Rock Type	Wo (%)	En (%)	Fs (%)
Ultramafic Komatiite	38.51 - 39.68	51.81 - 52.61	7.21 - 8.01
Komatiite	36.64 - 44.39	41.84 - 51.51	9.39 - 17.26
Basaltic Komatiite	34.36 - 45.57	43.05 - 53.22	9.94 - 12.62

Table 3a: Correlation matrices of clinopyroxene cations (ultramafic komatiites).

	Si	Al (iv)	Al (vi)	Fe (3+)	Cr	Ti	Fe (2+)	Mn	Mg	Ca	Na	K
Si	1	-1	-0.64	0.20	-0.13	-0.70	-1.00	-0.46	0.82	0.76	0.02	-0.46
Al (iv)		1	0.64	-0.20	0.13	0.70	1.00	0.46	-0.82	-0.76	-0.02	0.46
Al (vi)			1	-0.88	-0.67	-0.10	0.67	0.97	-0.97	0.00	-0.78	0.97
Fe (3+)				1	0.94	0.56	-0.23	-0.96	0.73	-0.48	0.98	-0.96
Cr					1	0.80	0.10	-0.82	0.46	-0.74	0.99	-0.82
Ti						1	0.68	-0.32	-0.16	-1.00	0.70	-0.32
Fe (2+)							1	0.48	-0.83	-0.74	-0.06	0.48
Mn								1	-0.89	0.23	-0.90	1.00
Mg									1	0.25	0.60	-0.89
Ca										1	-0.63	0.23
Na											1	-0.90
K												1

Table 3b: Correlation matrices of clinopyroxene cations (komatiites).

	Si	Al (iv)	Al (vi)	Fe (3+)	Cr	Ti	Fe (2+)	Mn	Mg	Ca	Na	K
Si	1	-1	-0.72	-0.23	-0.70	-0.04	0.47	0.59	-0.04	0.00	-0.11	0.00
Al (iv)		1	0.72	0.23	0.70	0.04	-0.47	-0.59	0.04	0.00	0.11	0.00
Al (vi)			1	-0.43	0.70	-0.15	-0.35	-0.40	-0.08	0.12	0.11	-0.20
Fe (3+)				1	-0.30	0.40	0.05	0.06	-0.15	0.05	0.20	0.16
Cr					1	-0.60	-0.79	-0.62	0.43	-0.06	-0.14	0.00
Ti						1	0.76	0.16	-0.55	-0.02	0.39	0.12
Fe (2+)							1	0.52	-0.45	-0.18	0.30	0.03
Mn								1	-0.55	0.34	0.47	-0.05
Mg									1	-0.75	-0.74	0.04
Ca										1	0.48	-0.07
Na											1	0.10
K												1

Table 3c: Correlation matrices of clinopyroxene cations (basaltic komatiites).

	Si	Al (iv)	Al (vi)	Fe (3+)	Cr	Ti	Fe (2+)	Mn	Mg	Ca	Na	K
Si	1											
Al (iv)	-1	1										
Al (vi)	-0.95	0.95	1									
Fe (3+)	-0.37	0.37	0.09	1								
Cr	0.18	-0.18	-0.31	0.07	1							
Ti	-0.96	0.96	0.88	0.33	-0.17	1						
Fe (2+)	0.12	-0.12	-0.01	-0.49	-0.16	-0.03	1					
Mn	0.28	-0.28	-0.22	-0.14	-0.31	-0.27	0.60	1				
Mg	0.93	-0.93	-0.94	-0.24	0.23	-0.87	0.26	0.42	1			
Ca	-0.76	0.76	0.76	0.27	-0.16	0.68	-0.58	-0.60	-0.92	1		
Na	-0.87	0.87	0.82	0.39	0.01	0.81	-0.20	-0.38	-0.88	0.76	1	
K	-0.31	0.31	0.28	0.14	-0.18	0.33	-0.25	-0.22	-0.32	0.35	0.20	1

Table 4a: Selected electron microprobe analyses of igneous augite in Barberton komatiites. *(data from Parman et al., 2003)*

Point no.	1	2	3	4	6	7	8	10	11	12	13	14
xtal	1	1	1	1	1	2	2	2	2	2	3	3
Oxides (wt %)												
SiO_2	53.70	55.30	53.00	54.20	53.40	54.10	54.30	54.10	53.40	53.20	53.80	55.00
TiO_2	0.20	0.19	0.21	0.22	0.19	0.18	0.18	0.20	0.21	0.22	0.22	0.20
Al_2O_3	1.10	0.99	1.00	0.96	1.14	1.31	0.98	1.18	0.96	1.15	1.06	1.15
Cr_2O_3	0.58	0.44	0.49	0.54	0.73	0.71	0.45	0.61	0.43	0.59	0.65	0.77
FeO^*	6.30	6.30	6.50	5.40	6.30	5.60	6.10	5.70	5.70	6.60	5.60	4.90
MnO	0.22	0.20	0.18	0.19	0.19	0.18	0.21	0.21	0.14	0.16	0.16	0.19
MgO	19.90	18.90	19.40	17.60	19.10	18.10	19.20	18.90	19.10	19.10	18.90	18.30
CaO	18.40	18.70	17.90	19.60	18.00	19.70	20.10	19.10	18.90	18.20	20.10	20.10
Na_2O	0.12	0.16	0.17	0.19	0.20	0.16	0.13	0.17	0.17	0.18	0.17	0.20
Total	100.50	101.20	99.80	98.90	99.30	100.00	101.60	100.10	99.00	99.50	99.80	100.80
Si	1.949	1.987	1.957	1.993	1.961	1.971	1.954	1.967	1.964	1.955	1.953	1.982
Al (iv)	0.047	0.013	0.043	0.007	0.039	0.029	0.042	0.033	0.036	0.045	0.045	0.018
Al (vi)	0.000	0.029	0.000	0.035	0.011	0.027	0.000	0.017	0.006	0.005	0.000	0.031
Fe (3+)	0.052	0.000	0.044	0.000	0.015	0.000	0.054	0.000	0.026	0.035	0.044	0.000
Cr	0.017	0.013	0.014	0.016	0.021	0.020	0.013	0.018	0.013	0.017	0.019	0.022
Ti	0.005	0.005	0.006	0.006	0.005	0.005	0.005	0.005	0.006	0.006	0.006	0.005
Fe (2+)	0.138	0.190	0.156	0.167	0.178	0.171	0.129	0.173	0.149	0.167	0.125	0.148
Mn	0.007	0.006	0.006	0.006	0.006	0.006	0.006	0.006	0.004	0.005	0.005	0.006
Mg	1.077	1.013	1.068	0.965	1.046	0.983	1.030	1.024	1.048	1.046	1.023	0.983
Ca	0.716	0.720	0.708	0.772	0.708	0.769	0.775	0.744	0.745	0.717	0.782	0.776
Na	0.008	0.011	0.012	0.014	0.014	0.011	0.009	0.012	0.012	0.013	0.012	0.014
K	0.000	0.000	0.000	0.000	0.000	0.000	0.000	0.000	0.000	0.000	0.000	0.000
TOTAL	4.017	3.987	4.014	3.980	4.005	3.992	4.017	4.000	4.008	4.011	4.014	3.985

* Total Fe analysed as FeO.

125

Table 4b: Major element compositions of clinopyroxenes in the Belingwe komatiites. *(data compiled from Shimizu et al., 2005)*

Oxides (wt %)	Komatiites					Basaltic komatiites		
	BW069	BW072	BW087	BW091	BX001	BW050	BW052	BW495
SiO_2	52.50	52.70	52.20	52.30	51.10	53.30	54.10	53.80
TiO_2	0.30	0.30	0.40	0.40	0.40	0.30	0.10	0.20
Al_2O_3	4.70	4.60	5.00	4.60	5.10	3.40	3.10	3.00
Cr_2O_3	0.40	0.10	0.20	0.20	0.40	0.20	0.30	0.30
FeO^*	5.70	7.60	5.20	7.00	8.30	6.90	6.60	6.40
MnO	0.20	0.10	0.20	0.20	0.20	0.20	0.10	0.10
MgO	16.10	17.70	16.30	17.60	14.30	18.00	18.90	18.90
CaO	19.80	16.70	20.10	17.40	19.90	17.50	16.60	16.80
Na_2O	0.30	0.20	0.20	0.30	0.20	0.10	0.20	0.30
Total	100.00	100.00	99.80	100.00	99.90	99.90	100.00	99.80
Si	1.913	1.916	1.903	1.905	1.890	1.939	1.956	1.951
Al (iv)	0.087	0.084	0.097	0.095	0.110	0.061	0.044	0.049
Al (vi)	0.115	0.113	0.117	0.102	0.112	0.085	0.088	0.079
Fe (3+)	0.000	0.000	0.000	0.000	0.000	0.000	0.000	0.000
Cr	0.012	0.003	0.006	0.006	0.012	0.006	0.009	0.009
Ti	0.008	0.008	0.011	0.011	0.011	0.008	0.003	0.005
Fe (2+)	0.174	0.232	0.159	0.213	0.257	0.211	0.201	0.195
Mn	0.006	0.003	0.006	0.006	0.006	0.006	0.003	0.003
Mg	0.875	0.959	0.886	0.955	0.788	0.976	1.019	1.022
Ca	0.773	0.651	0.785	0.679	0.788	0.682	0.643	0.653
Na	0.021	0.014	0.014	0.021	0.014	0.007	0.014	0.021
K	0.000	0.000	0.000	0.000	0.000	0.000	0.000	0.000
TOTAL	3.984	3.984	3.984	3.994	3.990	3.981	3.979	3.986

* Total Fe analysed as FeO.

Table 4c: Representative clinopyroxene compositions from Gorgona komatiites.
(data compiled from Aitken and Echeverria, 1984)

Oxides (wt %)	GOR-156 Type 3 komatiite		GOR-126 Type 2A komatiite			
	1	2	1	2	3	4
SiO_2	50.00	49.60	49.10	48.50	46.30	45.90
TiO_2	0.85	0.67	0.49	0.49	0.90	1.14
Al_2O_3	4.90	4.70	8.60	9.80	10.90	11.40
Cr_2O_3	0.82	0.47	0.35	0.31	0.22	0.18
FeO*	8.20	8.50	7.80	8.60	7.50	7.60
MnO	0.15	0.14	n.d	n.d	n.d	n.d
MgO	13.90	14.60	18.40	17.60	12.20	11.50
CaO	21.50	20.20	15.00	14.40	22.30	22.70
Na_2O	n.d	n.d	n.d	0.29	n.d	n.d
Total	100.30	99.00	99.74	100.00	100.20	100.50
Si	1.856	1.863	1.790	1.768	1.717	1.703
Al (iv)	0.144	0.137	0.210	0.232	0.283	0.297
Al (vi)	0.070	0.072	0.160	0.189	0.193	0.202
Fe (3+)	0.004	0.020	0.020	0.040	0.051	0.039
Cr	0.024	0.014	0.010	0.009	0.006	0.005
Ti	0.024	0.019	0.013	0.013	0.025	0.032
Fe (2+)	0.251	0.247	0.217	0.221	0.181	0.196
Mn	0.005	0.004	0.000	0.000	0.000	0.000
Mg	0.769	0.818	1.000	0.957	0.674	0.636
Ca	0.855	0.813	0.586	0.562	0.886	0.902
Na	0.000	0.000	0.000	0.020	0.000	0.000
K	0.000	0.000	0.000	0.000	0.000	0.000
TOTAL	4.001	4.006	4.006	4.013	4.016	4.012

* Total Fe analysed as FeO.
n.d. = not detected.

127

Table 4d: Representative clinopyroxene compositions from Gorgona komatiites.
(data compiled from Echeverria, 1980)

Oxides (wt %)	6	6(2)	42D	71	72	73
SiO2	45.2	46.4	46.3	45.6	49	48.6
TiO2	1.18	0.94	1.02	0.75	1.1	1.13
Al2O3	12.7	10.9	10.3	10.7	6.43	9.72
Cr2O3	0.25	0.31	n.d	0.16	0.56	0.31
FeO*	8.27	9.97	7.39	12.1	9.27	9.9
MnO	0.14	0.18	0.16	0.23	0.14	0.23
MgO	11.7	14.7	12.7	12.5	13.1	11.9
CaO	21.2	16.9	21.6	17.5	20.5	19.3
Na2O	0.31	0.16	0.29	0.41	0.07	0.47
NiO	n.d	n.d	0.05	0.06	0.05	0.05
Total	101	100.5	99.8	100	100.2	101.6
Si	1.670	1.713	1.725	1.715	1.825	1.780
Al (iv)	0.330	0.287	0.275	0.285	0.175	0.220
Al (vi)	0.223	0.187	0.178	0.189	0.107	0.200
Fe (3+)	0.084	0.074	0.090	0.116	0.000	0.000
Cr	0.007	0.009	0.000	0.005	0.016	0.009
Ti	0.033	0.026	0.029	0.021	0.031	0.031
Fe (2+)	0.169	0.232	0.138	0.261	0.289	0.304
Mn	0.004	0.006	0.005	0.007	0.004	0.007
Mg	0.644	0.809	0.706	0.701	0.727	0.650
Ca	0.839	0.668	0.862	0.705	0.818	0.757
Na	0.022	0.011	0.021	0.030	0.005	0.033
K	0.000	0.000	0.000	0.000	0.000	0.000
TOTAL	4.027	4.023	4.029	4.035	3.998	3.992

* Total Fe analysed as FeO.
n.d. = not detected.

Table 5a: Microprobe average analyses and atomic proportions of Ca-clinopyroxenes in ophiolitic basalts from Northern Apennines, External and Internal Ligurides, Italy (Beccaluva et al., 1989).

Oxides (wt %)	BC1	BC4	MZ84	11A	16A	MZ67	A22	ROS2	RIP2	LI21	LI76
SiO2	50.99	45.90	51.08	51.35	51.75	51.86	48.87	48.79	49.54	49.49	49.79
TiO2	1.18	4.68	1.25	1.05	1.27	1.17	2.26	2.22	1.63	1.69	1.75
Al2O3	2.66	6.28	3.58	2.68	2.48	2.87	4.84	4.96	4.23	4.05	3.61
Fe2O3	1.68	3.06	1.18	0.84	0.66	0.28	1.79	2.40	2.65	2.52	1.10
FeO	9.32	7.89	6.84	9.53	9.01	8.00	7.22	6.52	5.05	8.10	9.18
MnO	0.30	0.04	0.20	0.37	0.27	0.21	0.22	0.23	0.17	0.38	0.26
MgO	14.92	10.88	15.29	15.45	14.33	14.92	12.68	13.59	14.90	14.74	13.52
CaO	18.49	20.71	20.19	17.96	19.91	20.25	21.00	20.71	20.70	18.62	19.75
Na2O	0.46	1.13	0.44	0.41	0.58	0.50	0.76	0.61	0.52	0.45	0.49
Cr2O3	0.06	0.19	0.23	0.03	0.05	0.12	0.13	0.21	0.28	0.39	0.20
Total	99.66	100.76	100.28	99.67	100.31	100.18	99.77	100.24	99.67	100.43	99.65
Si	1.9321	1.7239	1.8836	1.9142	1.9212	1.9172	1.8300	1.8145	1.8395	1.8393	1.8700
Ti	0.0247	0.1322	0.0347	0.0294	0.0355	0.0325	0.0636	0.0621	0.0455	0.0472	0.0494
Al (tot.)	0.0815	0.2780	0.1556	0.1178	0.1085	0.1251	0.2136	0.2174	0.1851	0.1774	0.1598
Fe (3+)	0.0303	0.0865	0.0327	0.0236	0.0184	0.0078	0.0504	0.0672	0.0740	0.0705	0.0311
Fe (2+)	0.2414	0.2478	0.2109	0.2971	0.2797	0.2473	0.2261	0.2028	0.1568	0.2518	0.2883
Mn	0.0081	0.0013	0.0062	0.0117	0.0085	0.0066	0.0070	0.0072	0.0053	0.0120	0.0083
Mg	0.8814	0.6090	0.8403	0.8583	0.7929	0.8220	0.7076	0.7532	0.8245	0.8164	0.7567
Ca	0.7727	0.8334	0.7977	0.7174	0.7920	0.8021	0.8426	0.8253	0.8236	0.7415	0.7948
Na	0.0265	0.0823	0.0315	0.0296	0.0418	0.0358	0.0552	0.0440	0.0374	0.0324	0.0357
Cr	0.0012	0.0056	0.0067	0.0009	0.0015	0.0035	0.0038	0.0062	0.0082	0.0115	0.0059
Total	3.9999	4.0000	3.9999	4.0000	4.0000	3.9999	3.9999	3.9999	3.9999	4.0000	4.0000

Table 5a continued:

Oxides (wt %)	LI76	LI78	LI31	LI32	LI33
SiO2	49.79	49.68	49.82	49.40	49.93
TiO2	1.75	2.56	1.50	2.02	1.70
Al2O3	3.61	4.41	3.77	4.59	4.37
Fe2O3	1.10	0.00	2.86	0.96	2.45
FeO	9.18	11.29	5.35	8.07	5.88
MnO	0.26	0.27	0.20	0.25	0.27
MgO	13.52	11.01	14.63	13.20	14.50
CaO	19.75	19.68	21.09	20.78	20.90
Na2O	0.49	0.84	0.49	0.52	0.53
Cr2O3	0.20	0.05	0.29	0.32	0.17
Total	99.65	99.59	100.00	100.11	100.70
Si	1.8700	1.8764	1.8491	1.8431	1.8405
Ti	0.0494	0.0727	0.0419	0.0567	0.0471
Al (tot.)	0.1598	0.1963	0.1649	0.2018	0.1899
Fe (3+)	0.0311	0.0000	0.0799	0.0270	0.0680
Fe (2+)	0.2883	0.3566	0.1661	0.2518	0.1813
Mn	0.0083	0.0086	0.0063	0.0079	0.0084
Mg	0.7567	0.6198	0.8093	0.7340	0.7966
Ca	0.7948	0.7565	0.8388	0.8307	0.8255
Na	0.0357	0.0469	0.0353	0.0376	0.0379
Cr	0.0059	0.0015	0.0085	0.0094	0.0050
Total	4.0000	3.9753	4.0001	4.0000	4.0002

Table 5b: Microprobe average analyses and atomic proportions of Ca-clinopyroxenes in alkali basalts.
(data from Leterrier et al., 1982)

site:	Oceanic islands		Intracontinental	
Oxides (wt %)	N80	N48	N38	N61
SiO2	49.09	47.51	48.16	45.16
TiO2	1.62	2.87	1.77	2.64
Al2O3	3.94	6.24	5.88	7.71
Cr2O3	0.34	0.40	0.17	0.19
FeO*	9.75	6.70	7.67	8.34
MnO	0.22	0.12	0.38	0.17
MgO	13.03	13.20	13.42	12.02
CaO	21.36	22.35	21.65	22.86
Na2O	0.41	0.54	0.67	0.64
Total	99.76	99.93	99.77	99.73
Si	1.8400	1.7630	1.7870	1.6870
Al (iv)	0.1600	0.2370	0.2130	0.3130
Al (vi)	0.0260	0.0380	0.0480	0.0330
Ti	0.0460	0.0810	0.0490	0.0740
Cr	0.0100	0.0120	0.0050	0.0060
Fe (3+)	0.0190	0.0700	0.1170	0.1880
Fe (2+)	0.2320	0.1380	0.1200	0.0840
Mn	0.0070	0.0040	0.0120	0.0050
Mg	0.7280	0.7340	0.7460	0.6720
Ca	0.8580	0.8890	0.8610	0.9150
Na	0.0300	0.0390	0.0480	0.0460
Total	3.9560	4.0050	4.0060	4.0230

* Total Fe analysed as FeO.

131

Table 5c: Microprobe average analyses and atomic proportions of Ca-clinopyroxenes in ophiolitic basalts from Troodos (Cyprus) and Pindos (Greece).   (Beccaluva et al., 1989)

Oxides (wt %)	CY9(1)	CY9(2)	CY32	CY39	AP267	AP197	AP95	719PIN	723PIN	732PIN
SiO_2	53.38	51.52	50.90	51.17	53.32	52.04	51.97	51.90	52.50	52.80
TiO_2	0.23	0.42	0.52	0.48	0.10	0.34	0.25	0.87	0.44	0.51
Al_2O_3	2.04	3.11	3.24	4.28	2.06	2.45	1.78	3.84	2.14	2.42
Fe_2O_3	0.00	0.00	1.84	0.43	0.00	0.00	2.27	0.00	0.00	0.00
FeO	7.40	11.34	8.27	5.03	7.07	10.56	7.92	6.83	9.68	8.01
MnO	0.22	0.30	0.27	0.17	0.19	0.23	0.28	0.18	0.26	0.20
MgO	16.08	14.79	15.41	15.79	17.57	15.07	15.60	16.50	16.10	15.80
CaO	19.64	17.40	19.22	21.49	19.20	18.69	20.11	19.40	17.40	18.90
Na_2O	0.13	0.14	0.15	0.16	0.10	0.10	0.13	0.27	0.21	0.25
Cr_2O_3	0.20	0.00	0.00	0.39	0.09	0.03	0.02	0.44	0.27	0.13
Total	99.32	99.02	99.82	99.39	99.70	99.51	100.33	100.23	99.00	99.02
Si	1.9714	1.9353	1.8941	1.8877	1.9571	1.9446	1.9268	1.8997	1.9575	1.9591
Ti	0.0064	0.0119	0.0146	0.0133	0.0028	0.0096	0.0070	0.0239	0.0123	0.0142
Al (tot.)	0.0888	0.1377	0.1421	0.1861	0.0891	0.1079	0.0778	0.1657	0.0940	0.1058
Fe (3+)	0.0000	0.0000	0.0515	0.0119	0.0000	0.0000	0.0633	0.0000	0.0000	0.0000
Fe (2+)	0.2286	0.3562	0.2574	0.1552	0.2170	0.3300	0.2456	0.2091	0.3018	0.2486
Mn	0.0069	0.0095	0.0085	0.0053	0.0059	0.0073	0.0088	0.0056	0.0082	0.0063
Mg	0.8851	0.8280	0.8546	0.8681	0.9611	0.8392	0.8620	0.9001	0.8946	0.8737
Ca	0.7772	0.7003	0.7664	0.8495	0.7551	0.7483	0.7989	0.7609	0.6951	0.7514
Na	0.0093	0.0102	0.0108	0.0114	0.0071	0.0072	0.0093	0.0192	0.0152	0.0180
Cr	0.0058	0.0000	0.0000	0.0114	0.0026	0.0009	0.0006	0.0127	0.0080	0.0038
Total	3.9795	3.9891	4.0000	3.9999	3.9978	3.9950	4.0001	3.9969	3.9867	3.9809

Table 5d: Chemical analyses of clinopyroxenes in ophiolitic gabbros from Sarikaraman, Central Anatolia, Turkey. (data from Yaliniz and Goncuoglu, 1999).

Oxides (wt %)	KY30-3	KY31-1	KY31-3	KY52-2	KY52-3	KY43-1	KY26-1	KY26-3
SiO2	51.80	52.19	53.22	52.44	50.87	50.85	53.42	54.03
TiO2	0.00	0.54	0.37	0.28	0.55	0.72	0.28	0.00
Al2O3	0.80	3.33	1.83	2.17	3.38	3.56	1.98	0.55
Fe2O3	1.74	0.00	1.35	0.23	2.81	0.15	0.66	1.08
FeO	9.58	6.03	3.51	5.50	3.27	6.01	4.45	3.22
MnO	0.37	0.22	0.00	0.00	0.21	0.00	0.18	0.20
MgO	12.45	15.72	15.98	17.40	16.65	16.09	16.51	16.60
CaO	23.25	21.95	24.01	20.64	20.96	20.88	22.64	24.65
Na2O	0.00	0.00	0.26	0.00	0.28	0.00	0.23	0.00
Cr2O3	0.00	0.38	0.23	0.45	0.47	0.35	0.23	0.00
Total	100.00	100.36	100.76	99.11	99.45	98.61	100.58	100.33
Si	1.9560	1.9130	1.9380	1.9350	1.8760	1.8940	1.9460	1.9730
Ti	0.0000	0.0150	0.0100	0.0080	0.0150	0.0200	0.0080	0.0000
Al (tot.)	0.0360	0.1440	0.0790	0.0950	0.1470	0.1570	0.0850	0.0240
Fe (3+)	0.0500	0.0000	0.0370	0.0060	0.0780	0.0040	0.0180	0.0300
Fe (2+)	0.3030	0.1850	0.1070	0.1700	0.1010	0.1870	0.1360	0.0980
Mn	0.0120	0.0070	0.0000	0.0000	0.0070	0.0000	0.0060	0.0060
Mg	0.7010	0.8590	0.8670	0.9570	0.9150	0.8940	0.8960	0.9040
Ca	0.9410	0.8620	0.9370	0.8160	0.8280	0.8340	0.8840	0.9650
Na	0.0000	0.0000	0.0190	0.0000	0.0200	0.0000	0.0160	0.0000
Cr	0.0000	0.0110	0.0070	0.0130	0.0140	0.0100	0.0070	0.0000
Total	3.9990	3.9960	4.0010	4.0000	4.0010	4.0000	4.0020	4.0000

Table 5e: Microprobe average analyses and atomic proportions of Ca-clinopyroxenes in basalts and basaltic andesites from Troodos (Cyprus) and Asprokambo Vourinos (Greece). (Beccaluva et al., 1989)

Oxides (wt%)	CY5	CY33	AP131	AP123	BA	740PIN	727PIN	TR9(1)	TR9(2)
SiO2	53.36	51.00	52.50	53.22	51.60	52.20	52.75	53.23	52.71
TiO2	0.06	0.38	0.03	0.00	0.13	0.10	0.07	0.07	0.12
Al2O3	1.66	4.02	2.14	1.87	2.57	1.78	2.50	1.56	1.50
Fe2O3	1.14	0.96	1.95	2.09	1.79	2.51	1.50	0.63	1.39
FeO	3.55	7.23	5.10	3.38	7.93	4.82	6.47	4.95	6.76
MnO	0.15	0.18	0.17	0.12	0.16	0.22	0.25	0.14	0.27
MgO	18.94	15.92	17.08	18.27	15.57	17.60	17.60	17.43	16.34
CaO	20.43	19.43	20.86	21.31	20.13	20.50	19.30	21.26	20.52
Na2O	0.05	0.14	0.08	0.06	0.04	0.09	0.07	0.07	0.15
Cr2O3	0.31	0.17	0.28	0.11	0.07	0.30	0.13	0.32	0.26
Total	99.65	99.43	100.19	100.43	99.99	100.12	100.64	99.66	100.02
Si	1.9443	1.8907	1.9248	1.9319	1.9156	1.9169	1.9243	1.9534	1.9463
Ti	0.0016	0.0106	0.0008	0.0000	0.0036	0.0028	0.0019	0.0019	0.0033
Al (tot.)	0.0713	0.1757	0.0925	0.0800	0.1125	0.0770	0.1075	0.0675	0.0653
Fe (3+)	0.0313	0.0268	0.0538	0.0571	0.0500	0.0694	0.0412	0.0174	0.0386
Fe (2+)	0.1082	0.2242	0.1564	0.1026	0.2462	0.1480	0.1974	0.1519	0.2088
Mn	0.0046	0.0057	0.0053	0.0037	0.0050	0.0068	0.0077	0.0044	0.0084
Mg	1.0285	0.8796	0.9332	0.9884	0.8614	0.9632	0.9569	0.9533	0.8992
Ca	0.7977	0.7718	0.8195	0.8289	0.8007	0.8066	0.7544	0.8360	0.8119
Na	0.0035	0.0101	0.0057	0.0042	0.0029	0.0064	0.0050	0.0050	0.0107
Cr	0.0089	0.0050	0.0081	0.0032	0.0021	0.0087	0.0037	0.0093	0.0076
Total	3.9999	4.0002	4.0001	4.0000	4.0000	4.0058	4.0000	4.0001	4.0001

Table 6: Laser ablation (ICP-MS) trace element analyses (averaged) of clinopyroxenes in SRG komatiitic rocks; whole rock REE composition and calculated augite composition in equilibrium with melt.

Trace elements	ultramafic komatiite (WP-00-8)	komatiite (ROQ-95-21A)	ROQ-95-21B	basaltic komatiite ROQ-95-2	ROQ-95-12A
Rb	0.965	0.680	0.772	0.716	0.894
Sr	17.349	11.119	10.544	8.189	11.653
Th	0.048	0.024	0.027	0.016	0.017
Nb	0.275	0.130	0.148	0.121	0.155
La	0.520	0.172	0.195	0.381	0.603
Ce	1.970	0.584	0.579	1.252	2.198
Pr	0.451	0.122	0.136	0.273	0.483
Nd	2.600	1.528	1.671	1.885	3.363
Zr	13.590	4.295	5.019	10.158	20.192
Hf	0.825	0.308	0.300	0.508	1.040
Sm	2.242	0.827	0.806	1.030	1.512
Ti*	2831	1347	1724	2412	3845
Eu	0.826	0.179	0.223	0.393	0.576
Gd	2.907	0.750	0.996	1.456	1.803
Tb	0.617	0.198	0.220	0.284	0.324
Dy	4.573	1.384	1.479	1.803	2.160
Y	23.039	7.370	9.522	9.715	12.493
Er	2.555	1.128	0.838	0.929	1.338
Yb	2.274	1.211	1.054	0.909	1.063
Lu	0.363	0.160	0.165	0.179	0.143

REE (ppm)	whole rock composition	calculated augite	whole rock composition	calculated augite	whole rock composition	calculated augite	whole rock composition	calculated augite	whole rock composition	calculated augite
La	0.34	0.036	2.20	0.23	2.56	0.268	2.62	0.274	1.84	0.193
Ce	0.97	0.122	5.34	0.669	6.22	0.779	7.69	0.964	5.85	0.734
Pr	0.16	-	0.80	-	0.90	-	1.20	-	0.97	-
Nd	0.85	2.243	4.02	1.153	4.47	1.281	6.43	1.843	5.01	1.436
Sm	0.31	0.148	1.34	0.64	1.43	0.684	2.05	0.979	1.67	0.797
Eu	0.12	0.065	0.44	0.246	0.49	0.274	0.67	0.376	0.61	0.337
Gd	0.42	0.252	1.90	1.133	2.03	1.207	2.45	1.459	2.05	1.221
Tb	0.07	-	0.30	-	0.34	-	0.40	-	0.34	-
Dy	0.51	0.317	2.16	1.345	2.31	1.437	2.56	1.592	2.21	1.374
Er	0.39	0.246	1.41	0.895	1.52	0.964	1.39	0.883	1.20	0.763
Yb	0.34	0.206	1.25	0.749	1.27	0.765	1.36	0.817	1.20	0.721
Lu	0.05	0.03	0.19	0.106	0.19	0.109	0.21	0.118	0.17	0.095

*: Ti values obtained by conversion from microprobe wt % values to ppm.

Note:
Fujimaki et al. (1984) did not determine the pertition coefficients of Pr and Tb.

135